AD NUMBER

AD874509

LIMITATION CHANGES

TO:

Approved for public release; distribution is unlimited.

FROM:

**Distribution authorized to U.S. Gov't. agencies and their contractors;
Administrative/Operational Use; JUN 1970. Other requests shall be referred to Army Aviation Materiel Labs., Fort Eustis, VA.**

AUTHORITY

USAAVLABS per DTIC form 55

USAAVLABS TECHNICAL REPORT 70-6A

THEORY OF STRUCTURAL DYNAMIC TESTING USING IMPEDANCE TECHNIQUES

VOLUME I

THEORETICAL DEVELOPMENT

By

William G. Flannelly

Alex Berman

Roger M. Barnsby

June 1970

U. S. ARMY AVIATION MATERIEL LABORATORIES
FORT EUSTIS, VIRGINIA

CONTRACT DAAJ02-68-C-0106

KAMAN AEROSPACE CORPORATION

BLOOMFIELD, CONNECTICUT

Disclaimers

The findings in this report are not to be construed as an official Department of the Army position unless so designated by other authorized documents.

When Government drawings, specifications, or other data are used for any purpose other than in connection with a definitely related Government procurement operation, the United States Government thereby incurs no responsibility nor any obligation whatsoever; and the fact that the Government may have formulated, furnished, or in any way supplied the said drawings, specifications, or other data is not to be regarded by implication or otherwise as in any manner licensing the holder or any other person or corporation, or conveying any rights or permission, to manufacture, use, or sell any patented invention that may in any way be related thereto.

Disposition Instructions

Destroy this report when no longer needed. Do not return it to the originator.

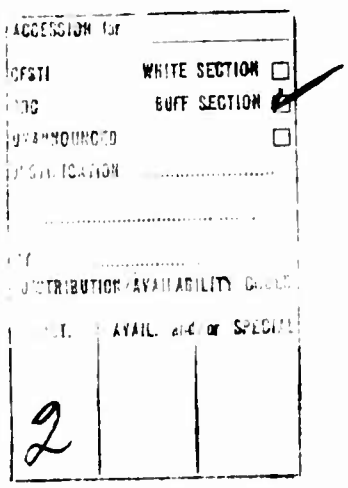

DEPARTMENT OF THE ARMY
HEADQUARTERS US ARMY AVIATION MATERIEL LABORATORIES
FORT EUSTIS, VIRGINIA 23604

Conventional methods of structural dynamic analysis are intuitive in nature. Equations of motion are obtained from an assumed model that, at best, has only a reasonable comparison to the actual structure. Because of their intuitive foundation, conventional analyses leave much to be desired with regard to the adequacy of proposed "fixes" or the dynamic effects of modifications such as gun pods, radar units, and external stores.

This contract was initiated to develop a theory of structural dynamic testing which could be used to determine, directly from measurable test data, the equations of motion, eigenfunctions, and natural frequencies of a complex structure such as a helicopter. Within the framework of the idealized assumptions, the following major goals have been achieved:

- Theory derived and proven - an exact method for identifying the parameters in n equations of motion of an n-degree-of-freedom linear structure was developed and shown to be theoretically correct.

- Theory shown to be numerically sound - the method of implementing the theory was designed to eliminate ill-behaved matrices and excessive sensitivity to experimental or measurement error.

- Theory found to be experimentally practical - precisely controlled statistical computer experiments demonstrated that the theory is operable using measured input data of the type common to helicopter structural testing and with errors in excess of the accuracy of available testing equipment.

A second contract has been awarded with the principal objectives of determining the adequacy of the chosen n degrees of freedom and the applicability of the theory of nonsymmetrical, three-dimensional structures.

Task 1F162204A13904
Contract DAAJ02-68-C-0106
USAAVLABS Technical Report 70-6A
June 1970

THEORY OF STRUCTURAL DYNAMIC TESTING USING IMPEDANCE TECHNIQUES

Final Report

Volume I
Theoretical Development

Kaman Report No. R-823

By

William G. Flannelly
Alex Berman
Roger M. Barnaby

Prepared By

Kaman Aerospace Corporation
Bloomfield, Connecticut

For

U. S. ARMY AVIATION MATERIEL LABORATORIES
FORT EUSTIS, VIRGINIA

ABSTRACT

It is shown that the mass, stiffness and damping parameters in Lagrange's equations of motion of an n-degree-of-freedom damped linear elastic structure can be determined directly from impedance-type test data without prior assumption of an intuitive mathematical model. The damping is assumed to be such that the modal vectors are orthogonal with respect to damping.

A method is derived for determination of the exact modal eigenvector of the dominant mode at any forcing frequency by iteration on the damped impedance measurements in matrix form. A similar eigenvalue equation yields the vector in the inverse transpose of the modal matrix; this vector, called the gamma vector, is identified with the dominant mode. The generalized masses, stiffnesses and damping terms are related to the mass, stiffness and damping matrices of the equations of motion through products of the gamma vectors.

Using the gamma vectors, obtained by iteration on test data, the natural frequencies and other modal parameters are determined. Natural frequencies which are not visible in response plots may be determined by this method.

Computer experiments were conducted to test the sensitivity of the theory to errors in input data.

The work performed under this contract is reported in two volumes. This volume contains the theoretical development, application of the theory and computer experiments demonstrating the theory's practicality.

Volume II documents the computer program.

TABLE OF CONTENTS

TABLE OF CONTENTS (Continued)

LIST OF ILLUSTRATIONS

LIST OF ILLUSTRATIONS (Continued)

LIST OF ILLUSTRATIONS (Continued)

LIST OF ILLUSTRATIONS (Continued)

LIST OF ILLUSTRATIONS (Continued)

LIST OF TABLES

LIST OF SYMBOLS

$[c]$	the damping matrix
$[d]$	a damping matrix; $[d] = \omega[c]$; for damping forces which are proportional to displacement
$[d]_i^*$	a damping matrix of unit rank associated with the i-th mode
EI	product of the modulus of elasticity and second moment of area
$\{f\}$	vector of external forces acting along the generalized coordinates
$\{\tilde{f}\}$	force phasor, $\{f\} = \{\tilde{f}\}e^{i\omega t}$
g_i	the structural damping coefficient of the i-th mode
i or j	indices; imaginary operator
κ_i	the generalized stiffness of the i-th mode
$[k]$	the stiffness matrix
$[k]_i^*$	the stiffness matrix of unit rank associated with the i-th mode
m_i	the generalized mass of the i-th mode
$[m]$	the mass matrix
$[m]_i^*$	the mass matrix of unit rank associated with the i-th mode
N or n	the number of degrees of freedom in the structure
$\{\dot{y}\}$	vector of velocities of the generalized coordinates
$\{\tilde{\dot{y}}\}$	velocity phasor, $\{\dot{y}\} = \{\tilde{\dot{y}}\}e^{i\omega t}$
$Y^*_{i(\omega)}$	generalized mobility of the i-th mode at forcing frequency
$[Y_{(\omega)}]$	matrix of mobilities at forcing frequency ω; $[Y_{(\omega)}] = [\partial\tilde{\dot{y}}_i/\partial\tilde{f}_j]_{(\omega)}$

LIST OF SYMBOLS (Continued)

$[z_{(\omega)}]$	matrix of element impedances at forcing frequency ω; $[z_{(\omega)}] = [\partial \tilde{f}_i / \partial \dot{\tilde{y}}_j]_{(\omega)}$
$Z^*_{i(\omega)}$	generalized impedance of the i-th mode at forcing frequency ω
$\overline{Z}^*_{i(\omega)}$	complex conjugate of the i-th mode generalized impedance at forcing frequency ω
$\lvert Z^*_{i(\omega)} \rvert$	absolute value of the i-th mode generalized impedance at forcing frequency ω
α	phase angle between velocity and force
$\{\beta\}_i$	i-th eigenvector of [z]
$\{\gamma\}_i$	the i-th column of $[\Gamma]$; the gamma vector of the i-th mode; a left-hand eigenvector of $[k]^{-1}[m]$
$[\Gamma]$	the left-hand eigenvectors of $[k]^{-1}[m]$; $[\Phi]^{-T}$
δ_i^j	Kronecker's delta
ε	dimensionless error factor
λ_i	the i-th eigenvalue of [z]
$\{\phi\}_i$	the modal vector of the i-th mode
$[\Phi]$	matrix of modal vectors
ω	forcing frequency
Ω_i	the natural frequency of the i-th mode

SUPERSCRIPTS

R	the real part of a complex quantity
I	the imaginary part of a complex quantity

LIST OF SYMBOLS (Continued)

*	a generalized parameter associated with a particular mode
-T	the inverse transpose

SUBSCRIPTS

(ω)	the forcing frequency at which the quantity was measured or calculated
d	dominant mode
h	at frequency high enough to be influenced by all N modes
k	forcing frequency

BLANK PAGE

INTRODUCTION

Because of the severe rotor-induced excitations, helicopter structures and helicopter components must be designed to withstand heavy dynamic loadings. The weight, performance, structural integrity and overall mission effectiveness of a helicopter are affected, in part, by the capability of the design engineer to predict and control the dynamic response of the fuselage and mechanical components.

Although most of the dynamic analysis of a helicopter takes place after the first static test ship is built, the helicopter dynamicist conventionally works with intuitively based equations of motion, or mathematical models as they are often called, and relies on structural dynamic testing for correlation and trial and error improvement purposes.

To obtain the equations of motion, the dynamicist must reduce the physical structure to idealized elements which lend themselves to analytical treatment. This process of abstraction requires skill and judgment and necessarily involves considerable uncertainty. When, after modifying the analysis or changing the assumptions upon which it is based, the analytical predictions of structural response eventually agree with the test results, the dynamicist can use his mathematical model to indicate structural changes which might cure an undesirable dynamic condition.

This report shows that sufficient information can be obtained from impedance-type shake testing of an n-degree-of-freedom helicopter to determine the linear, structurally damped equations of motion directly from the test information, without further idealizing the helicopter structure. The only input information required in this theory is measured mobilities and the approximate frequency of the n-th mode. The modal eigenvectors (mode shapes), "undamped" natural frequencies and damping coefficients can also be determined with this theory using the measured mobilities, as these quantities cannot always be approximated directly from the dynamic responses.

When the equations of motion can be determined from test data in helicopter engineering practice, the dynamicist can avoid most of the uncertainties of present-day analytical prediction of structural dynamics. The interface between analysis and test, which is now largely at the output end of both, will begin to disappear as the abstraction of theoretical analysis and the physical reality of testing

blend more into a single engineering method for defining the helicopter structure and predicting its performance. With the consequent increase in the reliability of dynamic prediction, the end-product helicopter will be produced with less engineering lead time, the user will be justified in placing greater confidence in the integrity of the ship, the effects of desired changes will be more rapidly evaluated, the number of trial and error fixes should be drastically reduced, and the analyst can improve his intuitive creation of mathematical models by one-to-one comparison of his idealized parameters in the equations of motion with those actually determined from the helicopter.

The work reported herein has not eliminated all idealized assumptions: retained are the assumptions that the structure has a finite number of degrees of freedom and that the structure can be described by second-order linear differential equations in which the dissipative term is proportional to amplitude. All assumptions, or prior knowledge, of the magnitude of damping or the magnitudes or distributions of mass and stiffness have been eliminated.

Methods for determining equations of motion from test data, a task referred to as System Identification, must be numerically as well as algebraically manipulatable. Many theoretically sound procedures, such as techniques for reversing the dominance of extreme eigenvalues in matrix iteration, are usually numerically impractical on a useful scale even with a computer. System Identification theories, to be practical in engineering, must be workable with a reasonable degree of experimental error. This is a most stringent requirement. To test the sensitivity to input error of the technique described in this report, a series of computer experiments incorporating experimental errors was carried out.

THEORY

ASSUMPTIONS

It is assumed, for the sake of rigor, either that the structure is describable as an n x n linear mathematical model, which is to say, among other things, that it has as many degrees of freedom as there are measured points of interest on the structure (i.e., the order of the response or "mobility" matrices), or that the modes which are ordinarily above the n-th mode, for n points of interest, have negligible effect on the response of the n-th mode. Violations of this assumption, which is more common than than not, in nature, plague all lumped parameter analyses.

It is also assumed that the mass and stiffness matrices are symmetrical and invariant with frequency. It is expected but not assumed that both are positive definite, that is, that the stiffness matrix can give rise to only a positive potential energy and the mass matrix can yield only a positive kinetic energy unless all motions or displacements are zero. An exception in the case of the stiffness matrix would be for a system with one or more of the six rigid-body degrees of freedom unconstrained, in which instance the stiffness matrix would be neither positive definite nor negative definite. This case is neither excluded nor considered in this report.

The theory is also based on the assumption that the damping, if any, is such that the modal eigenvectors (mode shapes) are orthogonal with respect to the damping. It is not necessary that the damping be small. This assumption regarding damping is both necessary and sufficient for the derivation of all the fundamental principles of this approach. However, for purposes of calculation, we can choose to represent this damping in any of several accepted fashions which do not violate the orthogonality assumption. Beginning with Soroka[1], it has been common for aeroelasticians to represent structural or hysteretic damping as a nondimensional constant multiplying the stiffness divided by the forcing frequency which puts the damping terms in phase with the velocity (essential for energy dissipation and therefore a necessity for all types of damping terms) but proportional to the displacement. Many structural dynamicists, on the other hand, prefer to consider the damping proportional to velocity (viscous damping) but nevertheless defined as a modal property (see Raney)[2]. The derivations presented here use Soroka's representation of structural damping

with the coefficients assigned uniquely to each mode. This choice was made to reflect most closely the current practices in helicopter aeroelastics work.

Other representations which could have been used include a damping coefficient proportional to the generalized mass and a coefficient proportional to any linear combination of the generalized mass and generalized stiffness. Some of these representations might be found to be approximations of Coulomb or "non-orthogonal" viscous damping sufficiently accurate for engineering purposes if and when there is an accumulation of experience in the identification of mathematical model lumped parameters of helicopters or other structures.

It is not assumed that the modes are necessarily all separated so that their existence could be determined from a visual examination of any or all driving-point or transfer plots; in other words, the procedure can reveal modes which are completely masked. This follows from the condition, discussed in the derivation, that the dominant eigenvalue must be greater than (not necessarily greater than the sum of all) the eigenvalues of the other modes.

DERIVATION

Derivation of the Modal Expressions for Mobility

The equations of motion of a linear system are

$$[m]\{\ddot{y}\} + [c]\{\dot{y}\} + [k]\{y\} = \{f\} \qquad (1)$$

Assume a steady-state solution of the form

$$\{\dot{y}\} = \{\tilde{\dot{y}}\}e^{i\omega t} \text{ and } \{f\} = \{\tilde{f}\}e^{i\omega t}$$

to give

$$\left[j([m]\omega - \frac{1}{\omega}[k]) + [c]\right]\{\tilde{\dot{y}}\} = \{\tilde{f}\} \text{ or } (j[z^{I}_{(\omega)}] + [z^{R}_{(\omega)}])\{\tilde{\dot{y}}\}$$

$$\equiv [z_{(\omega)}]\{\tilde{\dot{y}}\} = \{\tilde{f}\} \qquad (2)$$

$z_{ij(\omega)}$ is called the Element Impedance (measured at ω) in this work, and it is seen from the above equation that

$$z_{ij} = \partial \tilde{f}_i / \partial \tilde{\dot{y}}_j$$

Premultiply Equation (2) by $[\Phi]^{-T}[\Phi]^{T}$ and postmultiply by $[\Phi][\Phi]^{-1}$ where $[\Phi]$ is the matrix of modal vectors. Then

$$[\Phi]^{-T}\left[j\left([\Phi]^{T}[m][\Phi]\omega - \frac{1}{\omega}[\Phi]^{T}[k][\Phi]\right) + [\Phi]^{T}[c][\Phi]\right][\Phi]^{-1} = [z] \tag{3}$$

The diagonal generalized mass matrix is given by

$$\left[\eta\right] = [\Phi]^{T}[m][\Phi] \tag{4}$$

and the diagonal generalized stiffness matrix by

$$\left[\kappa\right] = [\Phi]^{T}[k][\Phi] \tag{5}$$

Assume that

$$[\Phi]^{T}[c][\Phi] = \frac{1}{\omega}\left[g\kappa\right] \tag{6}$$

such as would be expected from structural damping in a lightly damped structure. Equation (3) now becomes

$$[z_{(\omega)}] = [\Phi]^{-T}\left[j(\eta\omega - \frac{1}{\omega}\kappa) + \frac{g\kappa}{\omega}\right][\Phi]^{-1} \tag{7}$$

Define the i-th modal impedance as

$$Z^{*}_{i(\omega)} = j(\eta_i\omega - \frac{1}{\omega}\kappa_i) + \frac{g_i\kappa_i}{\omega},$$

and substitute into Equation (3) to give

$$[z_{(\omega)}] = [\Phi]^{-T}\left[Z^{*}_{(\omega)}\right][\Phi]^{-1} \tag{8}$$

The mobility is defined by $Y_{ij} \equiv \partial\dot{\tilde{y}}_i/\partial\tilde{f}_j$ and is equal to the ratio of the velocity phasor along the coordinate i to the external force phasor along the coordinate j when no other forces are externally applied.

$$[Y] = [\partial\tilde{\dot{y}}/\partial\tilde{f}] = [\partial\tilde{f}/\partial\tilde{\dot{y}}]^{-1} \equiv [z]^{-1} \tag{9}$$

Therefore, from Equation (8) it is seen that

$$[Y_{(\omega)}] = [\Phi]\left[\frac{1}{Z^{*}_{(\omega)}}\right][\Phi]^{T} \equiv [\Phi]\left[Y^{*}_{(\omega)}\right][\Phi]^{T} \tag{10}$$

The modal mobility of the i-th mode measured at ω is

$$Y^{*}_{i(\omega)} = Y^{*R}_{i(\omega)} + jY^{*}_{i(\omega)} = \frac{1}{Z^{*}_{i(\omega)}} = \frac{\bar{Z}^{*}_{i(\omega)}}{(Z^{*}_{i(\omega)})^{2}}$$

$$= \frac{Z^{*R}_{i(\omega)} - iZ^{*I}_{i(\omega)}}{(Z^{*R}_{i(\omega)})^{2} + (Z^{*I}_{i(\omega)})^{2}} = \frac{\frac{g_i\kappa_i}{\omega} - j(\eta_i\omega - \frac{\kappa_i}{\omega})}{(\frac{g_i\kappa_i}{\omega})^{2} + (\eta_i\omega - \frac{\kappa_i}{\omega})^{2}}$$

$$= \frac{1}{\omega\eta_i}\left(\frac{\omega^2}{\Omega_i^2}\right)\frac{g_i}{g_i^2 + \left(\frac{\omega^2}{\Omega_i^2} - 1\right)^2} - \frac{j}{\omega\eta_i}\left(\frac{\omega^2}{\Omega_i^2}\right)\frac{\left(\frac{\omega^2}{\Omega_i^2} - 1\right)}{g_i^2 + \left(\frac{\omega^2}{\Omega_i^2} - 1\right)^2} \tag{11}$$

Figures 1 and 2 illustrate the influence of the i-th mode on the real and imaginary mobilities measured at ω. It is seen that the magnitude of the real modal mobility drops sharply as the forcing frequency gets further from resonance: three orders of magnitude in less than two octaves for $g = .10$. From Equation (10), we write the real mobility,

$$[Y^{R}_{(\omega)}] = [\Phi]\left[Y^{*R}_{(\omega)}\right][\Phi]^{T} \tag{12}$$

and we note that because the real modal mobilities of modes far removed from the forcing frequency become negligible, compared to nearby modes, the real mobility matrix at any frequency is usually significantly affected only by modes in the vicinity of the forcing frequency. Looking at this

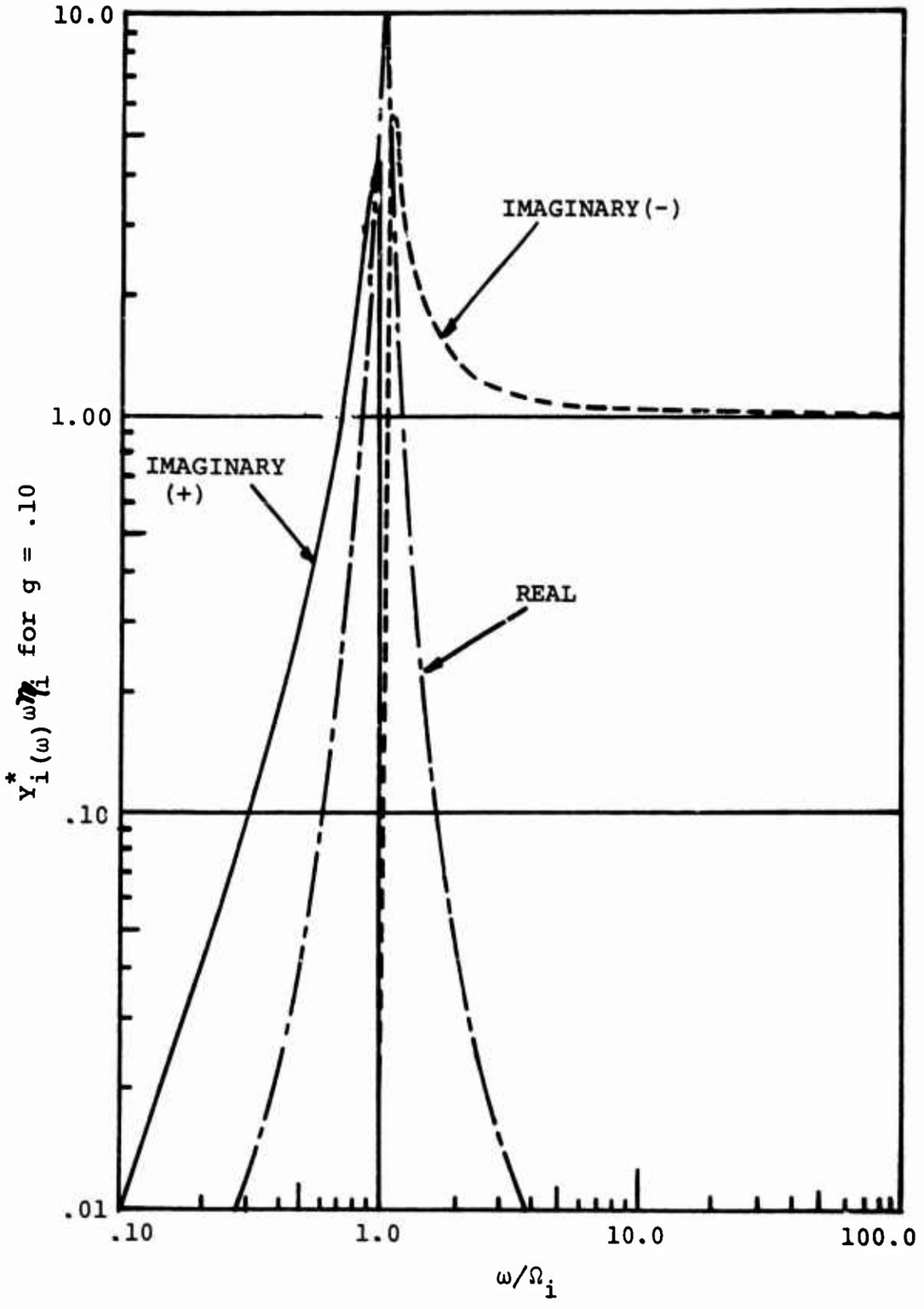

Figure 1. Dimensionless Plot Showing the Influence of the i-th Mode on the Mobility at ω for g = .10.

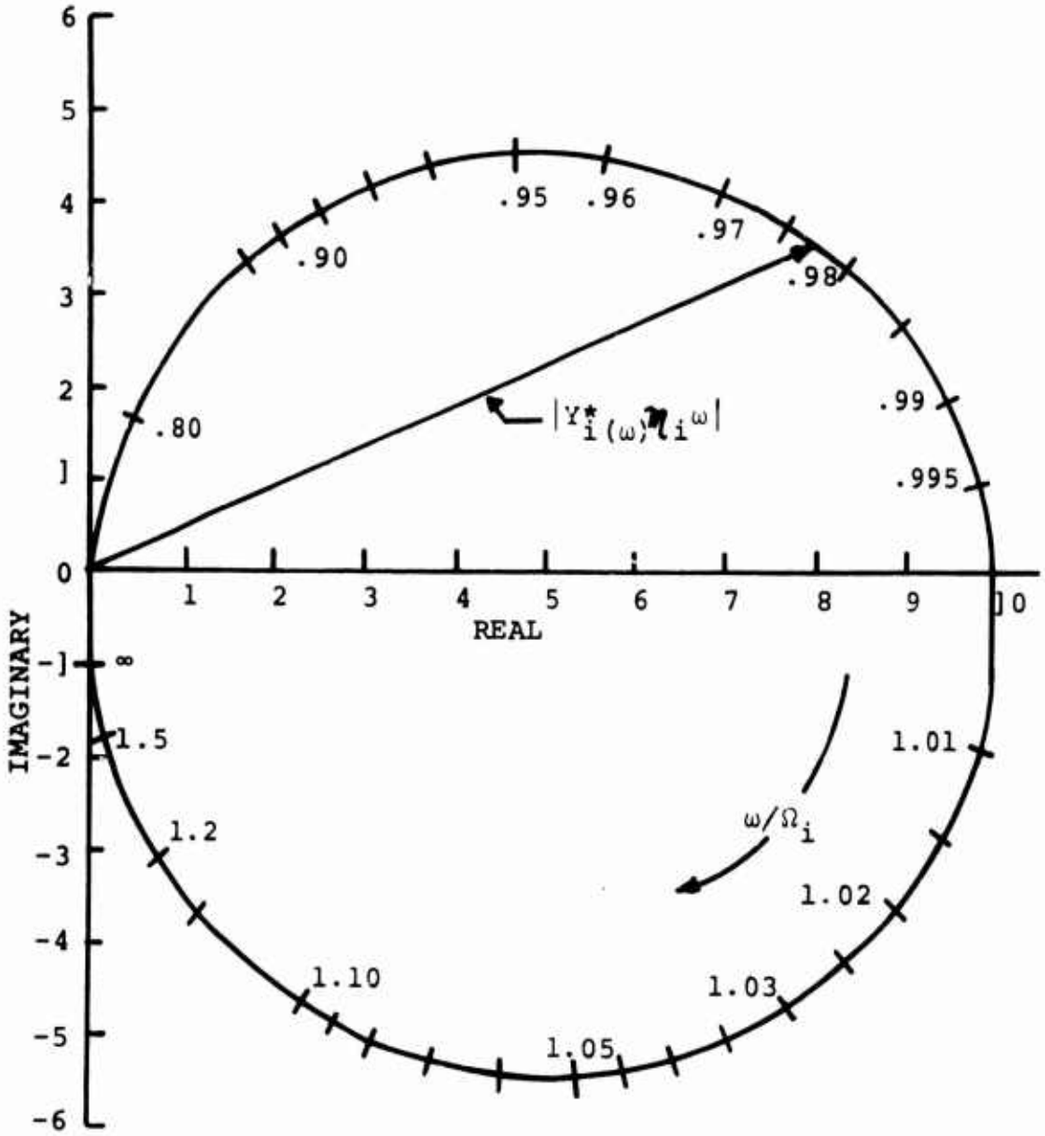

Figure 2. Dimensionless Plot Showing the Influence of the i-th Mode on the Mobility at ω for g = .10.

another way, any measured real mobility matrix reflects the influence of only the most dominant modes in that frequency-of-measurement region. Therefore, it is numerically impractical to use the real mobility matrix measured at only one frequency to determine parameters other than those associated with neighboring modes.

Figure 1 shows that the effect of the i-th mode on imaginary mobility measurements far below Ω_i is negligible. However, the effect on imaginary mobility matrices asymptotically approaches a constant with increasing frequency above Ω_i. An imaginary mobility matrix contains the effect of all lower modes in proportion to, or greater than, the magnitudes of their generalized masses. Therefore, it is numerically impractical to use imaginary mobility matrices to determine properties associated with natural frequencies far above the forcing frequency.

Were it not for these characteristics of the modal mobility, it would be possible to determine the system parameters from the n equations in n unknowns obtained from mobility matrices measured at any two forcing frequencies. However, the precision of measurement which would be required to do this for most systems (say, six or seven significant figures for a decade frequency range) is impossible to achieve. The mode-by-mode approach derived below avoids this problem.

Derivation of the Dominant Mode Eigenvalue Problem

Equation (10) may be written

$$[Y_{(\omega)}] = [\Phi]\left[Y^*_{(\omega)}\right][\Phi]^T = \sum_{i=1}^{N} Y^*_{i(\omega)}\{\phi\}_i\{\phi\}_i^T \qquad (13)$$

where $\{\phi\}$ is a column in $[\Phi]$ and N is the order of the matrices. Define $[\Gamma] \equiv [\Phi]^{-T}$ and write Equation (8) as

$$[Y_{(\omega)}]^{-1} = [z_{(\omega)}] = [\Gamma]\left[\frac{1}{Y^*_{(\omega)}}\right][\Gamma]^T = \sum_{i=1}^{N} \frac{1}{Y^*_{i(\omega)}}\{\gamma\}_i\{\gamma\}_i^T \qquad (14)$$

where $\{\gamma\}$ is a column in $[\Gamma]$. Note that $\{\gamma\}_i^T\{\phi\}_j = \delta_i^j$ by definition of the inverse.

Similarly,

$$[Y^R_{(\omega)}] = \sum_{i=1}^{N} Y^{*R}_{i(\omega)} \{\phi\}_i \{\phi\}_i^T$$

$$[Y^I_{(\omega)}] = \sum_{i=1}^{N} Y^{*I}_{i(\omega)} \{\phi\}_j \{\phi\}_i^T$$

$$[Y^R_{(\omega)}]^{-1} = \sum_{i=1}^{N} \frac{1}{Y^{*R}_{i(\omega)}} \{\gamma\}_i \{\gamma\}_i^T$$

$$[Y^I_{(\omega)}]^{-1} = \sum_{i=1}^{N} \frac{1}{Y^{*I}_{i(\omega)}} \{\gamma\}_i \{\gamma\}_i^T \qquad (15)$$

Each matrix $Y^*_{i(\omega)} \{\phi\}_i \{\phi\}_i^T$ and $\frac{1}{Y^*_{i(\omega)}} \{\gamma\}_i \{\gamma\}_i^T$ in Equations (13) and (14) is of rank one, but the summation of as many of these successive modal matrices as the order N of the matrix is a nonsingular matrix.

Consider an imaginary mobility matrix measured at a frequency ω_h which is high enough to be significantly influenced by all N modes; ω_h would usually be in the vicinity of or above the N-th mode. Take the inverse of this matrix and postmultiply by a real mobility matrix measured at any frequency ω_k:

$$[Y^I_{(\omega_h)}]^{-1} [Y^R_{(\omega_k)}] = \sum_{i=k}^{N} \frac{Y^{*R}_{i(\omega_k)}}{Y^{*I}_{i(\omega_h)}} \{\gamma\}_i \{\phi\}_i^T \qquad (16)$$

It is seen that because $\{\phi\}_i^T \{\gamma\}_j = \delta_i^j$, Equation (16) becomes the eigenvalue problem

$$[Y^I_{(\omega_h)}]^{-1} [Y^R_{(\omega_k)}] \{\gamma\}_i = \frac{Y^{*R}_{i(\omega_k)}}{Y^{*I}_{i(\omega_h)}} \{\gamma\}_i \qquad (17)$$

Among the quotients $Y^{*R}_{i(\omega_k)}/Y^{*I}_{i(\omega_h)}$ there will be one quotient, say $Y^{*R}_{d(\omega_k)}/Y^{*I}_{d(\omega_h)}$, which is greater than any other: this is the dominant mode. If Equation (17) is multiplied by an arbitrary vector $\{\chi\} = \sum_{i=1}^{N} a_i\{\gamma\}_i$ and the multiplication is iterated in the conventional manner, the process will converge on the eigenvector and eigenvalue of the dominant mode. The eigenvalue $Y^{*R}_{d(\omega_k)}/Y^{*I}_{d(\omega_h)}$ is not presently used in this theory. The eigenvector is the gamma vector of the dominant mode, $\{\gamma\}_d$. Usually, the dominant mode natural frequency will be the nearest natural frequency to the forcing frequency ω_k.

If the dominant mode is removed from Equation (17), then the iterations will converge on the next most dominant mode. Removing the dominant mode from the real and imaginary matrices of Equation (16), we write

$$\left([Y^{I}_{(\omega_h)}]^{-1} - \frac{1}{Y^{*I}_{d(\omega_h)}}\{\gamma\}_d\{\gamma\}^T_d\right)\left([Y^{R}_{(\omega_k)}] - Y^{*R}_{d(\omega_k)}\{\phi\}_d\{\phi\}^T_d\right)$$

$$= [Y^{I}_{(\omega_h)}]^{-1}[Y^{R}_{(\omega_k)}] - Y^{*R}_{d(\omega_k)}[Y^{I}_{(\omega_h)}]^{-1}\{\phi\}_d\{\phi\}^T_d$$

$$- \frac{1}{Y^{*I}_{d(\omega_h)}}\{\gamma\}_d\{\gamma\}^T_d[Y^{R}_{(\omega_k)}] + \frac{Y^{*R}_{d(\omega_k)}}{Y^{*I}_{d(\omega_h)}}\{\gamma\}_d\{\gamma\}^T_d = [Y^{I}_{(\omega_h)}]^{-1}[Y^{R}_{(\omega_k)}]$$

$$- \frac{Y^{*R}_{d(\omega_k)}}{Y^{*I}_{d(\omega_h)}}\{\gamma\}_d\{\phi\}^T_d - \frac{1}{Y^{*I}_{d(\omega_h)}}\{\gamma\}_d\{\gamma\}^T_d[Y^{R}_{(\omega_k)}] + \frac{Y^{*R}_{d(\omega_k)}}{Y^{*I}_{d(\omega_h)}}\{\gamma\}_d\{\gamma\}^T_d$$

$$= \left([Y^{I}_{(\omega_h)}]^{-1} - \frac{1}{Y^{*I}_{d(\omega_h)}}\{\gamma\}_d\{\gamma\}^T_d\right)[Y^{R}_{(\omega_k)}] \qquad (18)$$

But

$$Y^{*I}_{d(\omega_h)} = \{\gamma\}^T_d [Y^I_{(\omega_h)}] \{\gamma\}_d \tag{19}$$

as can be seen from Equation (13). Therefore,

$$\left([Y^I_{(\omega_h)}]^{-1} - \frac{1}{\{\gamma\}^T_d [Y^I_{(\omega_h)}] \{\gamma\}_d} \{\gamma\}_d \{\gamma\}^T_d\right) [Y^R_{(\omega_k)}] \{\gamma\}_{d\pm1}$$

$$= \frac{Y^{*R}_{d\pm1(\omega_k)}}{Y^{*I}_{d\pm1(\omega_h)}} \{\gamma\}_{d\pm1} \tag{20}$$

where the subscript d±1 designates the second most dominant mode in the segment of the frequency spectrum defined by the eigenvalue.

The transpose of Equation (16) is an eigenvalue problem, the eigenvector of which is the modal vector $\{\phi\}_d$. The eigenvalue of Equation (16) is identical to the eigenvalue of its transpose. The modal vector $\{\phi\}_d$ is obtained upon convergence after iterating using the transpose of Equation (16).

Determination of Modal Parameters

It follows from Equation (13) that the modal mobilities are given by

$$\left[Y^*_{(\omega)}\right] = [\Gamma]^T [Y_{(\omega)}] [\Gamma] \tag{21}$$

and, therefore, the orthogonality condition for gamma vectors is

$$\{\gamma\}^T_i [Y_{(\omega)}] \{\gamma\}_j = Y^*_{i(\omega)} \delta^j_i$$

The modal impedance of the i-th mode at ω_j is

$$Z^*_{i(\omega_j)} = \frac{\bar{Y}^*_{i(\omega_j)}}{|Y^*_{i(\omega_j)}|^2} = \frac{g_i \kappa_i}{\omega_j} + j(\eta_i \omega_j - \frac{1}{\omega_j}\kappa_i)$$

It follows that

$$Z^{*I}_{i(\omega_j)} = \frac{-Y^{*I}_{i(\omega_j)}}{|Y^*_{i(\omega_j)}|^2} = \frac{\{\gamma\}_i^T \left[Y^I_{i(\omega_j)}\right] \{\gamma\}_i}{(\{\gamma\}_i^T [Y^R_{i(\omega_j)}] \{\gamma\}_i)^2 + (\{\gamma\}_i^T [Y^I_{i(\omega_j)}] \{\gamma\}_i)^2}$$

and

$$Z^{*R}_{i(\omega_j)} = \frac{Y^{*R}_{i(\omega_j)}}{|Y^*_{i(\omega_j)}|^2} = \frac{\{\gamma\}_i^T \left[Y^R_{i(\omega_j)}\right] \{\gamma\}_i}{(\{\gamma\}_i^T [Y^R_{i(\omega_j)}] \{\gamma\}_i)^2 + (\{\gamma\}_i^T [Y^I_{i(\omega_j)}] \{\gamma\}_i)^2} \qquad (22)$$

Then

$$\omega_h Z^{*I}_{i(\omega_h)} - \omega_j Z^{*I}_{i(\omega_j)} = \eta_i (\omega_h^2 - \omega_j^2) \qquad (23)$$

and

$$\omega_j^2 \omega_h Z^{*I}_{i(\omega_h)} - \omega_h^2 \omega_j Z^{*I}_{i(\omega_j)} = \kappa_i (\omega_h^2 - \omega_j^2) \qquad (24)$$

Dividing Equation (24) by (23), we obtain the natural frequency of the i-th mode:

$$\Omega_i^2 = \frac{\kappa_i}{\eta_i} = \omega_j \omega_h \frac{\omega_j Z^{*I}_{i(\omega_h)} - \omega_h Z^{*I}_{i(\omega_j)}}{\omega_h Z^{*I}_{i(\omega_h)} - \omega_j Z^{*}_{i(\omega_j)}} \qquad (25)$$

From Equation (23), we find the generalized mass of the i-th mode:

$$\mathcal{M}_i = \frac{\omega_h Z^{*I}_{i(\omega_h)} - \omega_j Z^{*I}_{i(\omega j)}}{\omega_h^2 - \omega_j^2} \tag{26}$$

The generalized stiffness is found from Equation (24) or by

$$\mathcal{K}_i = \Omega_i^2 \mathcal{M}_i \tag{27}$$

The damping coefficient for the i-th mode is most readily given by

$$g_i = \frac{\omega_j Z^{*R}_{i(\omega_j)}}{\mathcal{K}_i} \tag{28}$$

which follows directly from Equation (7), and may also be obtained by

$$g_i = \left(\frac{\omega_j^2}{\Omega_i^2} - 1\right) \frac{Z^{*R}_{i(\omega_i)}}{Z^{*I}_{i(\omega_j)}} \tag{29}$$

Using a measurement of real mobility taken precisely at resonance, we may calculate the damping coefficient from

$$g_i = \frac{1}{Y^{*R}_{i(\Omega_i)} \Omega_i \mathcal{M}_i} \tag{30}$$

This follows from Equation (11).

Parameters of the Mathematical Model

Premultiply Equation (4) by $[\Gamma]$ and postmultiply by $[\Gamma]^T$ to obtain

$$[m] = \sum_{i=1}^{N} \mathcal{M}_i \{\gamma\}_i \{\gamma\}_i^T \equiv \sum_{i=1}^{N} [m]^*_i \tag{31}$$

In similar fashion,

$$[k] = \sum_{i=1}^{N} \kappa_i \{\gamma\}_i \{\gamma\}_i^T \equiv \sum_{i=1}^{N} [k]_i^* \tag{32}$$

Set $\frac{1}{\omega}[d] = [c]$ and note from Equation (6) that

$$[d] = \sum_{i=1}^{N} g_i \kappa_i \{\gamma\}_i \{\gamma\}_i^T \equiv \sum_{i=1}^{N} [d]_i^* \tag{33}$$

METHOD OF APPLYING THE THEORY

SUSPENDING THE AIRCRAFT

It is immaterial at this point in the research how the aircraft is suspended except that it is important, of course, that the manner of support does not cause the aircraft to dynamically couple with other structures such as that of the hangar, the floor, or the ground. If a relatively stiff suspension like the landing gear is used, then the ship should be parked on a pad of sufficiently high impedance that, for the frequency range tested, it may be considered infinite; then the landing gear component impedance terminates at ground.

Soft suspension may, of course, be used to simulate the aircraft in free flight, and this is the common procedure. However, as shown previously in the derivation, the imaginary mobility at every frequency is affected by the modes of all lower natural frequencies, no matter how low. It follows that the conventional criterion for free flight simulation (that the suspension natural frequency must be very low compared to the lowest flexural natural frequency) is a necessary condition but not a sufficient condition for free flight dynamic simulation in any dynamic test. No further consideration is given to this question in this report.

TEST SETUP

Choosing the Points

The dynamicist selects n "points of interest" on the structure. These correspond to the points he would use in a conventional analysis and include the points at which the major forces of flight would be applied and the points at which response is of greatest consequence to the mission of the aircraft. For example, the hub and the pilot's seat of a helicopter would certainly be among the points of interest.

A motion transducer (e.g., accelerometer) is placed at each of the n points of interest and is oriented in the direction of motion for which the equations are to be written. A unidirectional exciter is placed at one of these points of interest and is oriented so that the line of action of the impressed force coincides with the principal direction of the transducer at that point. The shaker provides the only

external force excitation (restraint reaction forces are not considered excitation), and only one shaker is used.

The aircraft is excited over a frequency spectrum encompassing as many modes as there are points of interest. The time rate-of-change of frequency should be slow enough in the frequency bands of interest so that the dynamic response is essentially in a steady state. The force and the motion of the n selected points are recorded.

The test is repeated for force excitation at each of the n points of interest, forcing at only one point each time.

Recording the Data

Although it would be possible to completely automate the procedure from the taking of test data through identification in the computer, a large amount of equipment and data storage would be required. Fortunately, by including a few manual steps, the procedure can be carried out with a minimum of present state-of-the-art measurement equipment and data storage devices.

The first step is to run a complete frequency sweep of the structure, with the shaker at only one position, and record or observe the responses at each of the n instrumented points. By noting the changes in the phase meter reading versus frequency or plotting the quadrature readings for several of the n responses in the manner of Kennedy and Pancu[3], the engineer can determine the approximate natural frequencies of the first n modes.

He then takes measurements of n responses and the force in a relatively narrow frequency bandwidth around each natural frequency and at a high frequency ω_h which is above or slightly below the n-th mode. The shaker is moved to another of the n points and a similar set of measurements is recorded. This process is repeated until the structure has been excited at each of the n points of interest. The data obtained are digitized and put in the form of a real and an imaginary mobility matrix for each selected frequency.

It is not necessary to digitize and store all the information at once. The only two mobility matrices that must be stored in the computer throughout the identification process are the real and imaginary n x n mobility matrices for ω_h. All other data can be digitized, put into matrix form, and provided on demand for computation after which they can be discarded.

THE IDENTIFICATION PROCESS

Figure 3 illustrates the logic steps in the identification process (it is not a flow chart for a computer program). The first step is to obtain the imaginary mobility matrix at the high frequency ω_h. Then take the real and imaginary mobility matrices at any frequency and iterate, using Equation (17), to obtain the gamma vector of the dominant mode at the chosen frequency. From Equations (22) and (25), an estimate of the identified natural frequency Ω_i of the dominant mode is determined.

If the identified natural frequency Ω_i is acceptably close, in terms of a chosen criterion, to the forcing frequency at which the mobilities were measured, then the modal parameters are calculated and stored. If the forcing frequency is not acceptably close to the identified natural frequency, then the mobilities at another frequency in that range are taken and the calculation repeated. The forcing frequency may be considered acceptably close to the natural frequency when the calculations at several successive frequencies yield the same identified natural frequency and gamma vector within very small percentage deviations. "Acceptably close", as will be shown later in this report, might be 20 percent above or below the natural frequency depending on the accuracy desired and the number of frequencies at which measurements were taken. However, with modern recording equipment, there is little excuse for not having measurements within a cycle or two of the natural frequency, particularly as the sweep can be nearly continuous along a band containing the natural frequency.

When the modal parameters of the dominant mode in the chosen frequency bandwidth are calculated, the calculations move on to the next measured bandwidth and so on until n modes have been covered.

Although the choice of the first bandwidth to be considered and the choice of the first forcing frequency within that bandwidth are completely arbitrary in the theory, it would be logically simplest to begin with the lowest measured frequency in the lowest bandwidth and progress successively upward in frequency.

When all n modal mass matrices, damping matrices, and stiffness matrices are calculated, they are summed according to Equations (31), (32), and (33) to give the coefficients in the equations of motion.

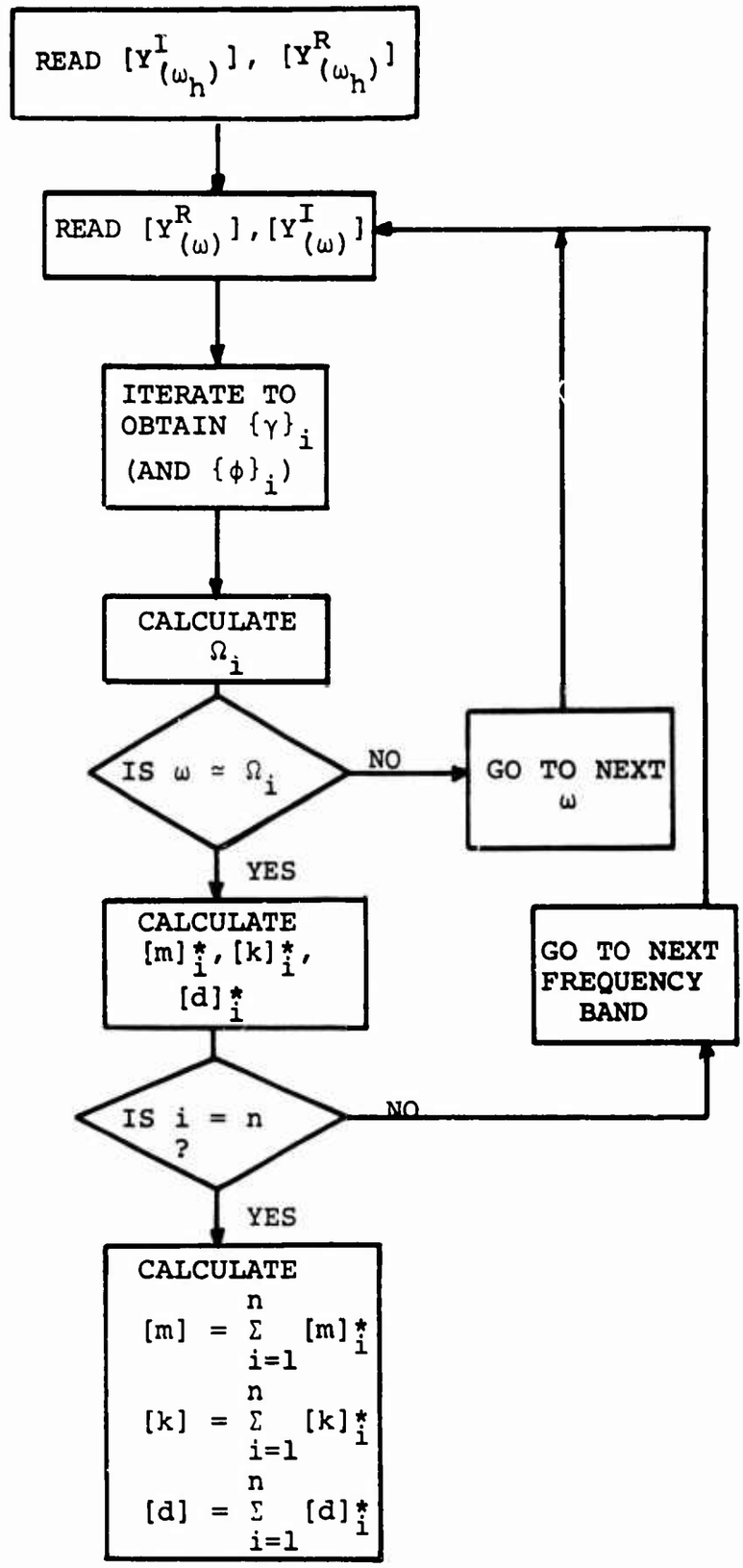

Figure 3. Chart of Identification Procedure.

TESTS OF THE THEORY

COMPUTER EXPERIMENTS

Advantages and Disadvantages

A series of computer experiments was designed to test the practicality of this theory, within the limitations of the assumptions, both in terms of the numerical operation on a computer and in terms of unavoidable experimental error in measuring mobility. The computer experiments offer very significant advantages over laboratory experiments at this stage of research. Computer experiments allow use of a control model for which the exact answers are known, thereby making it possible to evaluate the accuracy of the identified parameters. The computer experiments can be conducted with complete knowledge of the types and magnitudes of input errors, something which would not be known in a laboratory test. Because the computer experiments can be run at very low cost and at very high speed, more information per dollar can be determined and the experiments can use a more complicated type of structure than would be practical in laboratory experiments designed to test the theory.

The major disadvantages to computer experiments are that they must be based on certain analytical assumptions and that they cannot, of course, simulate the degree of reality that physical experiments reflect. Computer experiments cannot prove that an engineering theory is practical but they can prove that it is impractical, should that be the case, in a most efficient and informative manner.

Simulated Test Data

A 9000-pound-gross-weight helicopter stiffly suspended at its main landing gear and tail gear was used as the analytical test model. The EI and mass parameters shown in Table I are based on the parameters of the Kaman UH-2 single-rotor utility helicopter, which is structurally typical of helicopters of its class.

The relatively stiff supports at the landing gear stations simulate a jack-type suspension resting on concrete pads which have essentially infinite ground impedance over the frequency range tested. When identification has been completed, the jack stiffnesses can be subtracted directly from the stiffness matrix to give the stiffness matrix of the free body. This can be accomplished by replacing the

diagonal term at the support locations by minus one times the sum of the off-diagonal terms in the row or column. The chosen stations, or points of interest, were selected to include the pilot's seat, main rotor hub station, main and tail gear, tail rotor and significant mass concentrations on the helicopter.

The helicopter was represented as an elastically continuous Bernoulli-Euler beam in transverse bending with 1/EI varying linearly between the stations listed in Table I and with up to 5 percent structural damping. The masses were concentrated as shown in Table I. The mobilities of this beam were calculated over the frequency spectrum and statistically polluted with errors to simulate test measurements.

TABLE I. MASS AND STIFFNESS PARAMETERS OF BEAM REPRESENTATION OF HELICOPTER

Station (in.)	Stiffness EI ($lb\text{-}in.^2 \times 10^7$)	Masses (lb)	Spring Rate to Ground (lb/in.)
0	350	11.2	-
60	350	2840.0	-
140	3000	2530.0	10,000
180	5700	2000.0	-
220	5600	1205.0	-
260	3600	203.0	-
300	2600	65.6	-
340	1600	46.0	-
400	650	92.0	10,000
460	500	115.0	-

ERRORS USED

Types

Measurements of the complex mobilities will be subject to experimental errors of various types such as errors in calibration, errors due to the capacitive reactance of loads, errors resulting from mismatching of equipment, errors due to extraneous signals, and errors due to random noise. Some errors will depend on such variable environmental conditions as temperature and humidity.

In general, all errors can be divided into two classes: "random" or "accidental" errors which, in a large number of replicated measurements, are likely to be negative as often as positive; and "systematic" or "bias" errors which bias the arithmetic mean of many measurements. Both types of measurement errors have been incorporated in this study.

There is no definitive probability distribution for errors of each type in impedance testing practice. Private discussions with several authorities in the fields of impedance testing yielded estimates of maximum accidental error ranging from plus or minus a few percent to plus or minus 10 percent. Estimates of maximum accidental phase angle error were vaguely stated either as plus or minus a few degrees or plus or minus 1 degree. Proper test conditions were assumed.

It would have been reasonable to have assumed the accidental measurement errors to be distributed according to the Gauss-Laplace law but, to simplify the calculations, the authors distributed the accidental error in a purely random manner using a random number computer subroutine. The resulting rectangular distribution of accidental error between the selected limits is very conservative compared to the customary definition of the limits at three standard deviations from the mean of a Gaussian curve.

Magnitudes

Using the very limited information available, the authors selected an 8 percent bias error on the absolute value of the amplitude/force ratio as reasonably representative of the bias error that could be expected in an impedance test

on a helicopter. An accidental error of plus or minus 8 percent on the absolute value of the amplitude/force ratio distributed randomly was considered to be a conservative representation of the accuracy attainable. An accidental error in phase measurement randomly distributed between plus and minus 2 degrees was judged to be within the present state of the art.

No bias error on phase angle was used because analysis showed that phase bias has a negligible effect in the operation of this theory.

In the course of the study, computer experiments were run on the developed impedance theory using errors ranging from plus or minus 2 percent to 10 percent randomly distributed on amplitude/force, bias errors from 2 percent to 10 percent on amplitude/force, and randomly distributed phase errors from plus or minus 1 degree to plus or minus 5 degrees.

Bias Phase Error

A real driving point mobility measured at a frequency ω_h greater than the n-th natural frequency may be expressed as

$$Y^R_{kk\omega_h} \simeq \frac{g}{\omega_h}\left\{\sum_{i=1}^{n-1}\frac{\Omega_i^2}{\eta_i\omega_h^2}\phi_{ki}^2 + \frac{1}{\eta_n}\left(\frac{\omega_h^2}{\Omega_n^2}\right)\frac{\phi_{kn}^2}{g^2+\left(\frac{\omega_h^2}{\Omega_n^2}-1\right)^2}\right\} \qquad (34)$$

and the imaginary driving point mobility as

$$Y^I_{kk\omega_h} \simeq \frac{-1}{\omega_h}\left\{\sum_{i=1}^{n-1}\frac{\phi_{ki}^2}{\eta_i} + \frac{1}{\eta_n}\left(\frac{\omega_h^2}{\Omega_n^2}\right)\frac{\frac{\omega_h^2}{\Omega_n^2}-1}{g^2+\left(\frac{\omega_h^2}{\Omega_n^2}-1\right)^2}\right\} \qquad (35)$$

It is seen that each of the first n-1 terms in Equation (34) is less than each corresponding term in Equation (35) by one or more orders of magnitude for values of g equal to or less than 10 percent. Unless ω_h is within only a few percent of the n-th natural frequency, the last term in Equation (35) will be larger than the last term in Equation (34). Therefore, we can expect the real driving point mobilities at ω_h

to be substantially smaller than the imaginary driving point mobilities. In general, this relationship will hold true for the off-diagonal terms also.

If the phase angle α is in error by a constant small amount ε, the measured imaginary mobility at high frequency can be expressed as

$$Y^I_{kl\omega_h \text{ measured}} = |Y|_{kl\omega_h} \sin(\alpha + \varepsilon) \simeq Y^I_{kl\omega_h} + \varepsilon Y^R_{kl\omega_h} \quad (36)$$

But $Y^R_{kl\omega_h}$ is small compared to $Y^I_{kl\omega_h}$, and ε is a small number in the neighborhood of .05 radian. The difference between the exact imaginary mobility at high frequency and that calculated with a small phase angle error is the product of two small numbers. Thus, we can conclude that high frequency imaginary mobility is negligibly affected by phase error.

However, a bias phase angle error can have a very significant effect on the magnitude of the real mobility elements. The kl-th measured real mobility is given by

$$Y^R_{kl\omega \text{ measured}} = |Y|_{kl\omega} \cos(\alpha + \varepsilon) \simeq Y^R_{kl\omega} - \varepsilon Y^I_{kl\omega} \quad (37)$$

Because ε is a bias phase error which is the same for every element, Equation (37) can be written in matrix form as

$$[Y^R_\omega]_{\text{measured}} = [Y^R_\omega] - \varepsilon [Y^I_\omega] \quad (38)$$

Premultiplying Equation (38) by the inverse of the imaginary mobility matrix measured at high frequency, ω_h gives the following expression for the eigenvalue problem of interest:

$$[Y^I_{\omega_h}]^{-1}[Y^R_\omega]_{\text{measured}} = [Y^I_{\omega_h}]^{-1}[Y^R_\omega] - \varepsilon [Y^I_{\omega_h}]^{-1}[Y^I_\omega] \quad (39)$$

But the eigenvectors of the first term and the eigenvectors of the second term are identically gamma. The eigenvalues of Equation (39) are not used in the theory, and the eigenvectors are the same whether or not the bias phase error ε

is zero. Bias phase error has therefore not been included in the computer experiments.

THE GAMMA VECTOR

As shown in Figure 3, the gamma vector is calculated by iteration using Equation (17) at each frequency of measurement ω_k. Figure 4 shows the manner in which the elements of the gamma vector vary versus frequency when calculated from input mobility data having 8 percent bias error and $\pm$8 percent random error on absolute amplitude and $\pm 2°$ random phase angle error. The frequency range covered in Figure 4, 1 to 30 cps, shows a performance that is typical throughout the entire range from 1 to 1400 cps. Three of the ten stations were eliminated from the plot of Figure 4 for purposes of clarity.

We notice in Figure 4 that the elements of the gamma vector become very nearly equal to the exact elements of the gamma vector of the dominant mode in the vicinity of a natural frequency. Only in those frequency bands where the degree of dominance of any one mode is eclipsed by the error range of the data do the magnitudes of the gamma vector elements fluctuate wildly. As can be seen in Figure 4, these bands are narrowly confined: e.g., 4 to 6 cps, 13 to 16 cps.

Figure 4 does not clearly show how close to the exact gamma vector the calculated gamma vector becomes at a forcing frequency near the natural frequency. Therefore, Figures 5 through 14 show comparisons of the exact gamma vector of each mode to the gamma vector calculated at the nearest forcing frequency to the natural frequency. The input mobility data is from a randomly selected case having the error ranges mentioned above.

In Figures 4 through 14, the gamma vectors are normalized on the largest element. It is evident from the derivation that the manner of normalization of the gamma vector is entirely arbitrary in this theory.

NATURAL FREQUENCIES

For each gamma vector that is obtained, the natural frequency of the dominant mode is calculated using Equation (25). Figures 15 through 17 show the exact natural frequencies as lines parallel to the ordinate lines and parallel to the abscissa. The calculated values of natural frequency cluster closely about the true value except in narrow bands between

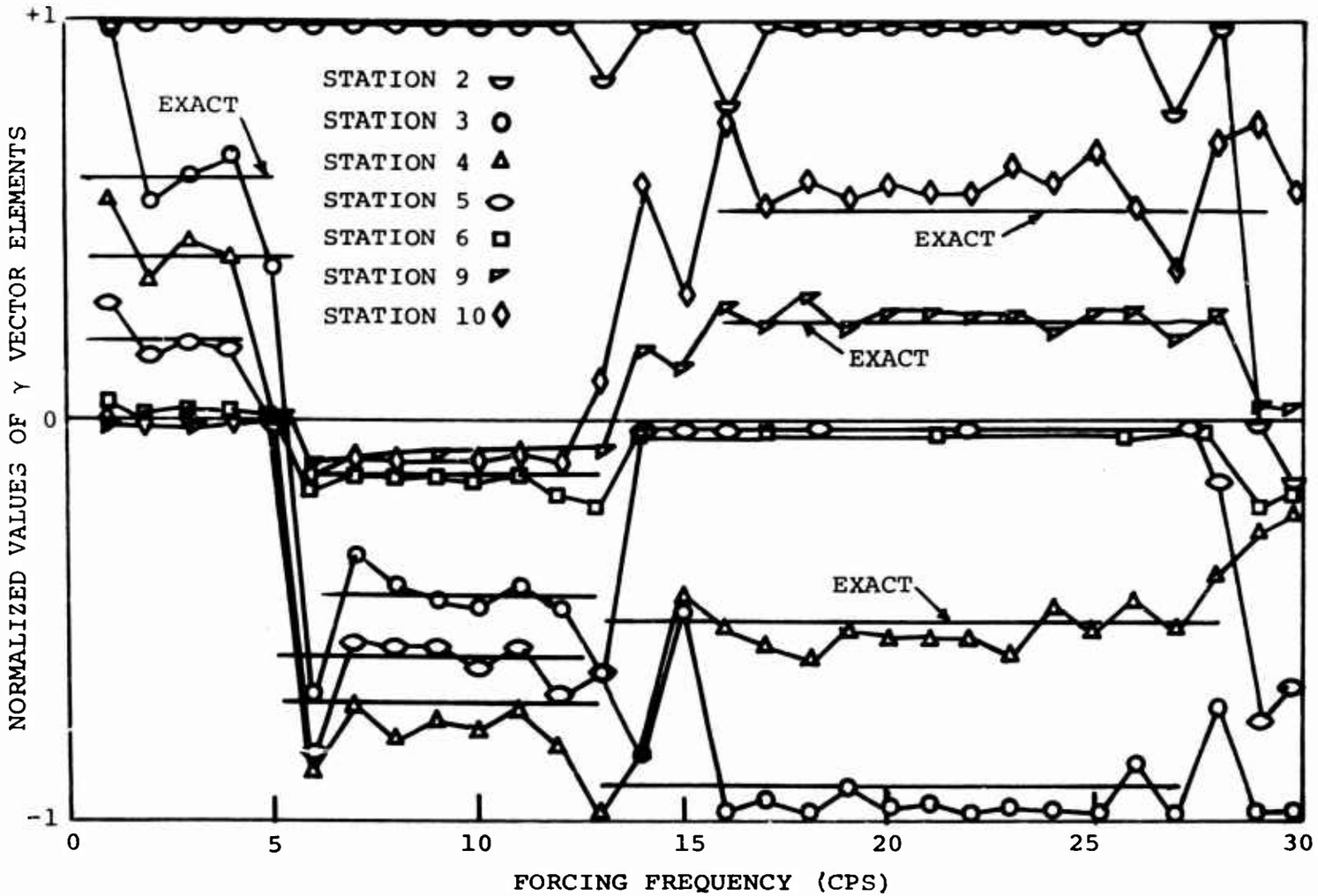

Figure 4. Variation of γ Vector Elements With Frequency. Input Mobility Data Had Errors of 8% Bias, ±8% Random and +2° Random on Phase. Damping g is 5%.

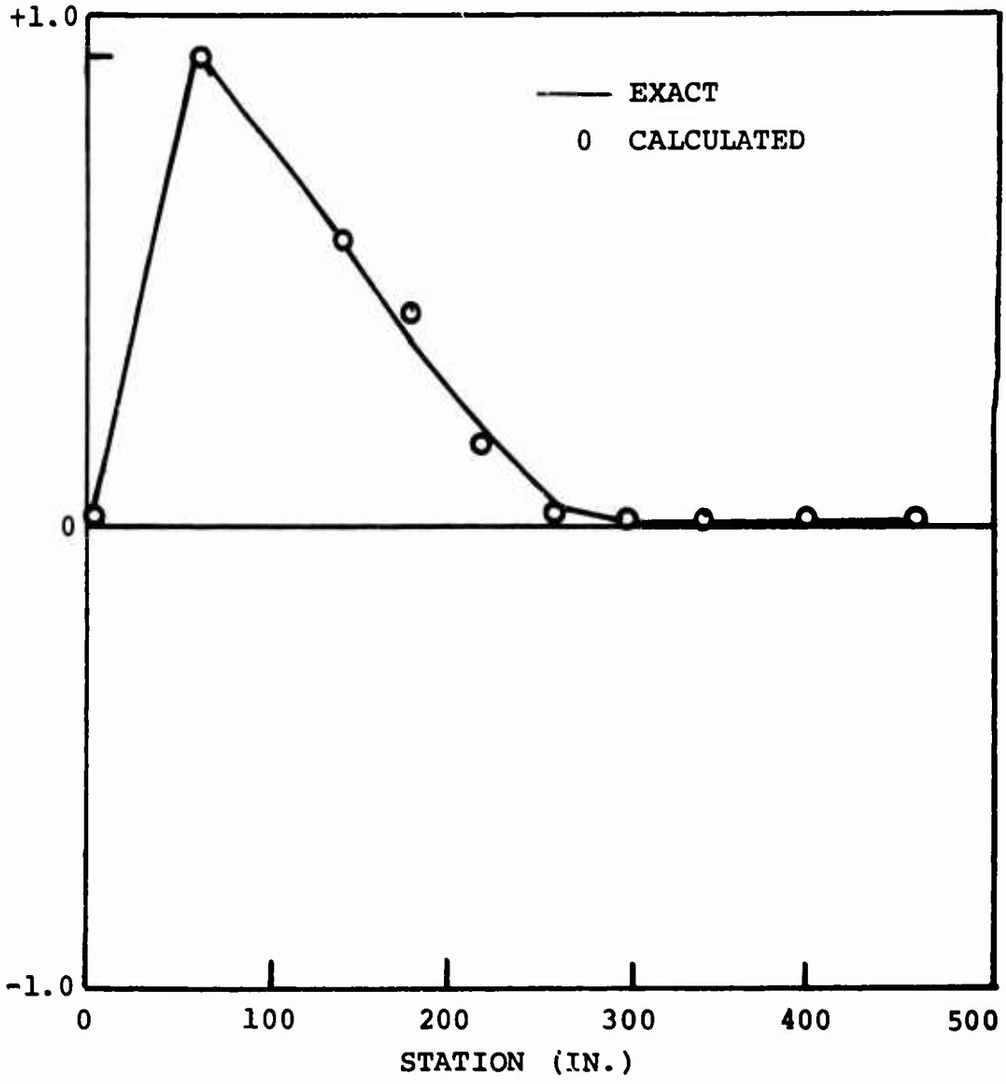

Figure 5. Gamma Vector of the First Mode Calculated at 3 cps Using Mobility Data With Error Ranges of 8% Bias and ±8% Random on Amplitude and ±2° Random on Phase Angle. The Damping g is 5%.

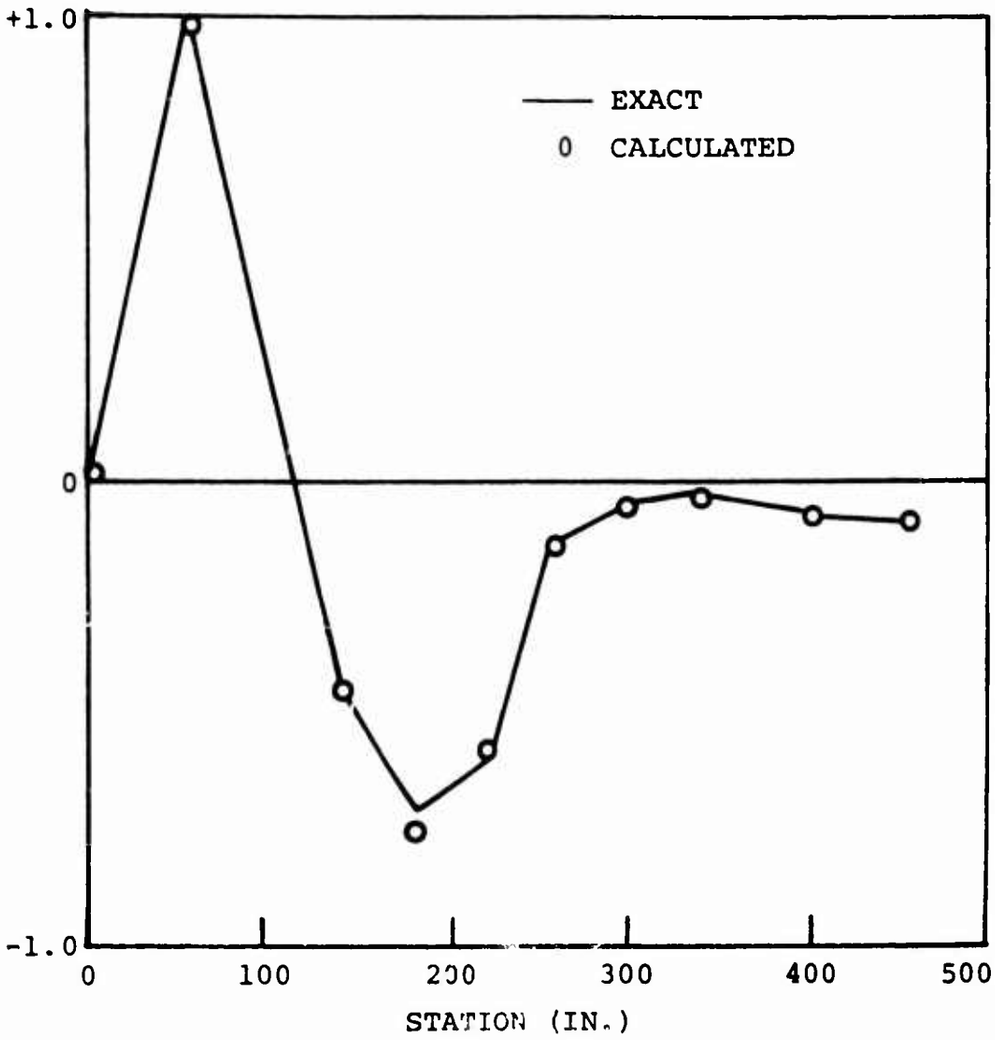

Figure 6. Gamma Vector of the Second Mode Calculated at 9 cps Using Mobility Data With Error Ranges of 8% Bias and ±8% Random on Amplitude and ±2° Random on Phase Angle. The Damping g is 5%.

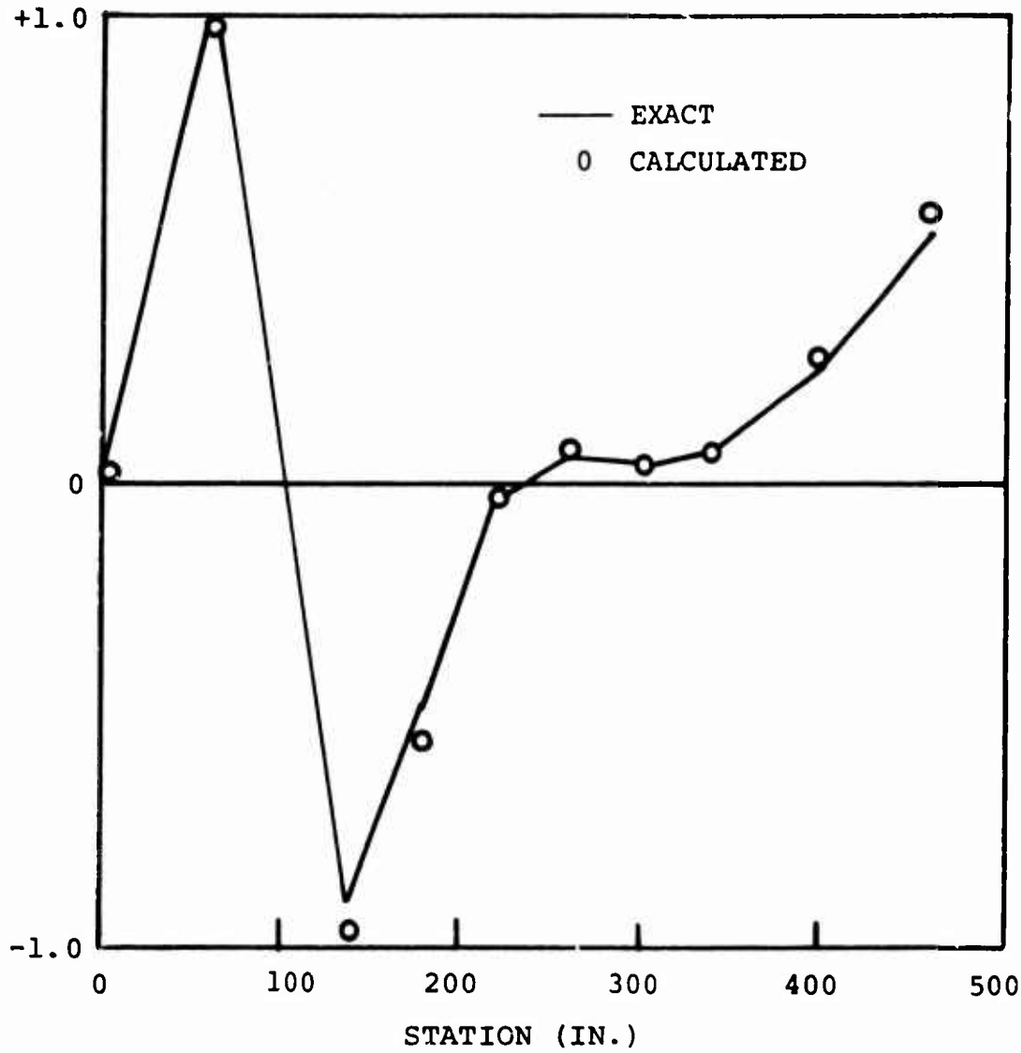

Figure 7. Gamma Vector of the Third Mode Calculated at 21 cps Using Mobility Data With Error Ranges of 8% Bias and +8% Random on Amplitude and $\pm\overline{2}°$ Random on Phase Angle. The Damping g is 5%.

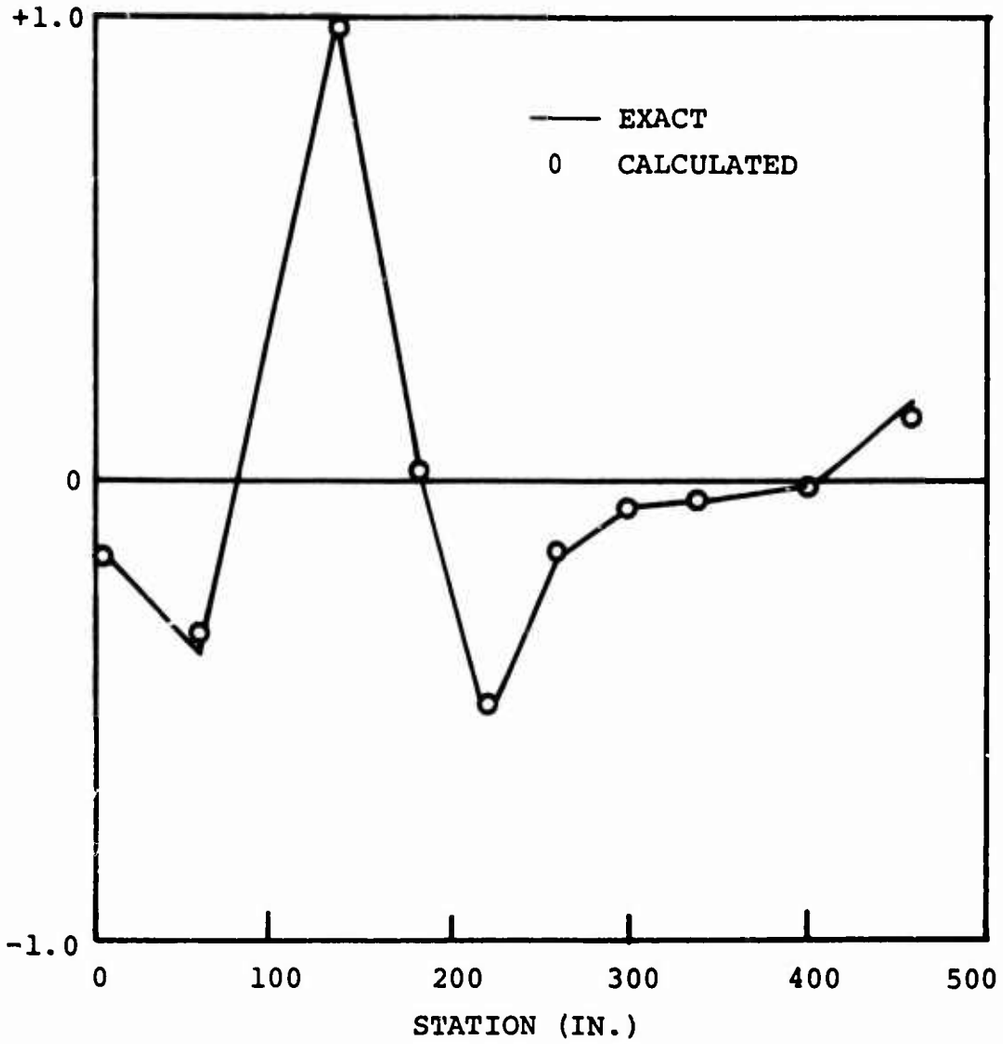

Figure 8. Gamma Vector of the Fourth Mode Calculated at 40 cps Using Mobility Data With Error Ranges of 8% Bias and ±8% Random on Amplitude and ±2° Random on Phase Angle. The Damping g is 5%.

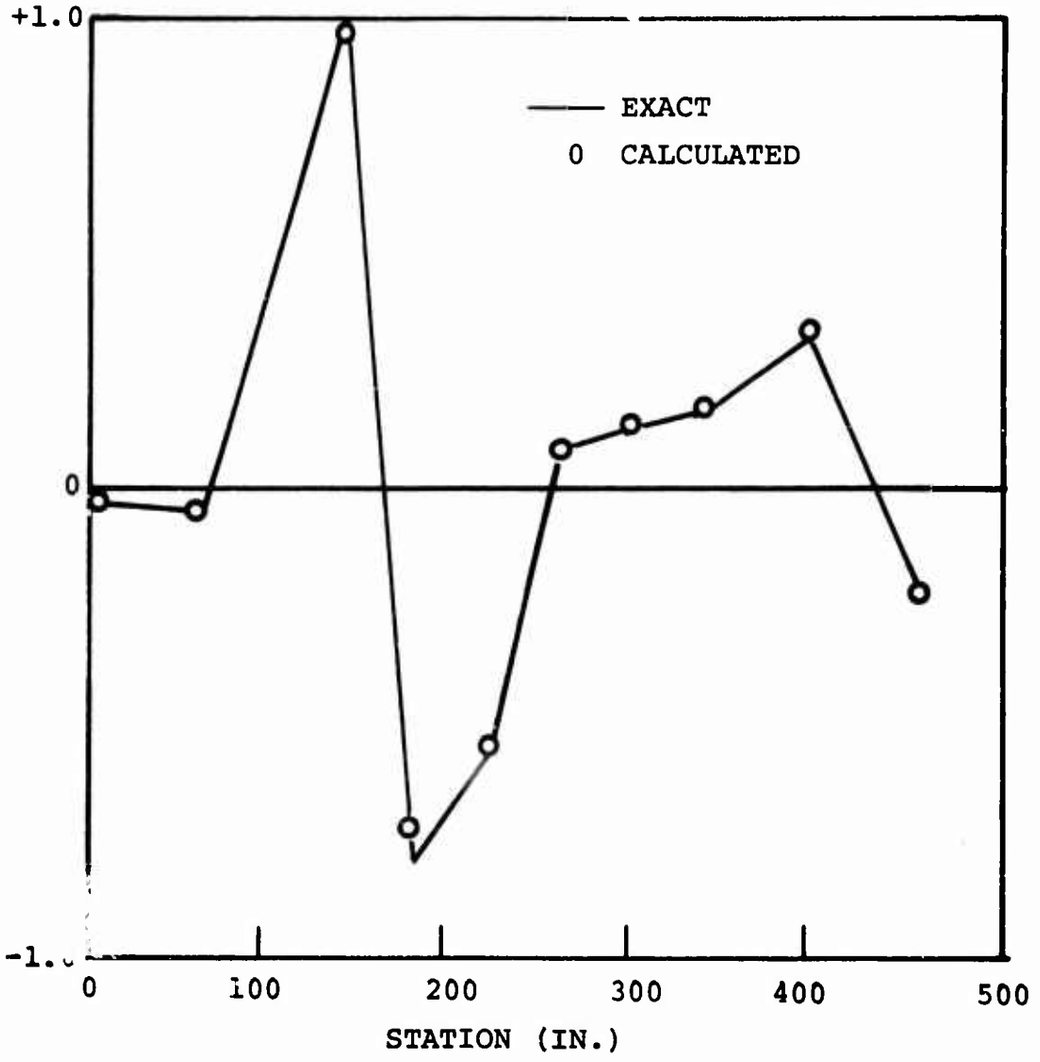

Figure 9. Gamma Vector of the Fifth Mode Calculated at 100 cps Using Mobility Data With Error Ranges of 8% Bias and +8% Random on Amplitude and $\pm\overline{2}°$ Random on Phase Angle. The Damping g is 5%.

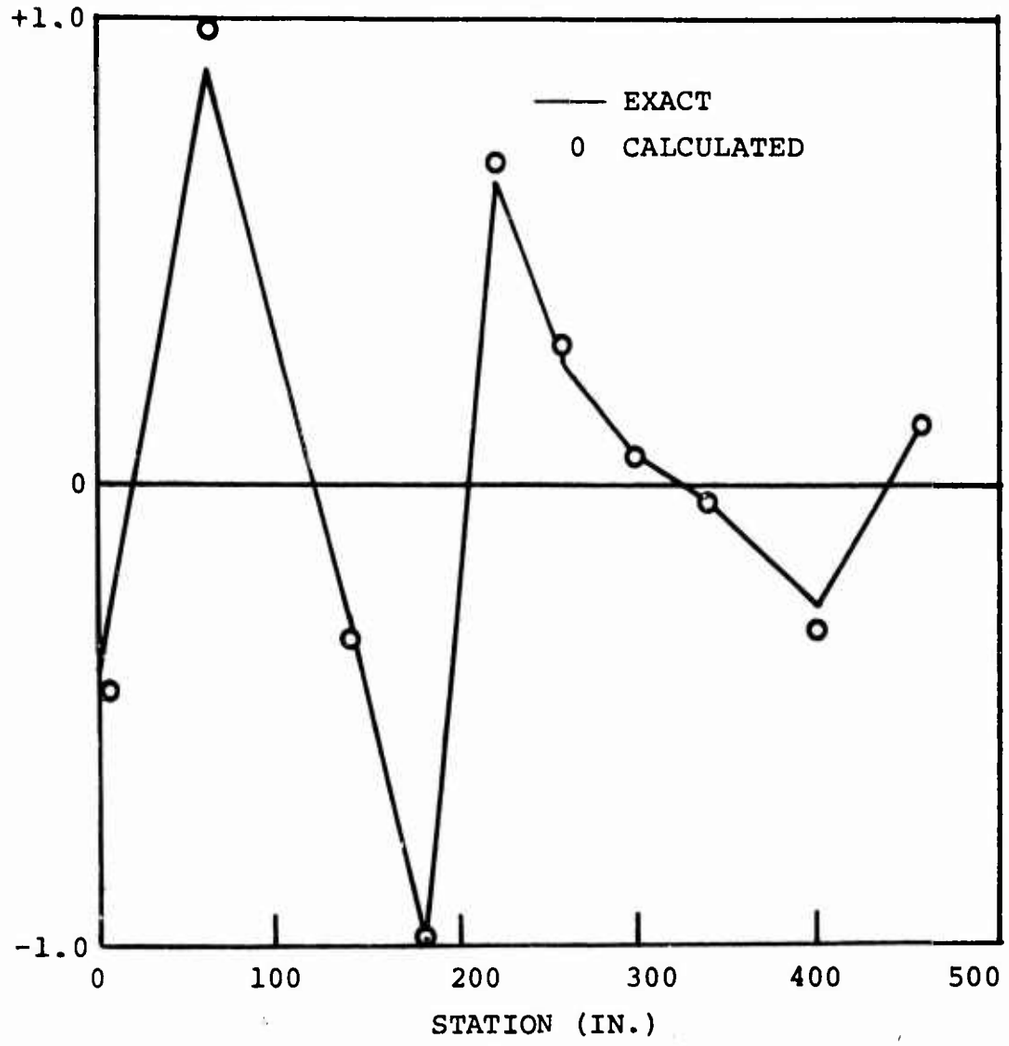

Figure 10. Gamma Vector of the Sixth Mode Calculated at 150 cps Using Mobility Data With Error Ranges of 8% Bias and +8% Random on Amplitude and +2° Random on Phase Angle. The Damping g is 5%.

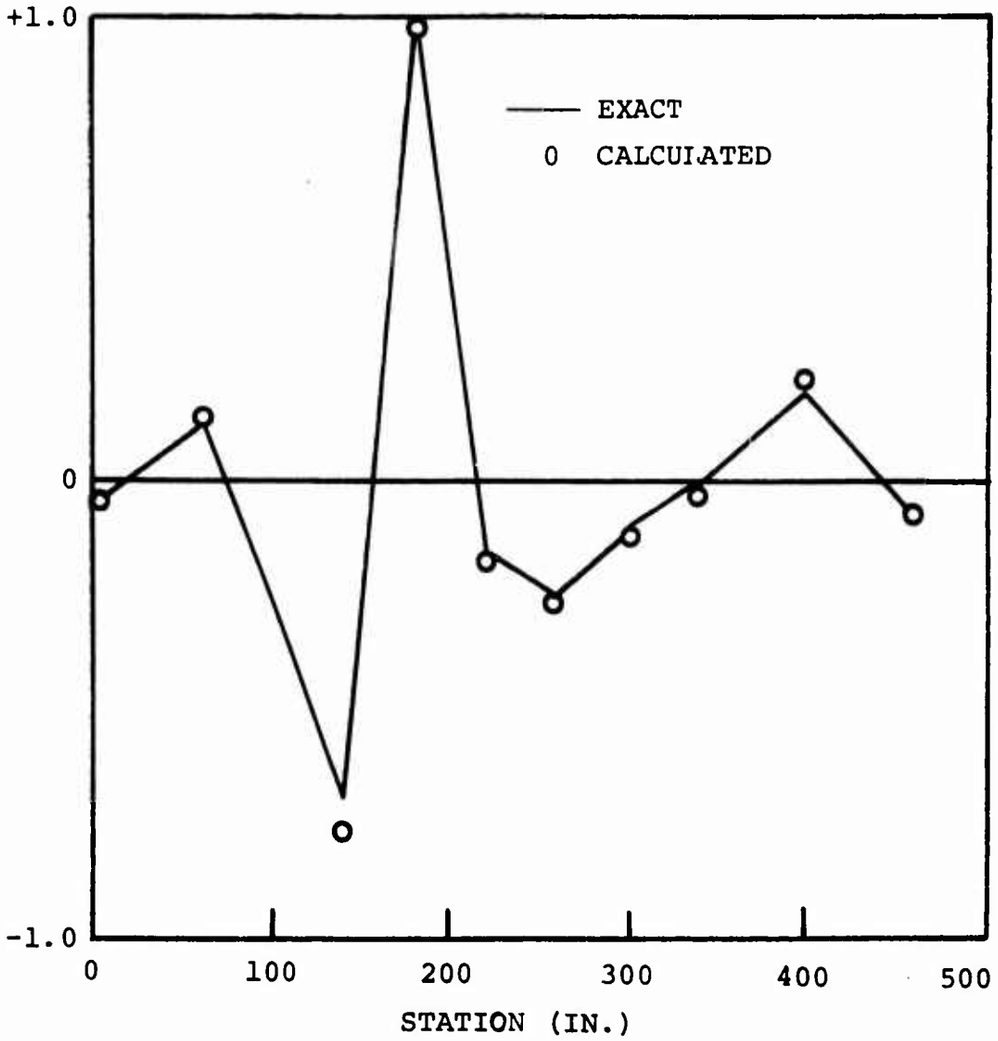

Figure 11. Gamma Vector of the Seventh Mode Calculated at 190 cps Using Mobility Data With Error Ranges of 8% Bias and +8% Random on Amplitude and $+\overline{2}°$ Random on Phase Angle. The Damping g is 5%.

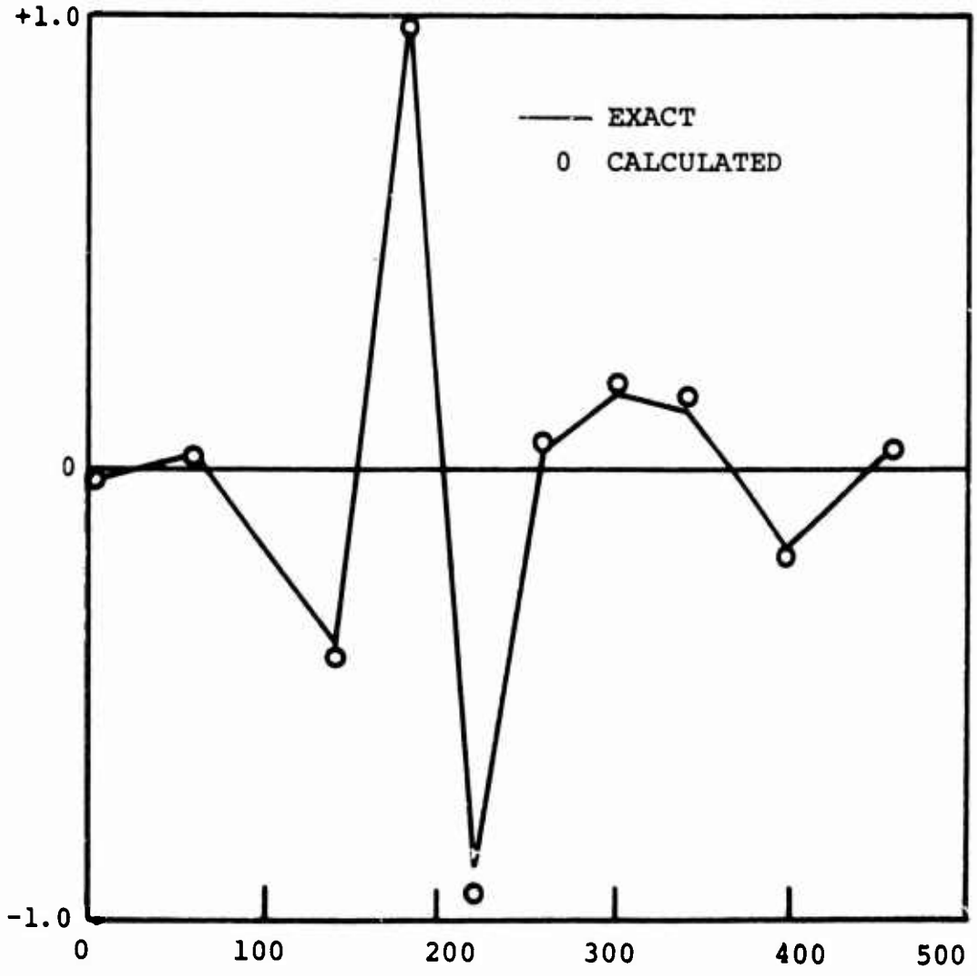

Figure 12. Gamma Vector of the Eighth Mode Calculated at 310 cps Using Mobility Data With Error Ranges of 8% Bias and +8% Random on Amplitude and $+\overline{2}°$ Random on Phase Angle. The Damping g is 5%.

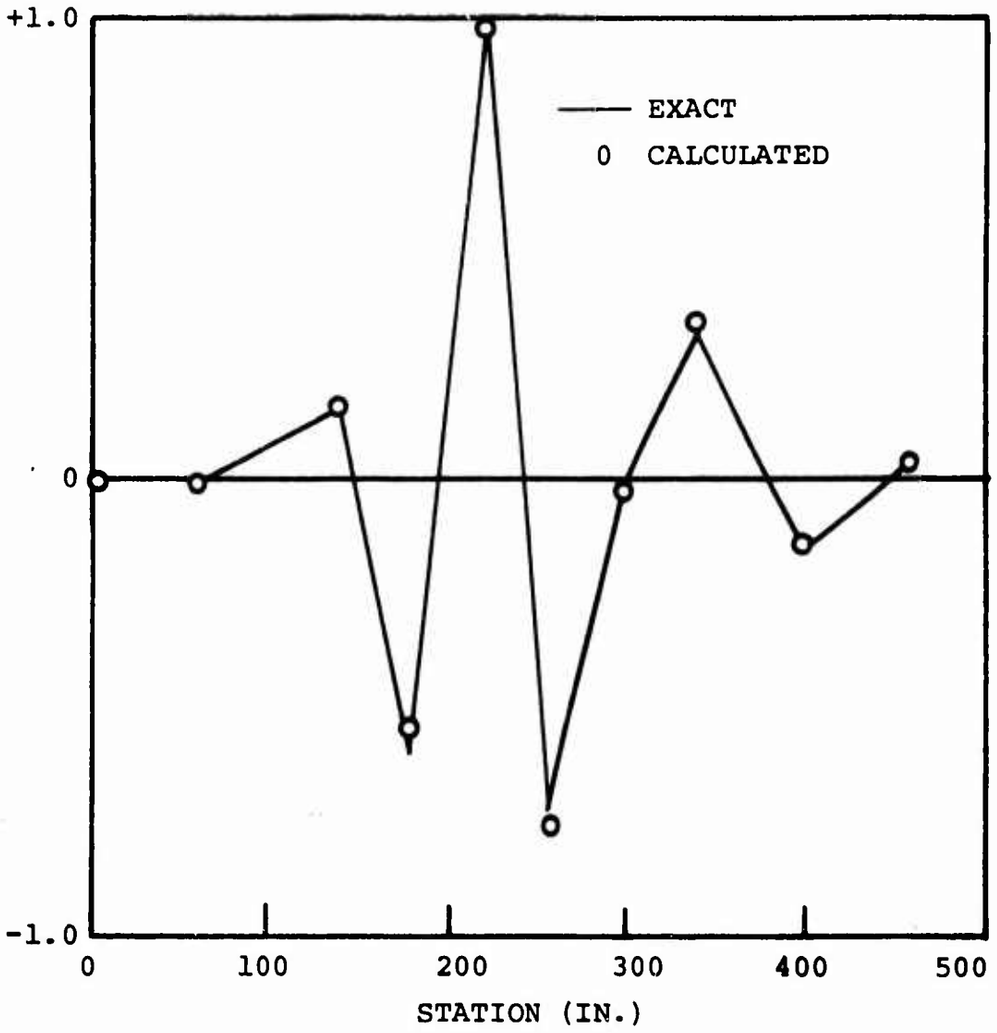

Figure 13. Gamma Vector of the Ninth Mode Calculated at 550 cps Using Mobility Data With Error Ranges of 8% Bias and +8% Random on Amplitude and +2° Random on Phase Angle. The Damping g is 5%.

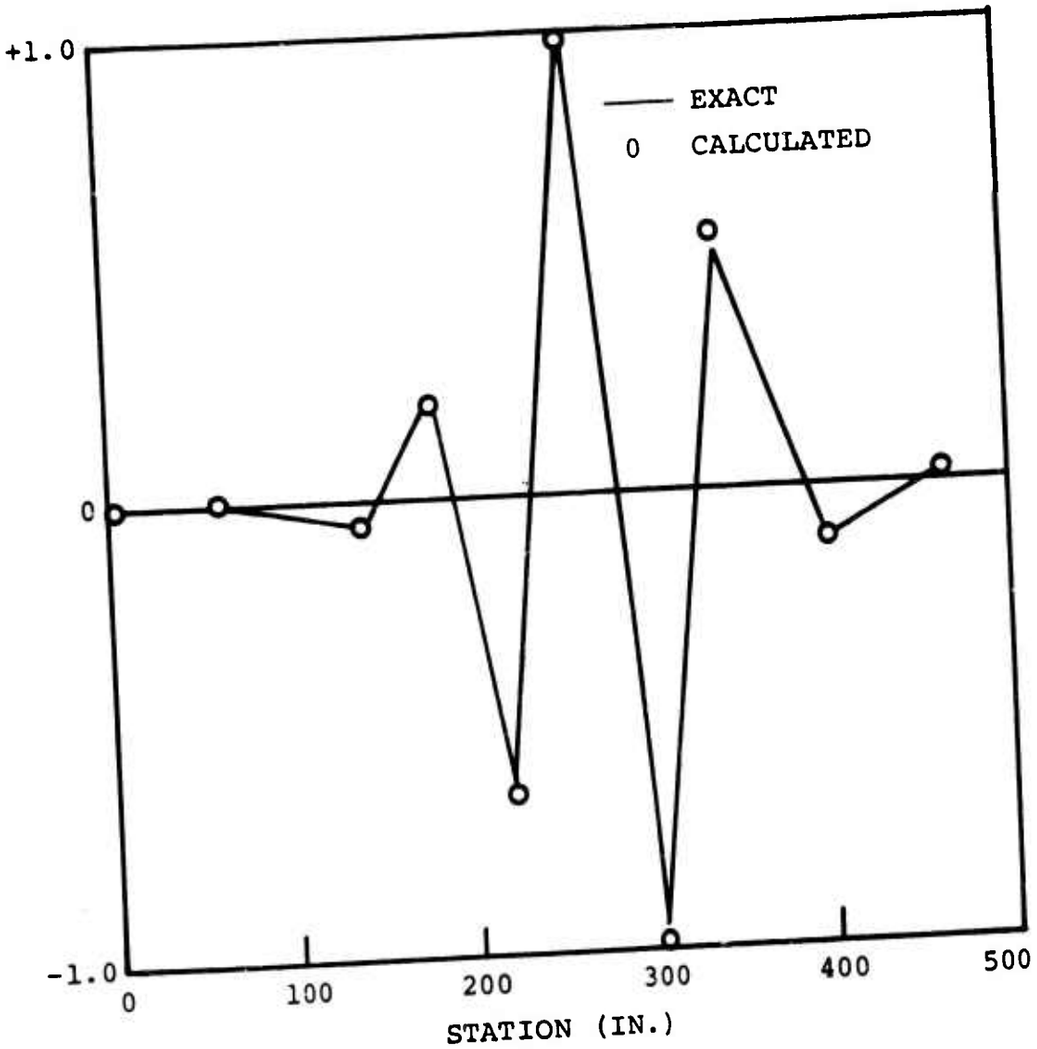

Figure 14. Gamma Vector of the Tenth Mode Calculated at 1150 cps Using Mobility Data With Error Ranges of 8% Bias and +8% Random on Amplitude and $\pm\overline{2}°$ Random on Phase Angle. The Damping g is 5%.

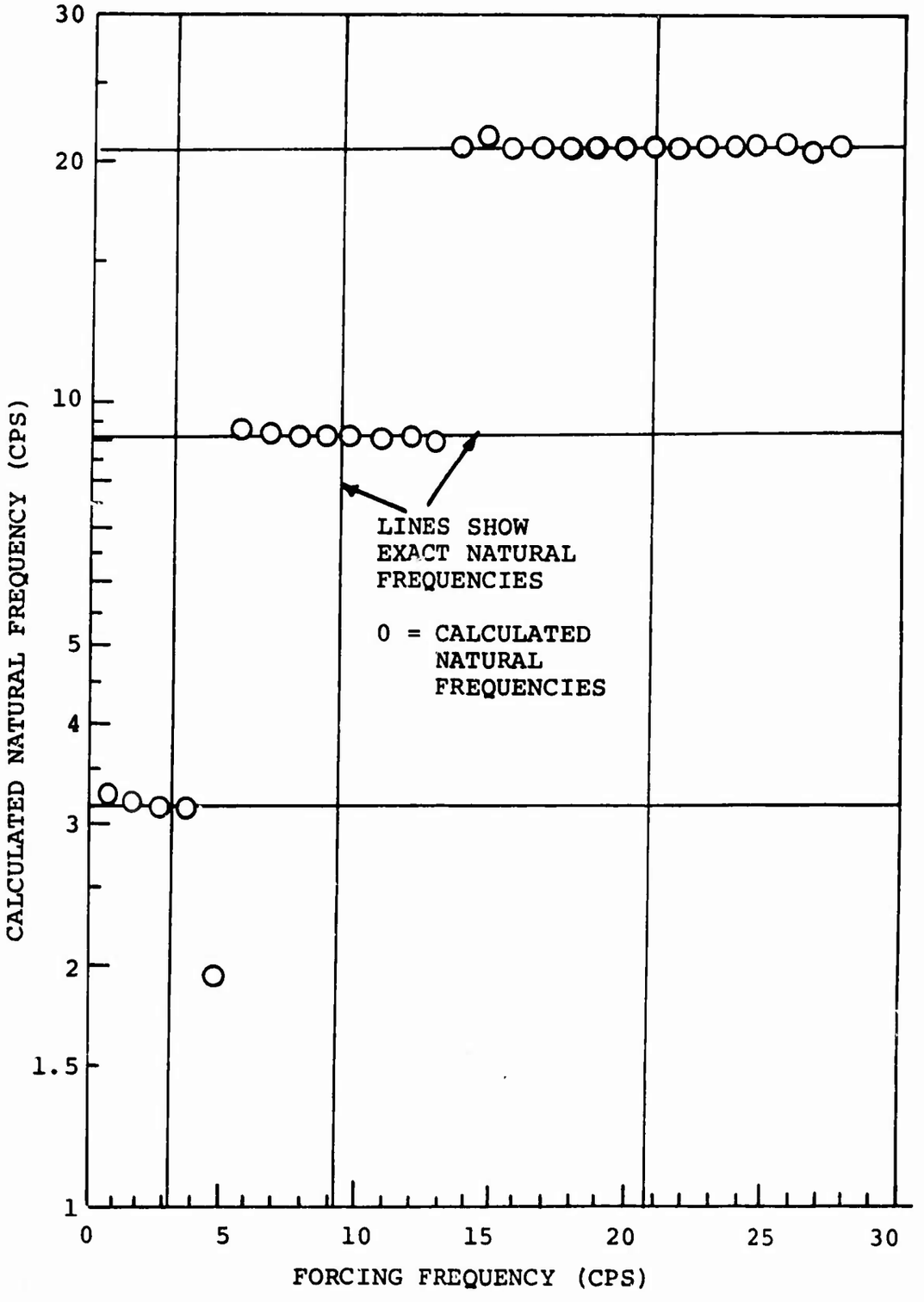

Figure 15. Natural Frequencies Calculated Using Test Data With ±8% Random Error and 8% Bias Error on Amplitude and ±2° Random Error on Phase. 5% Damping.

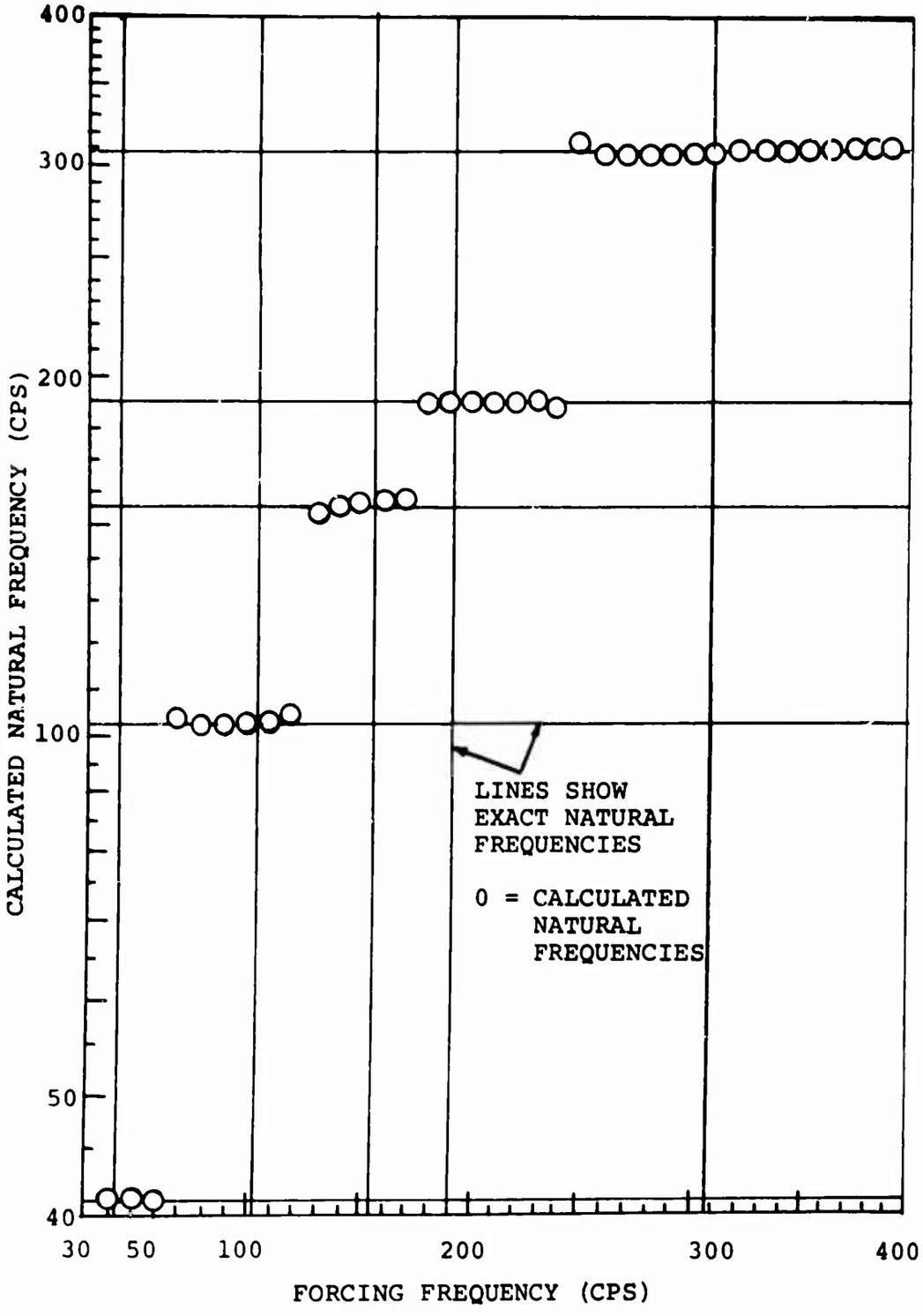

Figure 16. Natural Frequencies Calculated Using Test Data With ±8% Random Error and 8% Bias Error on Amplitude and ±2° Random Error on Phase. 5% Damping.

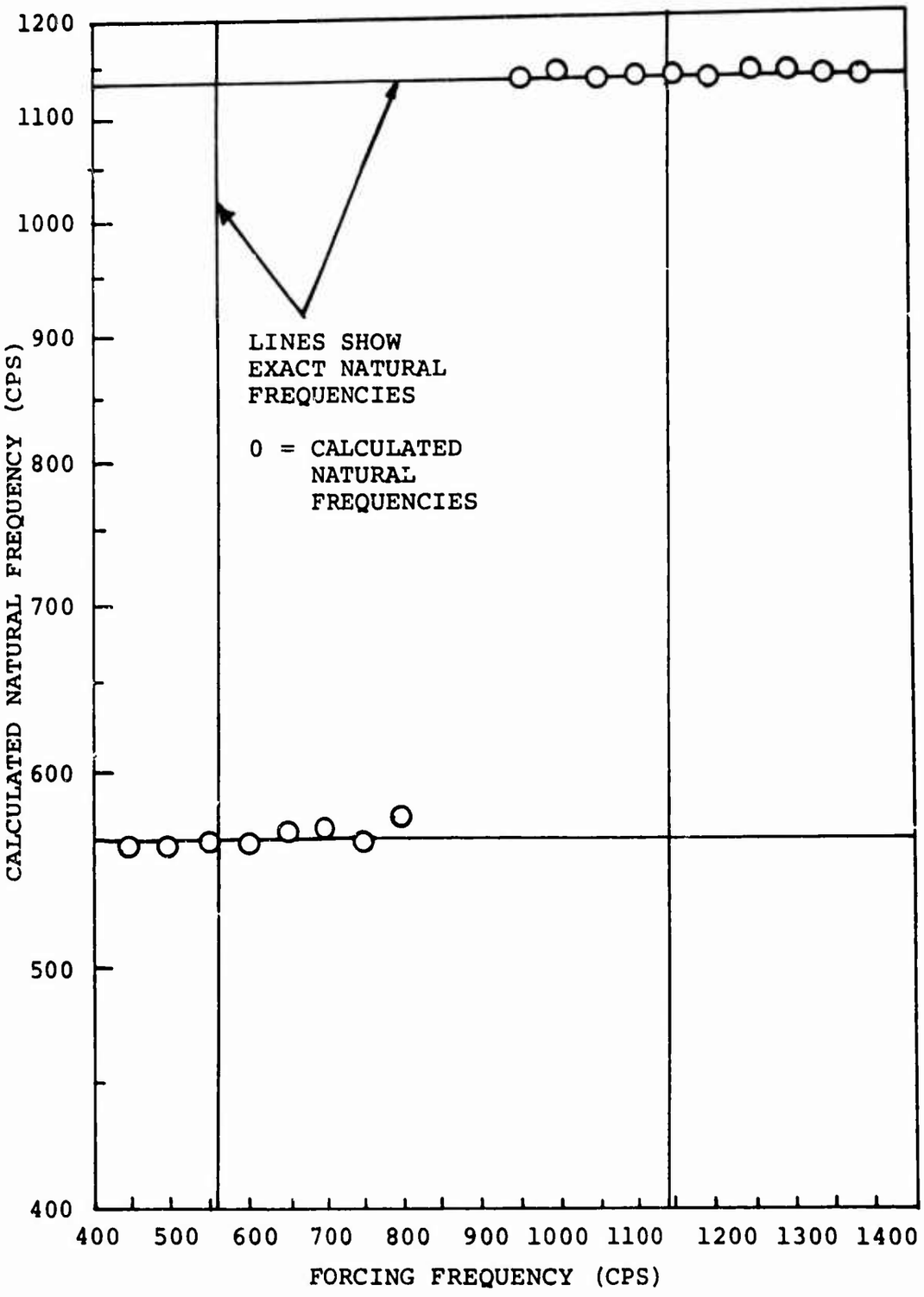

Figure 17. Natural Frequencies Calculated Using Test Data With ±8% Random Error and 8% Bias Error on Amplitude and ±2° Random Error on Phase. 5% Damping.

the modes, such as at 5 cps where neither the first nor the second mode is clearly dominant.

Figures 15 through 17 illustrate the process of identification which is examined in this report. Consider that we know that there are ten modes between 0 and 1500 cps, but we do not know precisely the values of these natural frequencies. At 1500 cps we measure a ten-by-ten matrix of mobilities which we call $[Y_{(\omega_h)}]$.

We take the ten-by-ten mobility matrix measured at 1 cps and determine the gamma vector which we use in Equation (25) to predict the first natural frequency at 3.24 cps. Now we take the measured ten-by-ten matrix of mobilities at 3 cps, the closest frequency to 3.24 cps for which we have measurements, and predict the first natural frequency to be 3.15 cps. Because the forcing frequency in this case, 3 cps, is very close to the predicted natural frequency, we accept 3.15 cps as the correct value. The gamma vector determined from the data taken at 3 cps is considered to be the first mode gamma vector.

Similarly, using data at 6 cps, we predict a natural frequency at 9.289 cps, so we take the data at 9 cps and predict the natural frequency to be 9.102 cps. The gamma vector found at 9 cps is then accepted as the second mode gamma vector. This process is continued throughout the range. It would have been possible to begin at any arbitrary frequency rather than calculate the modes in sequence, but there seems to be no advantage in so doing. Note that the calculations pertaining to any given mode are independent of the calculations pertaining to the other modes.

With a little care and some confirming calculations at additional frequencies, we will avoid the confusion that might result from operating at "crossover" frequencies such as at 5 cps.

Table II shows a possible sequence of calculations of the natural frequencies. In these experiments, mobility data were measured in simulation at once every cycle per second between 1 cps and 30 cps, once every 10 cycles per second between 30 cps and 400 cps, and once every 50 cycles per second between 400 cps and 1400 cp .

TABLE II. NATURAL FREQUENCY PREDICTIONS USING MOBILITY DATA WITH 8 PERCENT BIAS ERROR, ±8 PERCENT RANDOM ERROR AND ±2° RANDOM PHASE ERROR

Forcing Frequency at Which Measurements Were Taken (cps)	Predicted Natural Frequency (cps)	Exact Natural Frequency (cps)
1	3.24	-
3	3.15	3.14
6	9.29	-
9	9.10	9.10
14	20.80	-
21	20.80	20.80
40	41.10	41.10
50	41.20	-
70	101.90	-
100	101.30	101.40
130	153.30	-
150	154.90	154.90
180	190.10	-
190	190.10	190.10
250	314.10	-
310	309.30	309.40
450	560.70	-
550	561.90	562.30
900	1231.60	-
1250	1147.50	-
1150	1145.20	1145.10

IDENTIFICATION OF DAMPING COEFFICIENT

The structural damping coefficient is determined using Equation (29). If the structure has a type of damping such as viscous damping which cannot be represented using a scalar multiplier, then the damping term may be approximated by identification of a different damping coefficient for each mode. However, in the test case used in this study, we employed the conventional representation of structural damping as a scalar multiplier of the stiffness matrix in phase with the velocity.

Table III shows the identified values of damping coefficient for each of the modes of a structure with a constant 5 percent structural damping coefficient. The input mobility data had an 8 percent bias error and a ± 8 percent random error on amplitude and a $\pm 2°$ random phase error.

TABLE III. IDENTIFIED STRUCTURAL DAMPING COEFFICIENT USING MOBILITY DATA WITH 8% BIAS AND ± 8% RANDOM ERROR ON AMPLITUDE AND $\pm 2°$ RANDOM PHASE ERROR. EXACT VALUE OF DAMPING COEFFICIENT IS .050.

Exact Natural Frequency (cps)	Forcing Frequency at Which Measurements Were Taken (cps)	Identified Value of Damping Coefficient
3.14	3	.051
9.10	9	.050
20.80	21	.049
41.10	40	.050
101.40	100	.048
154.90	150	.045
190.10	190	.050
309.40	310	.049
562.30	550	.048
1145.10	1150	.049

IDENTIFIED MASSES AND STIFFNESSES

Figure 18 shows the identified mass matrix obtained using a typical case of input mobility data polluted with 8 percent random and bias error on amplitude and 2° random phase error. Comparison with the exact mass matrix, shown in Figure 19, shows reasonably close agreement. The identified mass matrix is fully populated, but the off-diagonal terms are all of small magnitude.

The question naturally arises whether by pure chance the random errors in this randomly selected case so fell as to yield an unusually accurate identification. To statistically study the effects of random input error, the computer was programmed to make identifications from 25 simulated replicated tests with errors of $\pm$8 percent random and 8 percent bias on amplitude and $\pm$2° phase angle error in the input mobility data.

In Figures 20 through 30, the exact value of the identified parameters is shown as a circle, the mean of the identified parameters as a short horizontal line, and the range of six standard deviations ($\pm$3 standard deviations) as a vertical line.

The mean value is the "expected value". It is most probable that the identified parameters from any one test will fall close to the mean. The probability of the magnitude of any identified parameter falling at or beyond the extremities of the vertical line is less than three parts in 1000.

In Figure 20, the range of error in the identification of the diagonal masses remains small over three orders of magnitude. The off-diagonal stiffness terms, urlike the off-diagonal mass terms, are not very small. Therefore, all the stiffness terms are shown, column by column, in Figures 21 through 30.

The mean of the identified values of the parameters is quite close to the exact value except when the value of the parameter is quite low. In general, these plots show that the error spread increases as the numerical significance of a parameter value (as compared to the maximum in the row or column) decreases. This is not a surprising finding.

Considerable care should be exercised in examining the plots. First, the logarithmic scale exaggerates the statistical spread below the mean. Secondly, the scales differ among various plots to magnify the numerical data. The ordinate scale of Figure 29, for example, is an order

$$\begin{bmatrix}
.0249 & .0013 & -.0027 & .0047 & -.0038 & -.0014 & -.0003 & .0002 & .0013 & -.0005 \\
.0013 & 6.5669 & .0155 & -.0285 & .0298 & .0073 & .0079 & .0053 & .0062 & .0087 \\
-.0027 & .0154 & 5.7224 & .0805 & -.0037 & -.0148 & -.0075 & -.0048 & -.0095 & -.0027 \\
.0047 & -.0285 & .0805 & 5.4196 & .0221 & .0004 & -.0080 & -.0021 & .0218 & -.0023 \\
-.0038 & .0298 & -.0037 & .0210 & 2.6838 & .0013 & .0037 & .0045 & -.0007 & .0016 \\
-.0014 & .0073 & -.0148 & .0004 & -.0013 & .4604 & .0096 & .0074 & .0007 & -.0020 \\
-.0003 & .0079 & -.0075 & -.0080 & .0037 & .0096 & .1734 & .0106 & .0000 & -.0011 \\
.0002 & .0053 & -.0048 & -.0021 & .0045 & .0074 & .0106 & .1296 & -.0004 & -.0010 \\
.0013 & .0062 & -.0095 & .0218 & -.0007 & .0007 & -.0000 & .0004 & .2215 & .0002 \\
-.0005 & .0087 & -.0027 & .0023 & .0016 & -.0020 & -.0011 & -.0010 & .0002 & .2787
\end{bmatrix} = [m] \text{ (lb-sec}^2\text{/in.)}$$

Figure 18. Identified Mass Matrix With Input Mobility Errors of 8% Bias and ±8% Random on Amplitude and ±2° Random on Phase.

$$
\begin{bmatrix}
.0290 & 0 & 0 & 0 & 0 & 0 & 0 & 0 & 0 & 0 \\
0 & 7.337 & 0 & 0 & 0 & 0 & 0 & 0 & 0 & 0 \\
0 & 0 & 6.540 & 0 & 0 & 0 & 0 & 0 & 0 & 0 \\
0 & 0 & 0 & 5.179 & 0 & 0 & 0 & 0 & 0 & 0 \\
0 & 0 & 0 & 0 & 3.129 & 0 & 0 & 0 & 0 & 0 \\
0 & 0 & 0 & 0 & 0 & .527 & 0 & 0 & 0 & 0 \\
0 & 0 & 0 & 0 & 0 & 0 & .170 & 0 & 0 & 0 \\
0 & 0 & 0 & 0 & 0 & 0 & 0 & .119 & 0 & 0 \\
0 & 0 & 0 & 0 & 0 & 0 & 0 & 0 & .238 & 0 \\
0 & 0 & 0 & 0 & 0 & 0 & 0 & 0 & 0 & .298
\end{bmatrix}
= [m] \quad (\text{lb-sec}^2/\text{in.})
$$

Figure 19. Exact Mass Matrix.

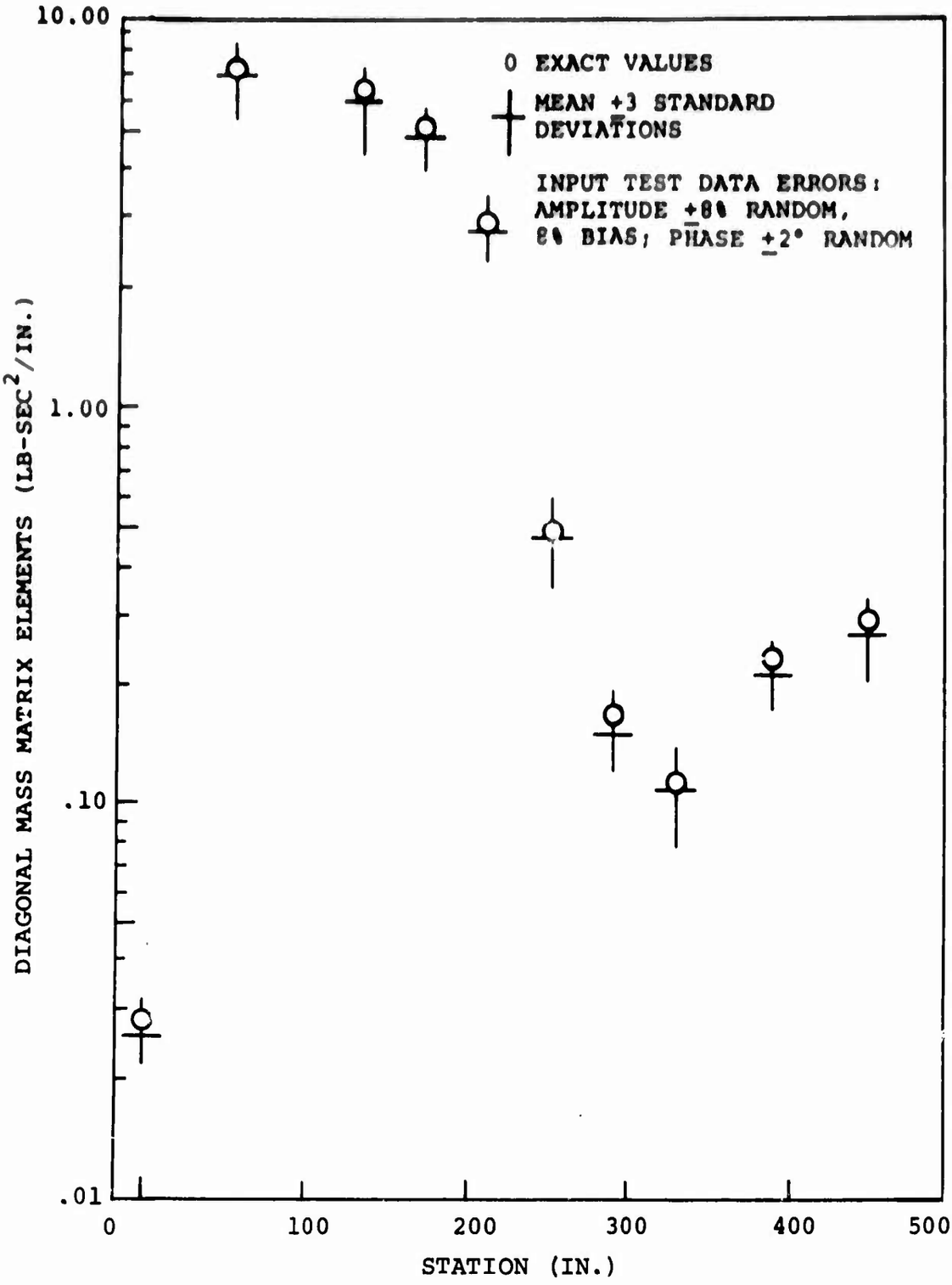

Figure 20. Identified Elements of Mass Matrix Diagonal.

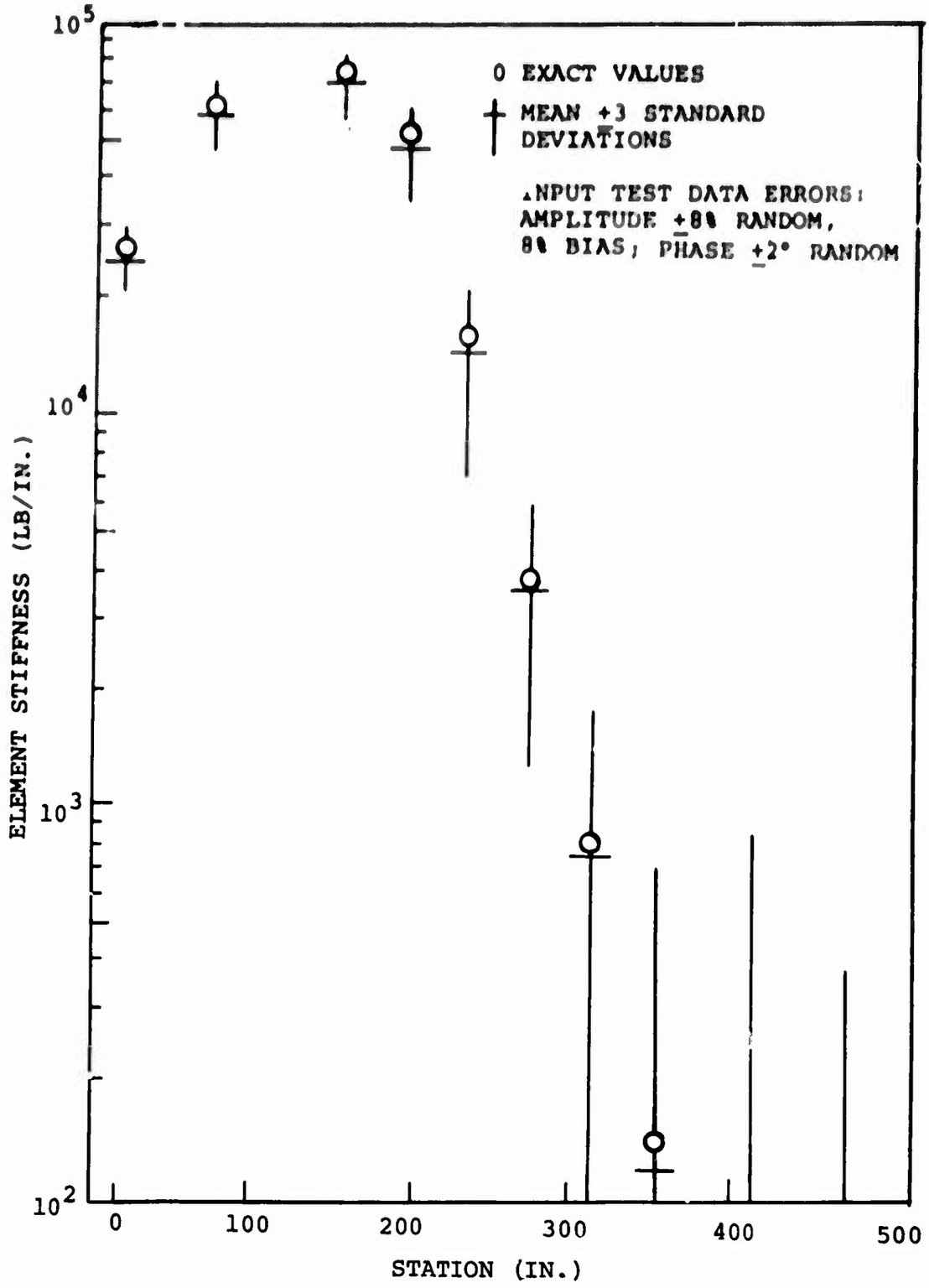

Figure 21. Identified Elements of Stiffness Matrix. Column One.

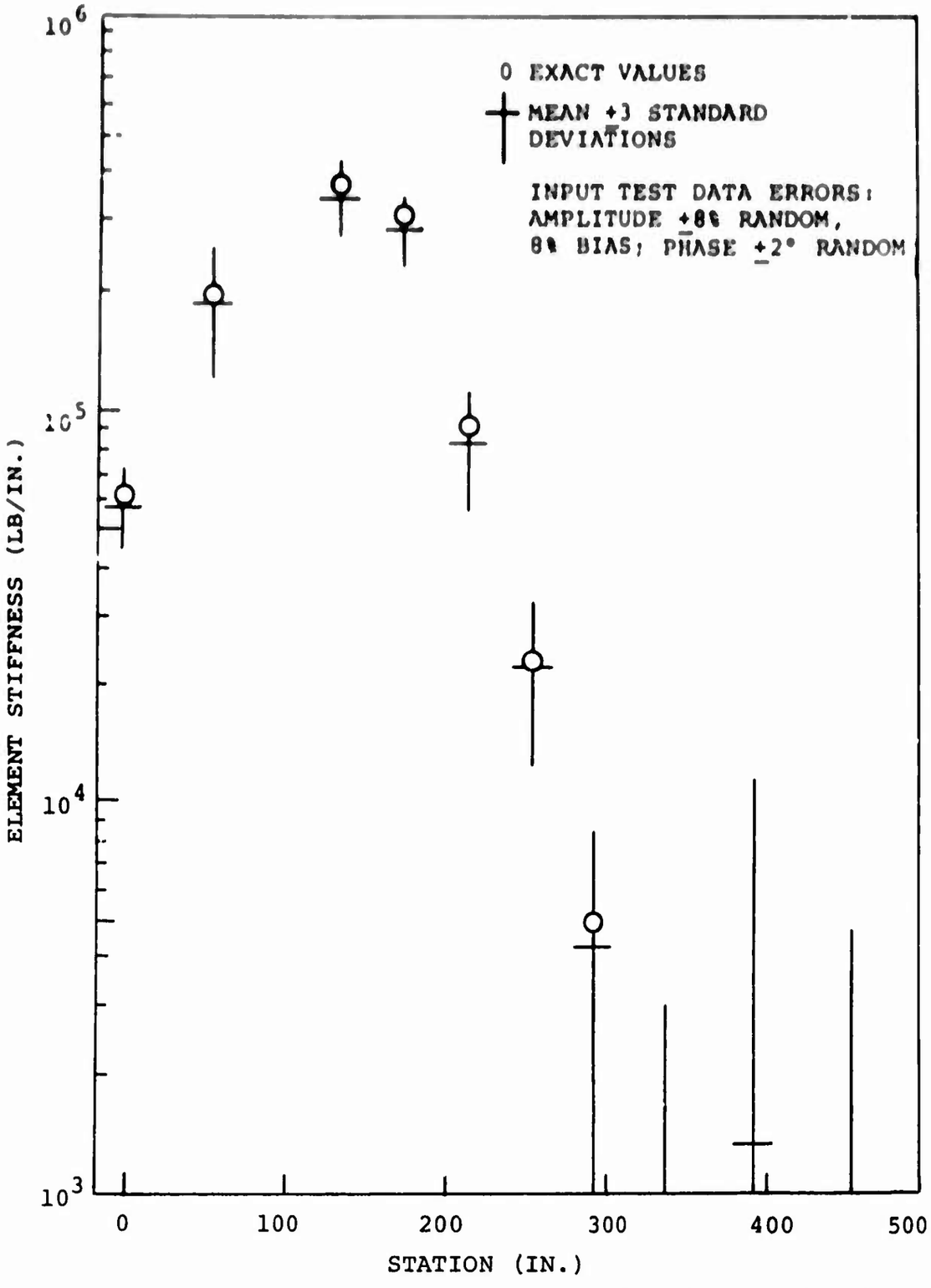

Figure 22. Identified Elements of Stiffness Matrix. Column Two.

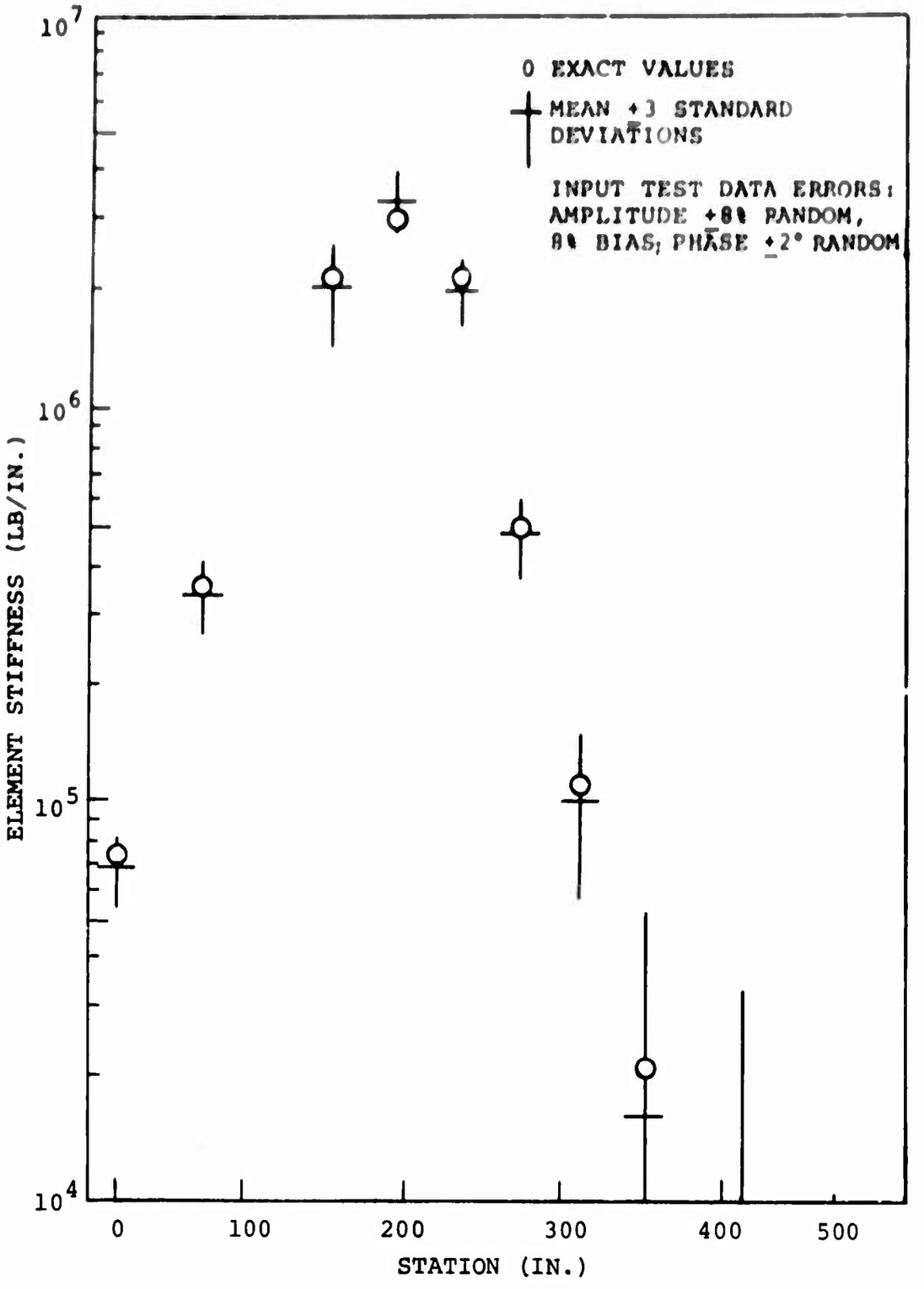

Figure 23. Identified Elements of Stiffness Matrix. Column Three.

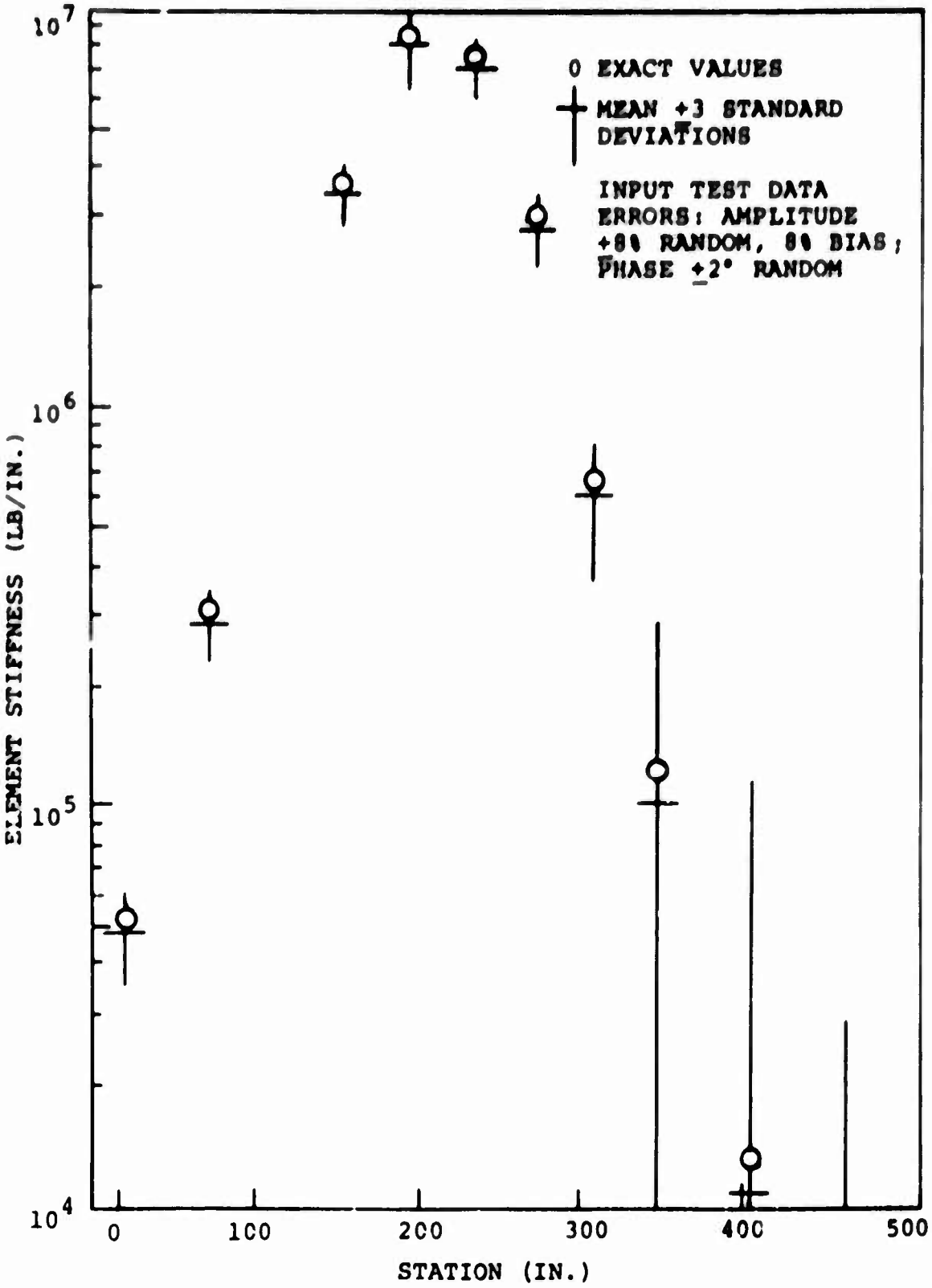

Figure 24. Identified Elements of Stiffness Matrix. Column Four.

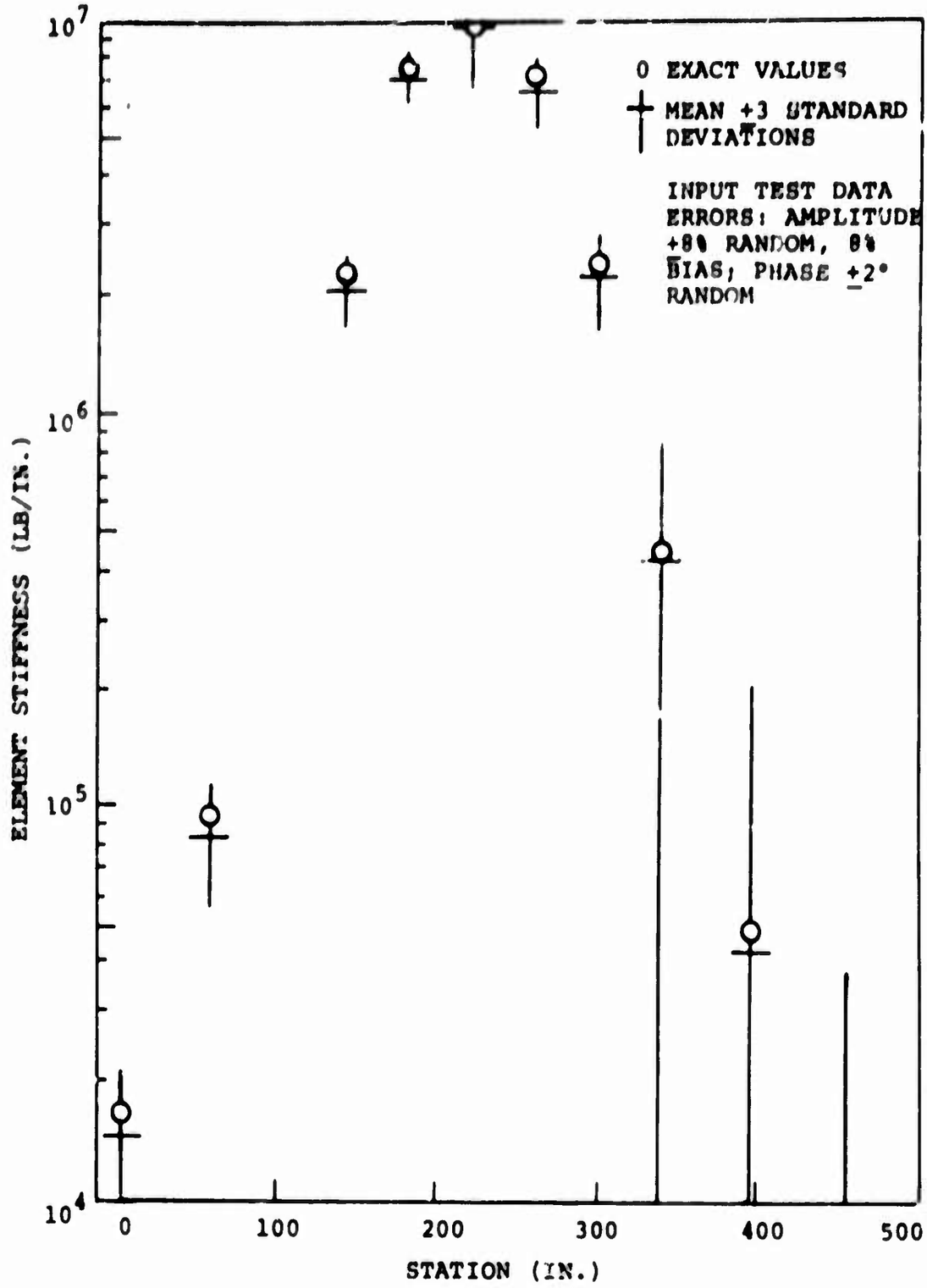

Figure 25. Identified Elements of Stiffness Matrix. Column Five.

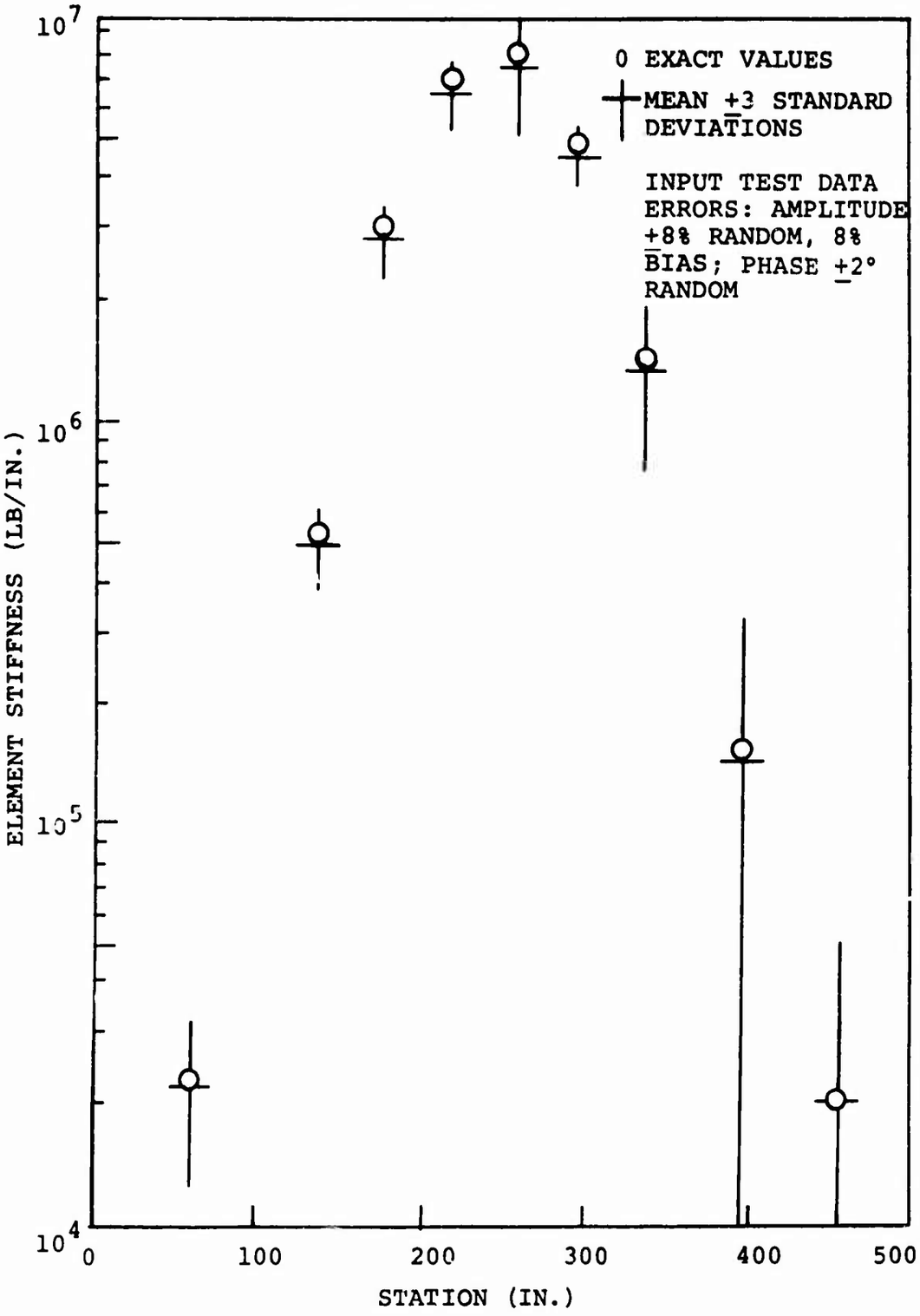

Figure 26. Identified Elements of Stiffness Matrix. Column Six.

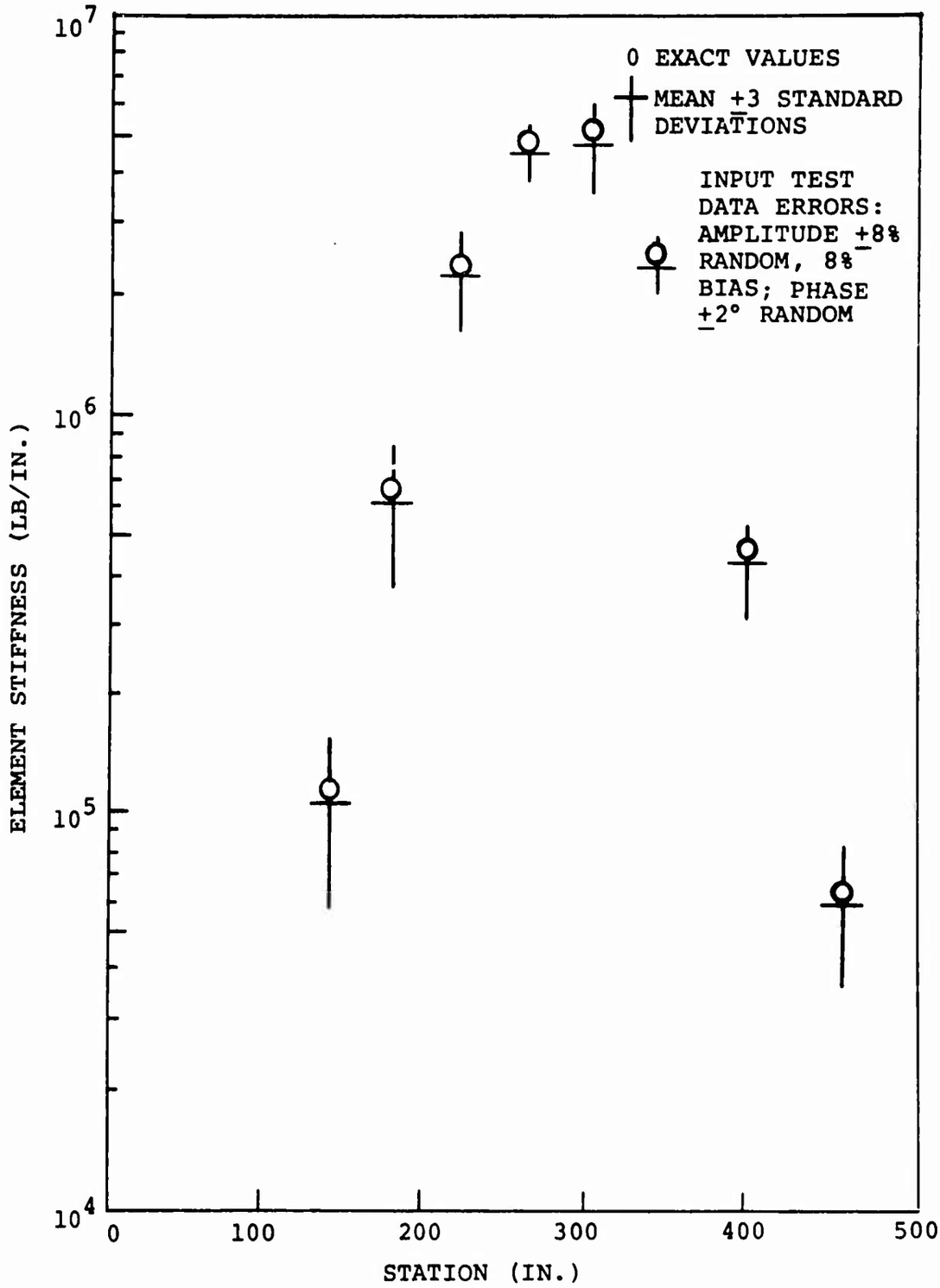

Figure 27. Identified Elements of Stiffness Matrix. Column Seven.

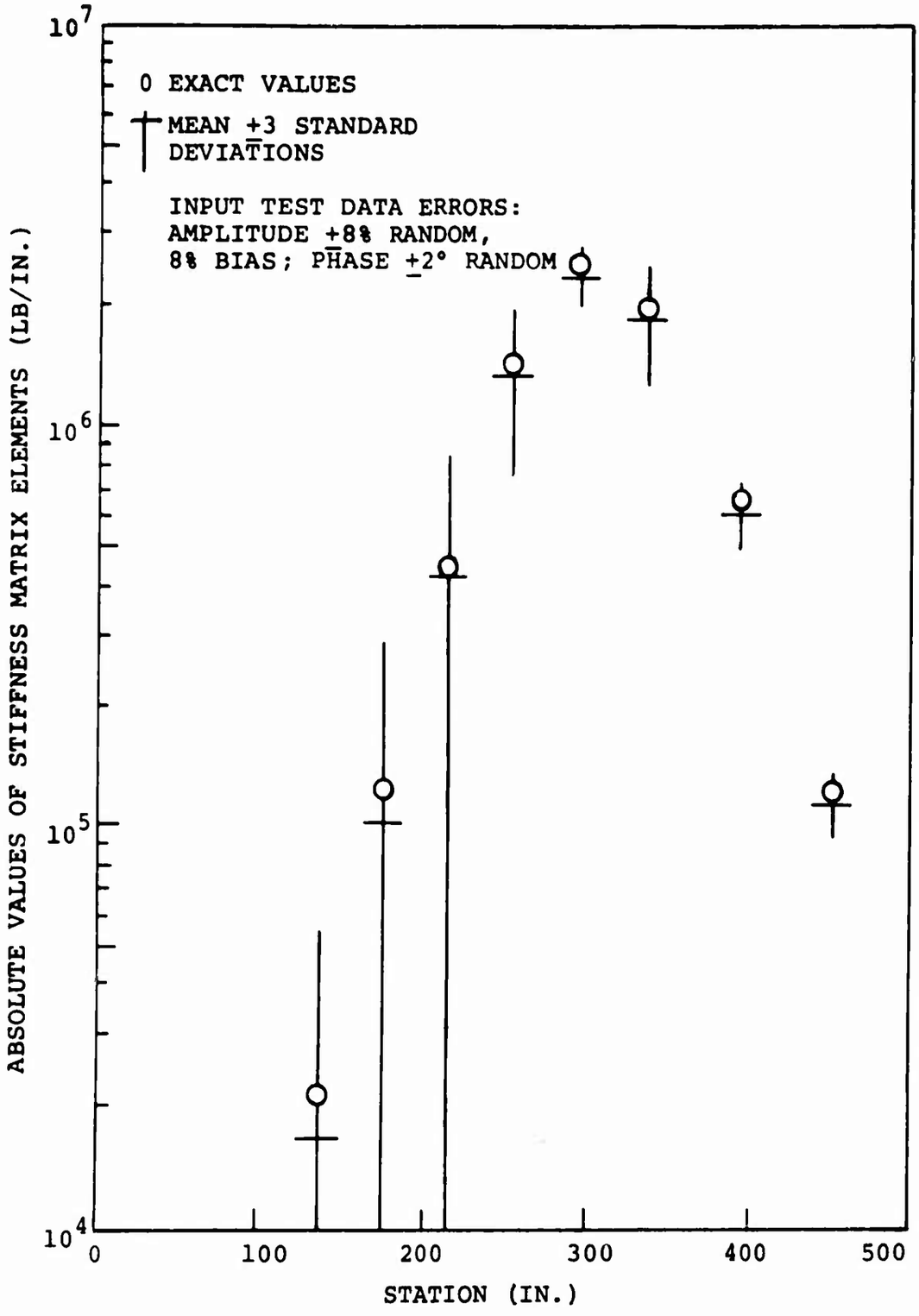

Figure 28. Identified Elements of Stiffness Matrix. Column Eight.

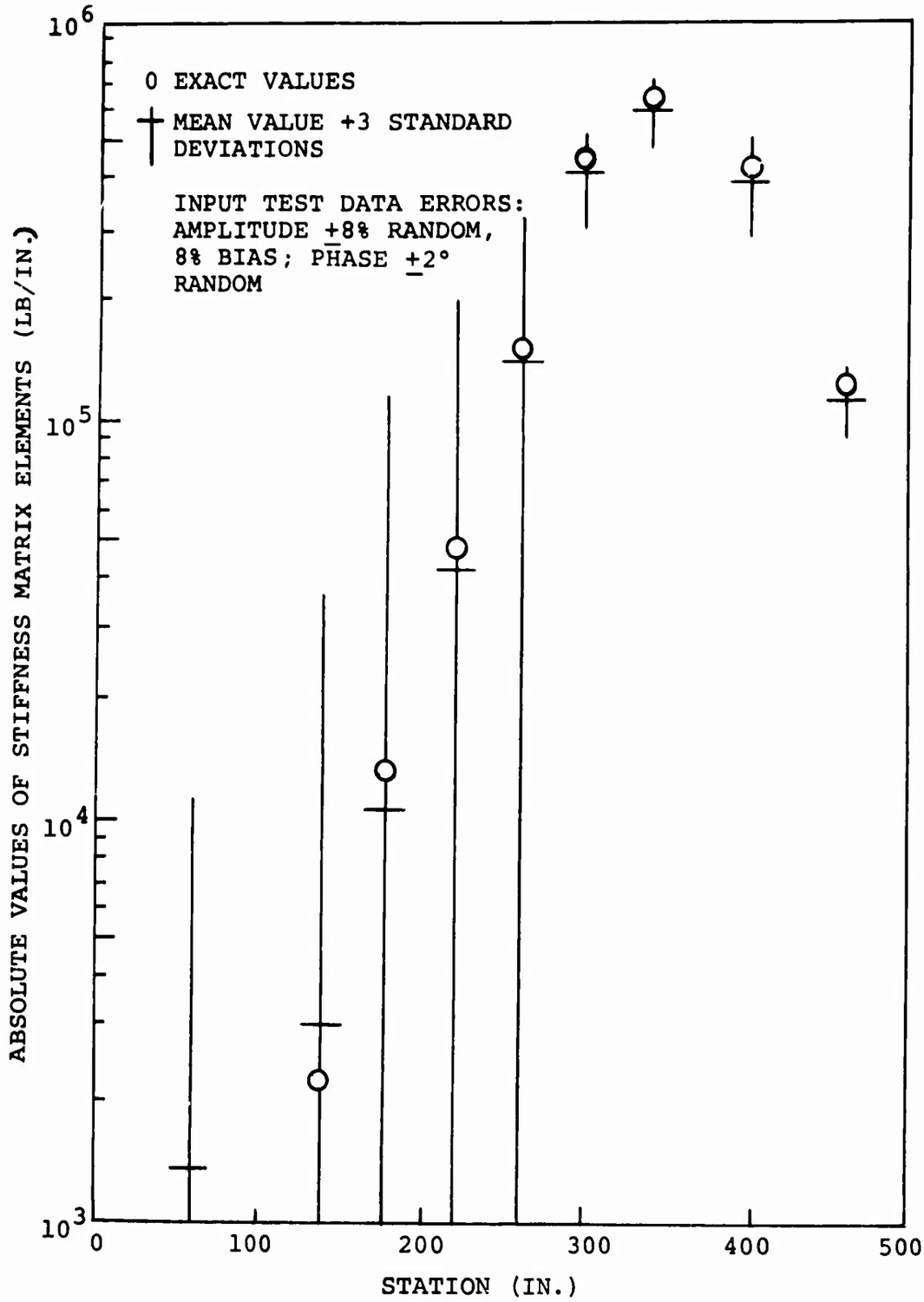

Figure 29. Identified Elements of Stiffness Matrix. Column Nine.

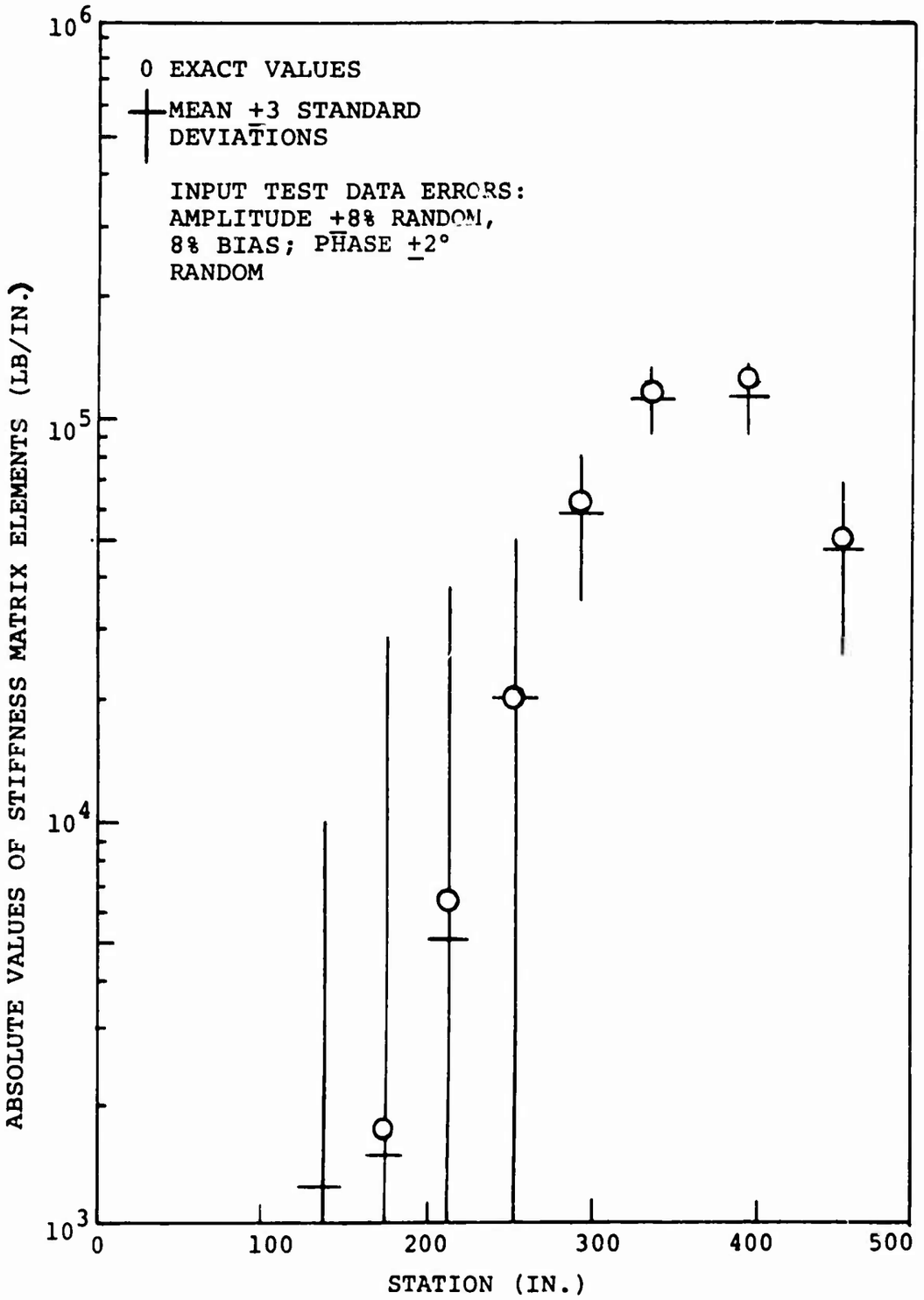

Figure 30. Identified Elements of Stiffness Matrix. Column Ten.

of magnitude lower than the ordinate scale of Figure 28.

It would appear from an examination of Figures 20 through 30 that the best identification would be obtained by taking the mean value of many identifications of a parameter, but computer experiments have shown that such is not the case. The "best identification" of a system's parameters requires not only that the value of each parameter approximate the "true" value, but that the values of all the parameters be mutually consistent as a set which describes the physical system. It was found through computer experiments that the mean values of identified parameters, each of which closely approximated the true value, collectively produced poor results in an attempt to reproduce the mobility data from which they were derived. On the other hand, parameters identified from one consistent set of mobility data (i.e., from one test) produced excellent results in reproducing the response even though most of the individual values were each poorer approximations of the true values than were the means of the identified parameters from many tests. The lack of consistency (or compatibility) in the system of equations formed using the means of the identified parameters was more important than the accuracy of the approximation of each term.

The conclusion is that statistical improvement in system identification from test data can be achieved by using the mean mobility data from replicated tests. The averages of the identified parameters from many tests should not be used; the data from many tests should be averaged and one set of consistent parameters identified using the averaged data.

REPRODUCTION OF RESPONSE

For an identification process to be satisfactory as an engineering tool, the equations of motion formed from the identified parameters should, when solved, yield a mobility response that approximates the actual response of the helicopter. As noted above, parameters which are accurate are not necessarily consistent. Only a consistent set of identified parameters will yield the mobility responses from which they were obtained.

Figures 31 through 41 show the magnitudes of the identified parameters of two specific cases from the sample population of 25 cases used in generating the data of Figures 20 through 30. Figures 31 through 41 illustrate the parameter values that might be identified from two separate tests in which there is 8 percent random and bias error on amplitude and

2° random error on phase. These two sets of identified parameters were used as the parameters in the linear equations of motion to generate mobility frequency responses. Figure 42 shows how closely each of these cases, along with a third case, approximates the exact response of the hub station to an excitation at the hub. It is interesting to note that gross differences in the identified values of off-diagonal stiffness terms, such as in Column One (Figure 32) or in Column Five (Figure 36), do not have a detectable effect on the mobility response of Figure 42.

The accuracy of the responses shown in Figure 42 for hub station driving point represents the sort of accuracy that has also been found for hub to pilot's seat responses. All the peaks and antiresonances evident in the exact response are evident in all the identified responses, and all occur at or very near the exact frequencies.

Figures 43 through 45 show the accuracy of response reproduction with three other levels of input data error from arbitrarily selected cases. The remarkably accurate reproduction of response for all levels of error from 2 percent to 10 percent indicates that the consistency of the identifications from individual tests is relatively insensitive to error.

Examination of this data leads us to the hypothesis that consistent, but inaccurate, identifications might be quite satisfactory for accurate predictions of the response of the helicopter to various forces and that consistency, rather than accuracy, of identified parameters might be the important factor in accurate determination of loads from accelerometer data on a mobility-calibrated aircraft.

When the identified parameters are used in equations of motion to reproduce the mobility response, the statistical distribution of mobility in values in the reproduced response is not the same as the distribution of error in the input, or measured, mobilities. Figures 46 through 53 show the error spread in the reproduced mobilities in comparison to the error spread in the corresponding measured mobilities, the latter of which is shown shaded. The sample population of mobility and phase consists of approximately 85 values of frequency across the spectrum.

Case 5C, for example, represents one test in which the measured mobilities are polluted with 5 percent bias error and $\pm$5 percent random error on absolute amplitude and $\pm$1° random error on phase. Figure 46 shows the distribution of amplitude error, at all measured frequencies, for the

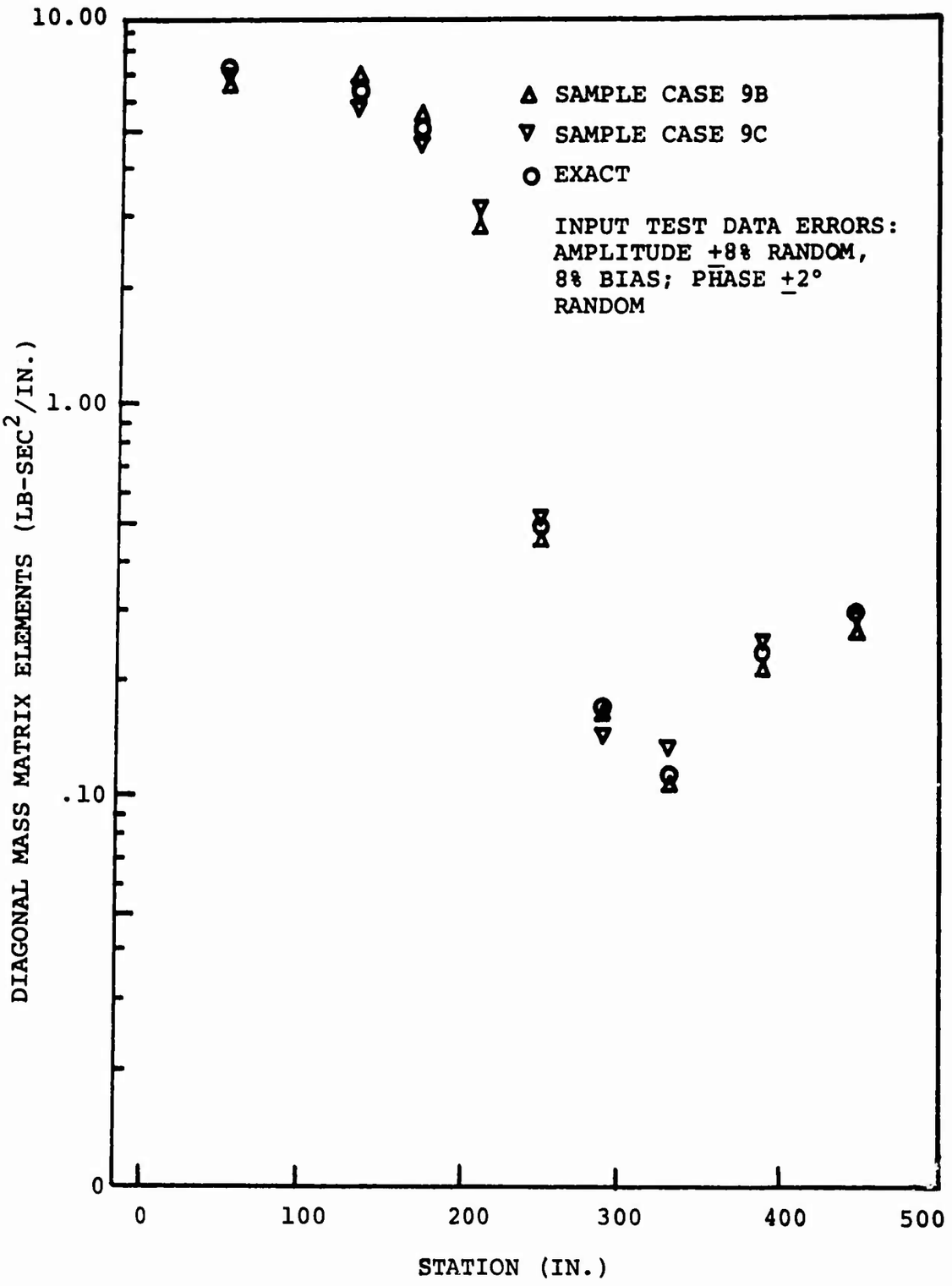

Figure 31. Two Sample Cases of Mass Identification.

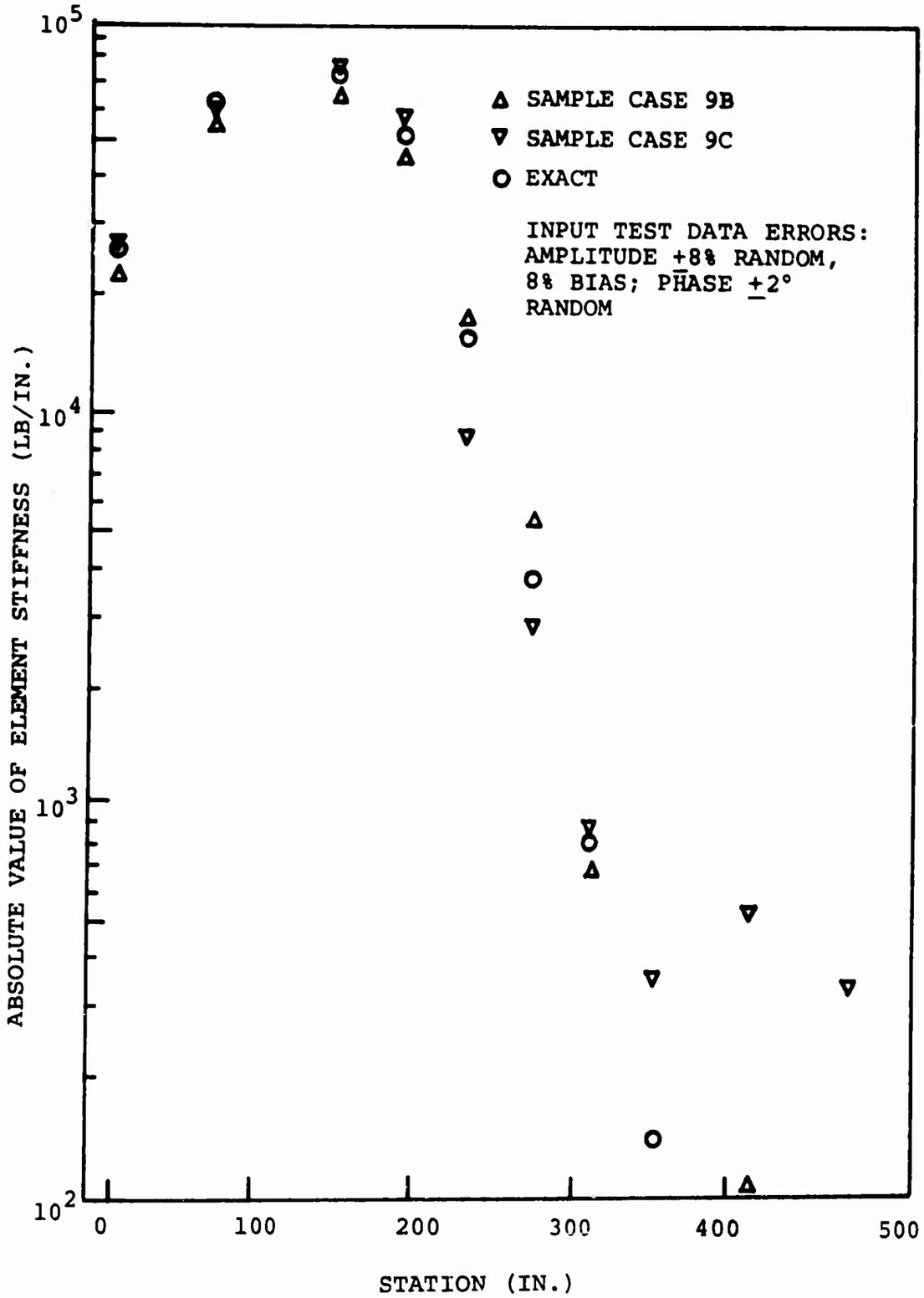

Figure 32. Two Sample Cases of Stiffness Identification. Column One.

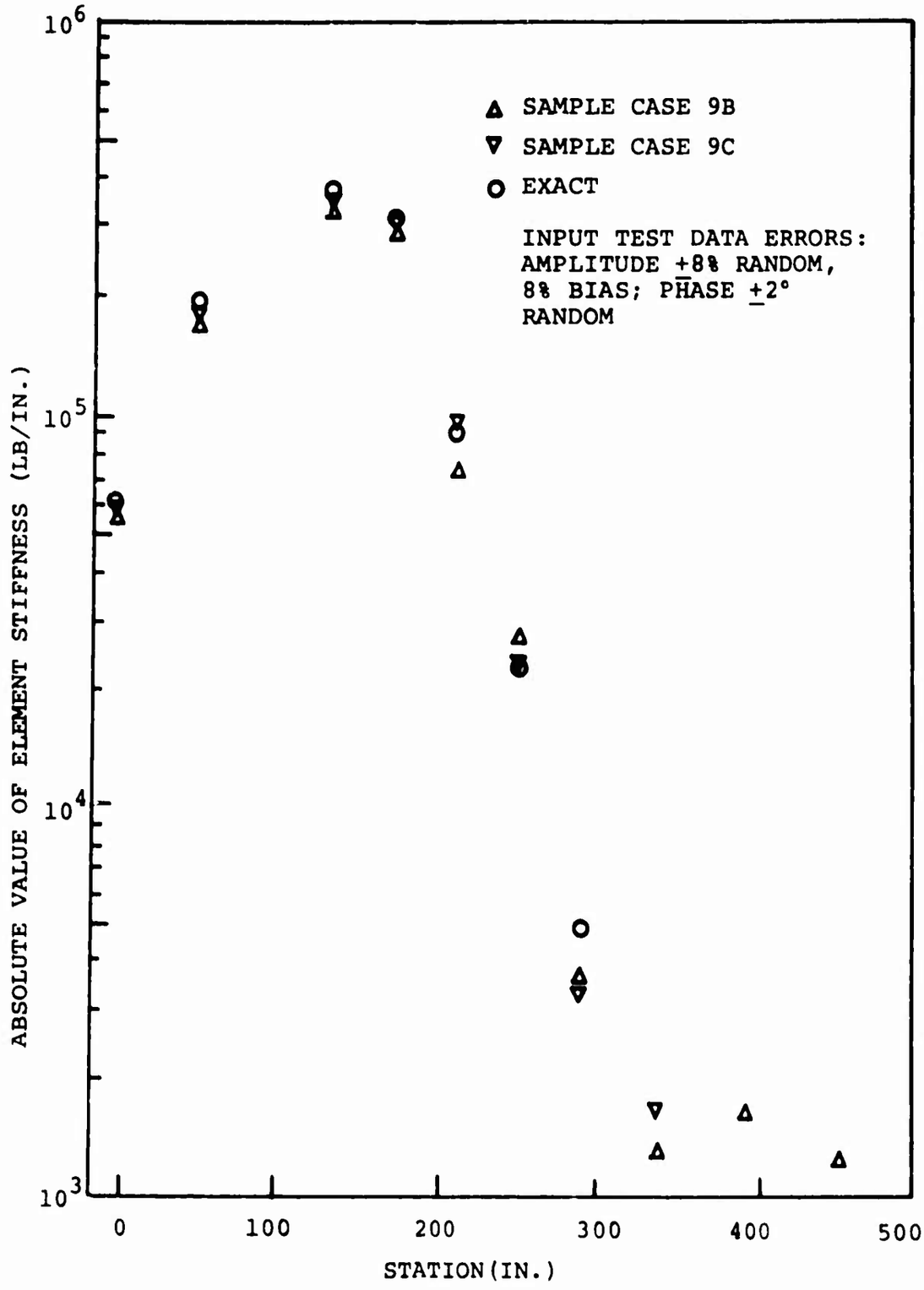

Figure 33. Two Sample Cases of Stiffness Identification. Column Two.

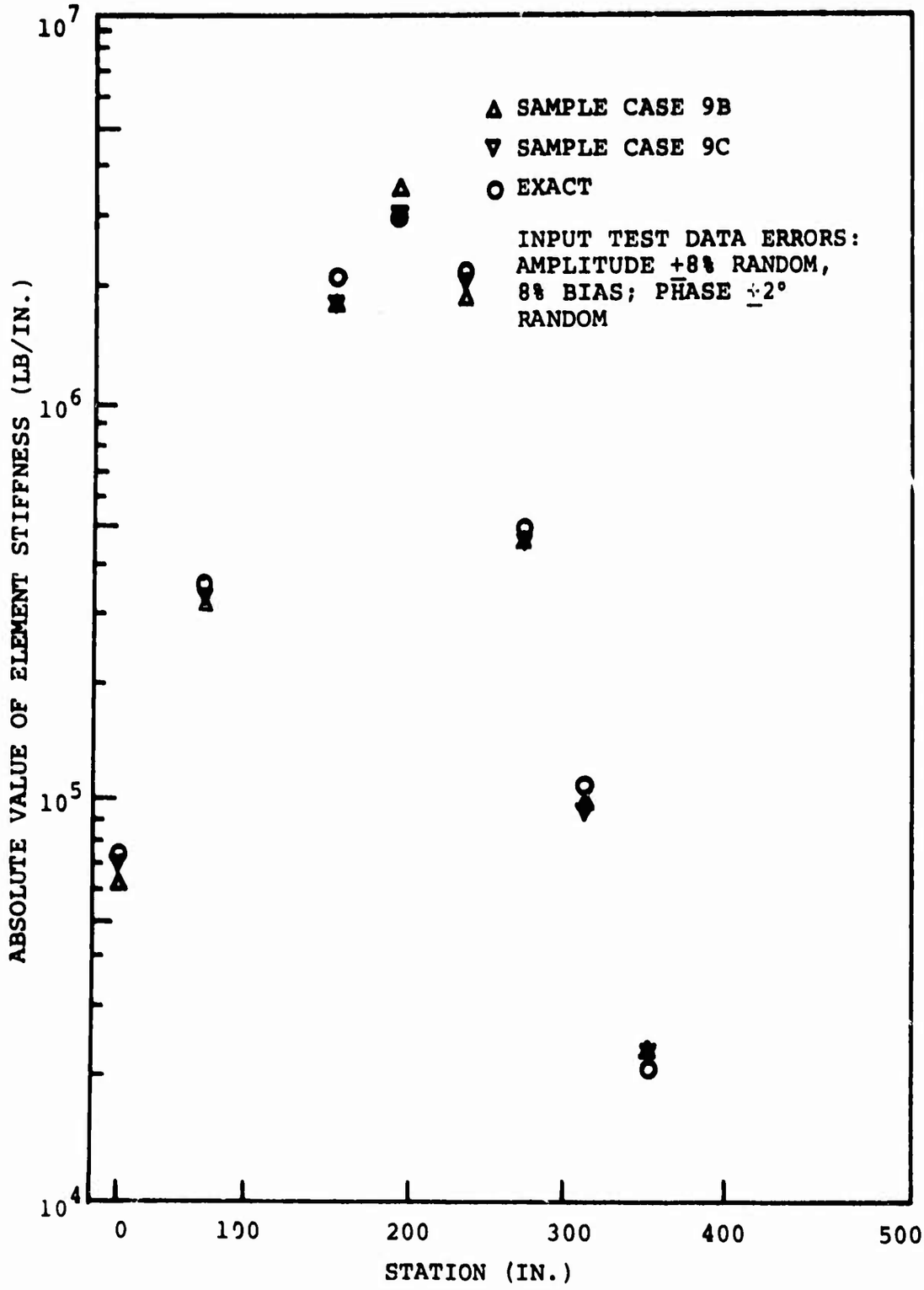

Figure 34. Two Sample Cases of Stiffness Identification. Column Three.

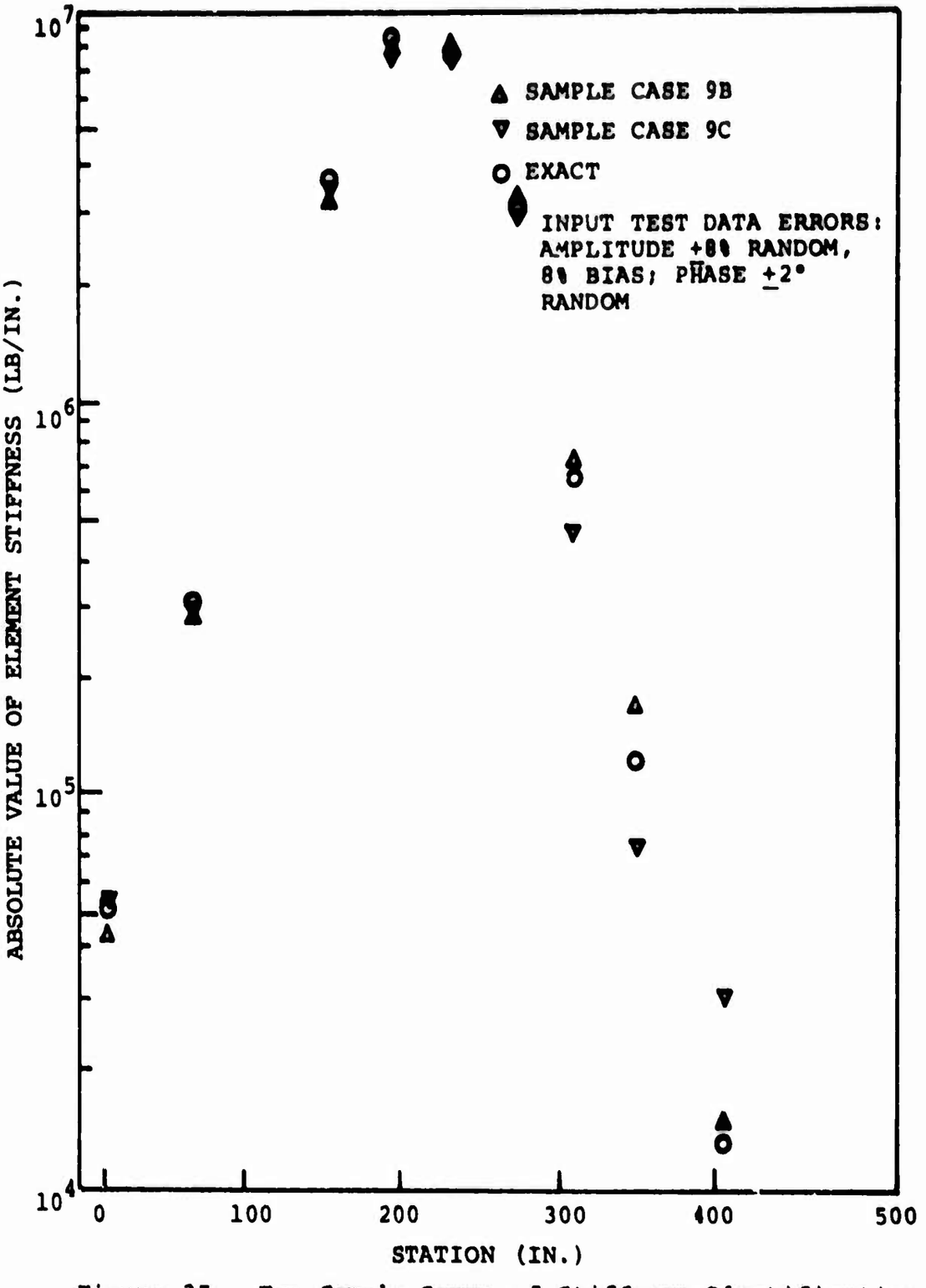

Figure 35. Two Sample Cases of Stiffness Identification. Column Four.

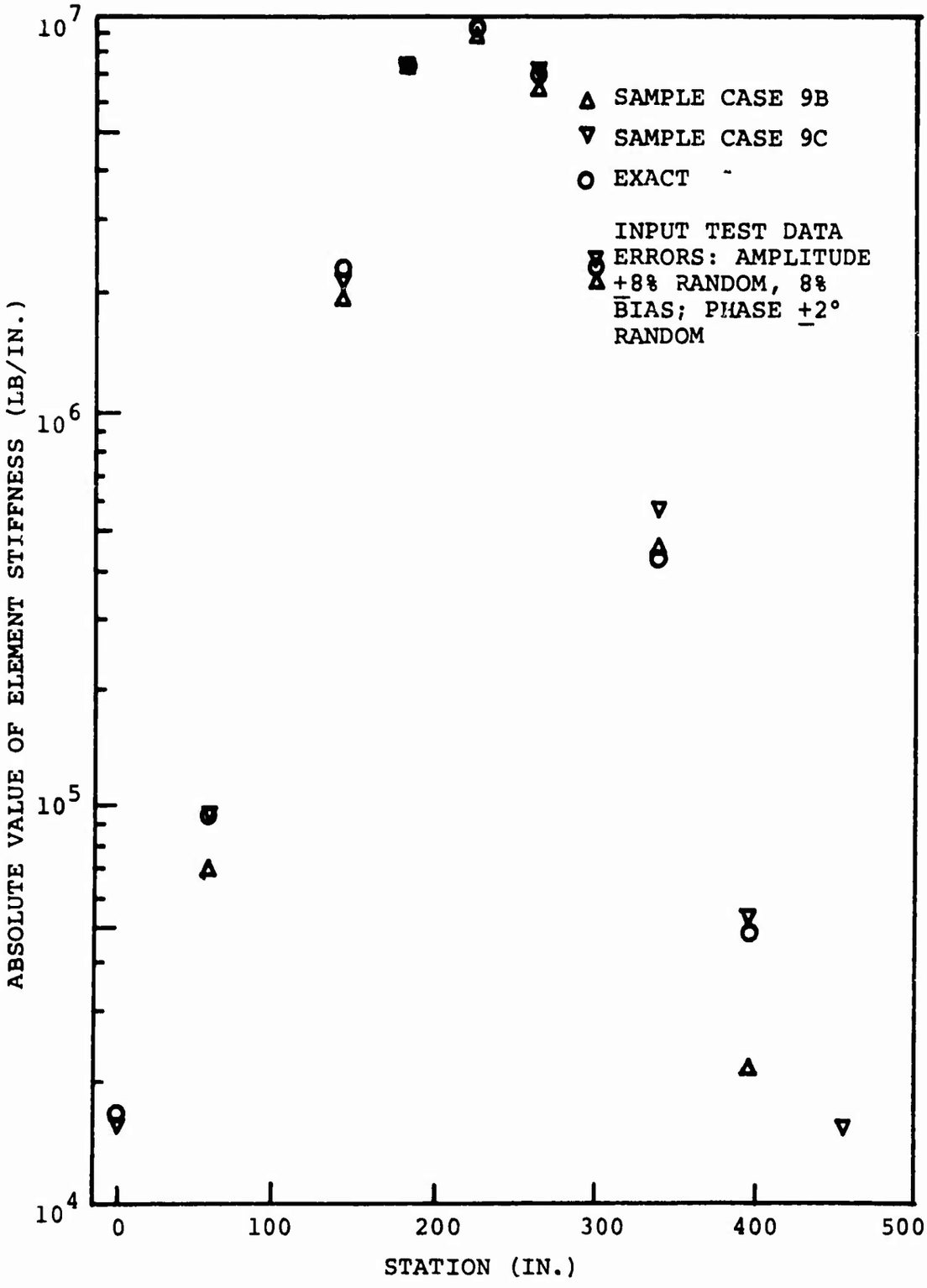

Figure 36. Two Sample Cases of Stiffness Identification. Column Five.

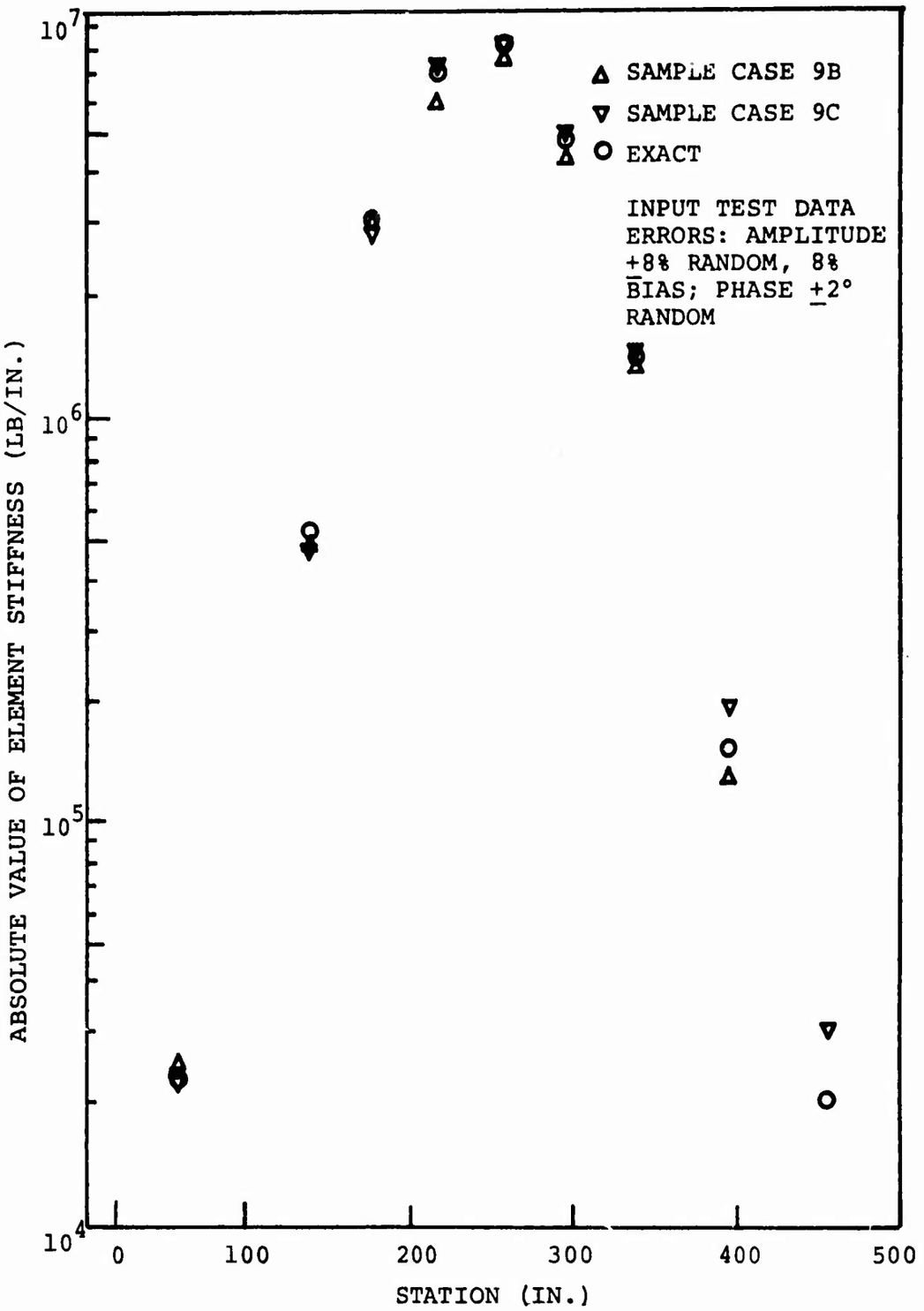

Figure 37. Two Sample Cases of Stiffness Identification. Column Six.

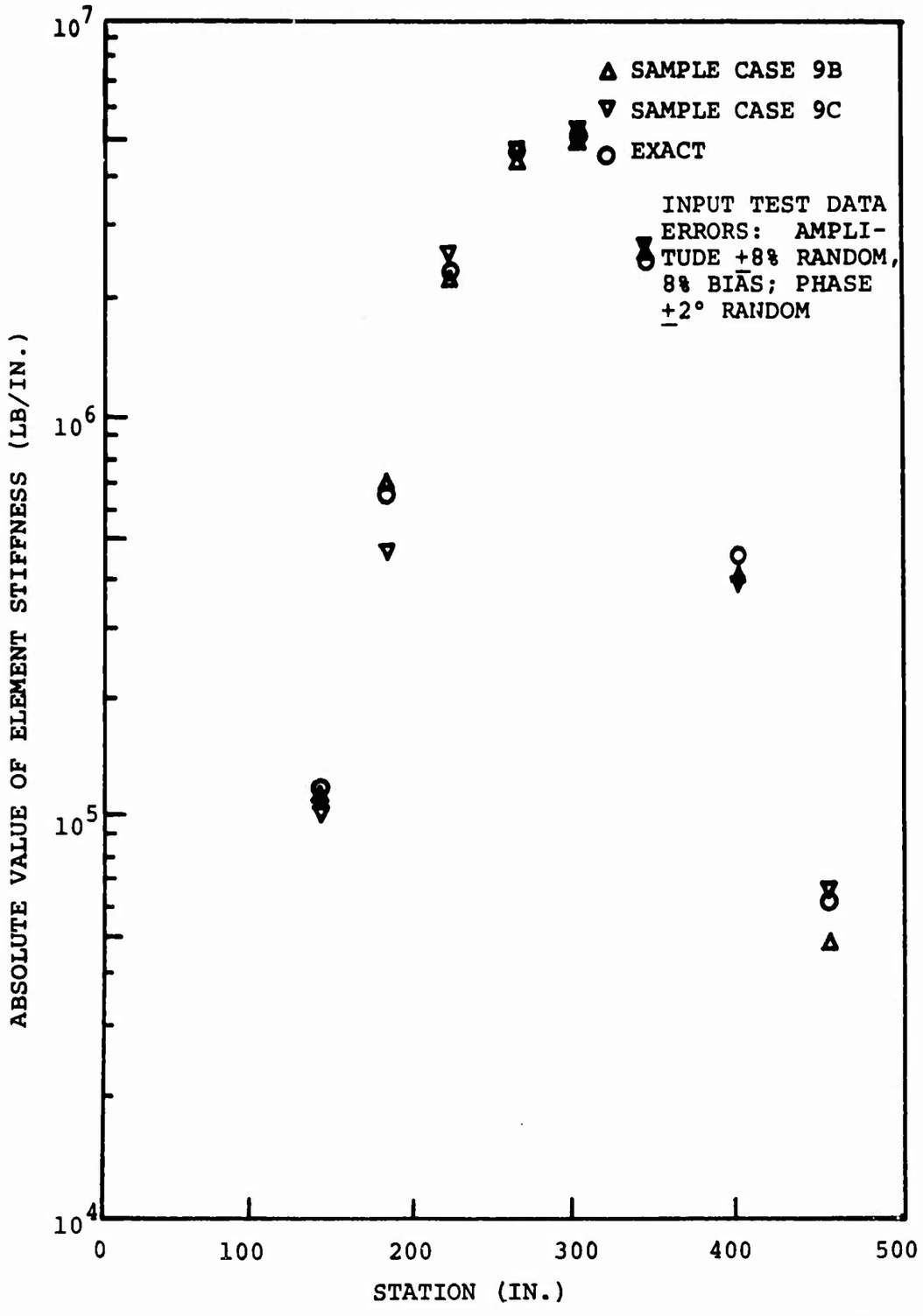

Figure 38. Two Sample Cases of Stiffness Identification. Column Seven.

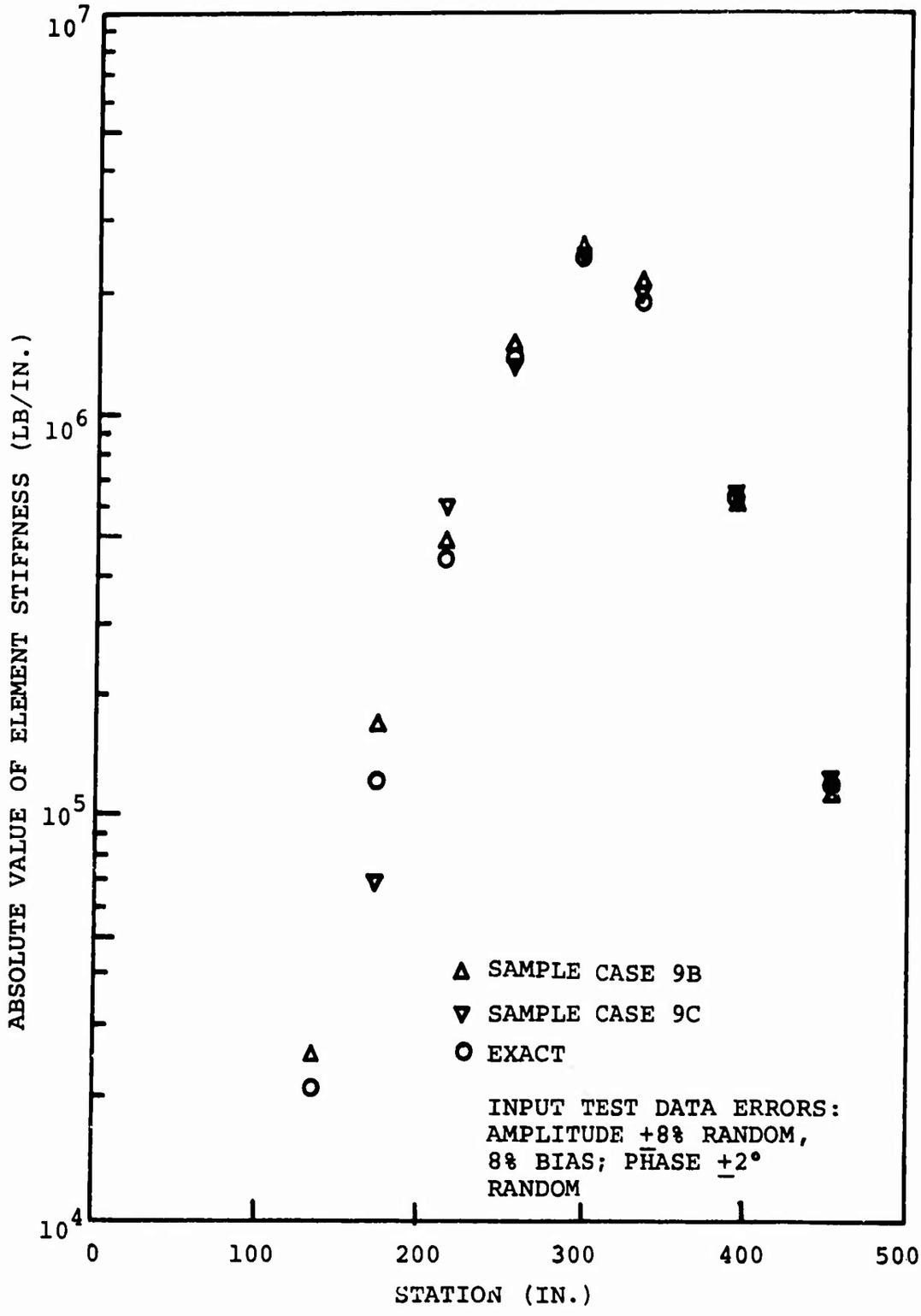

Figure 39. Two Sample Cases of Stiffness Identification. Column Eight.

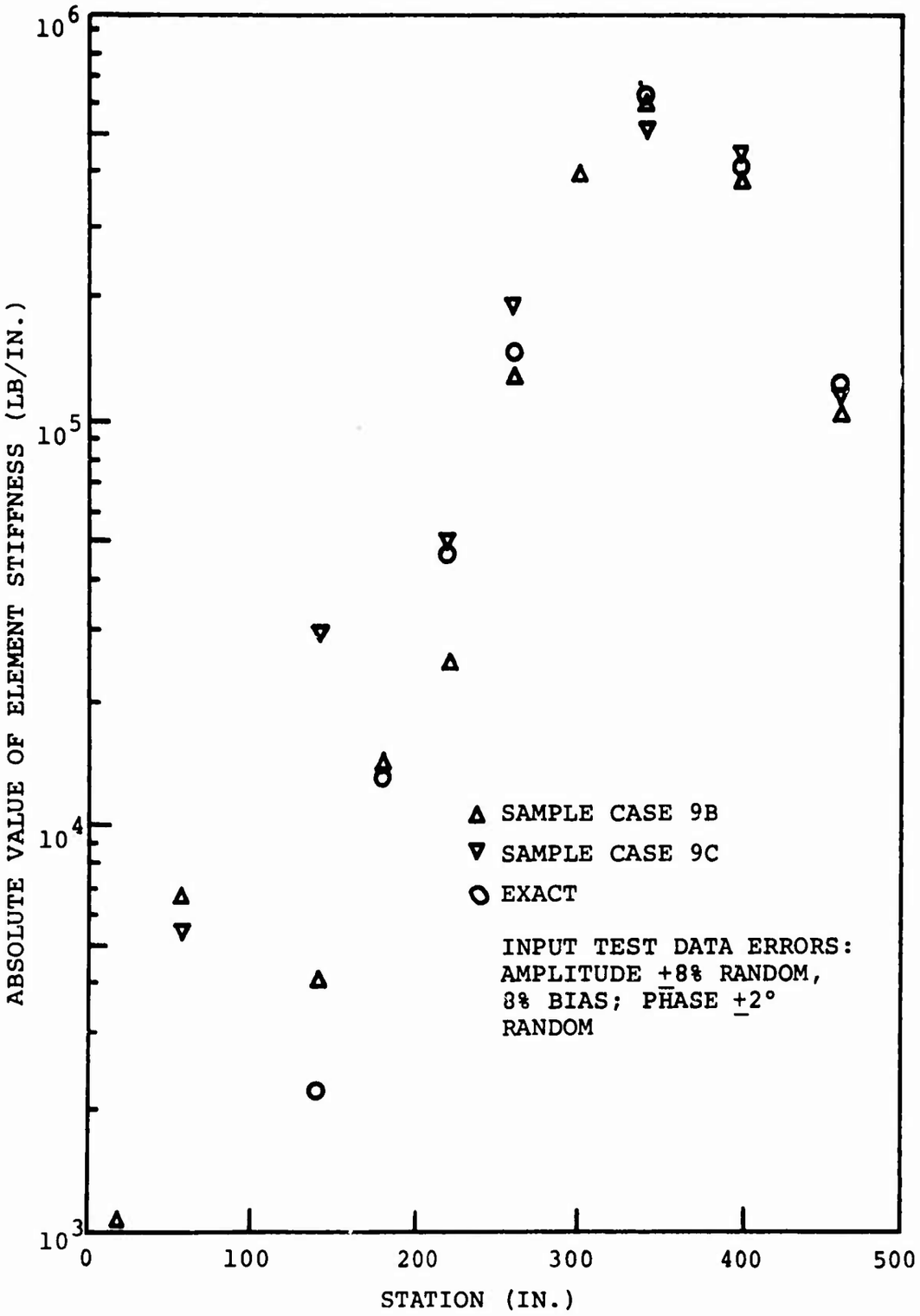

Figure 40. Two Sample Cases of Stiffness Identification. Column Nine.

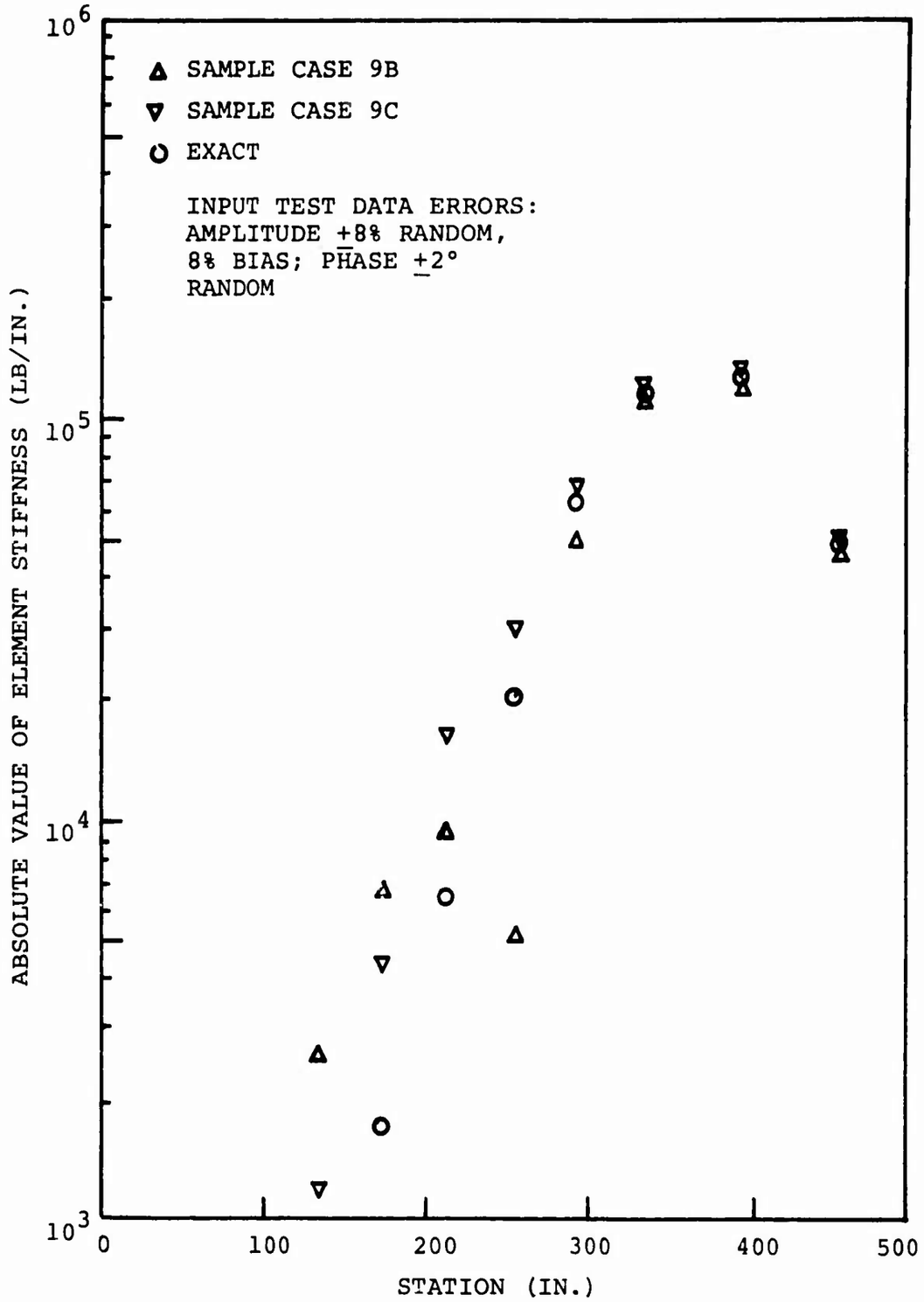

Figure 41. Two Sample Cases of Stiffness Identification. Column Ten.

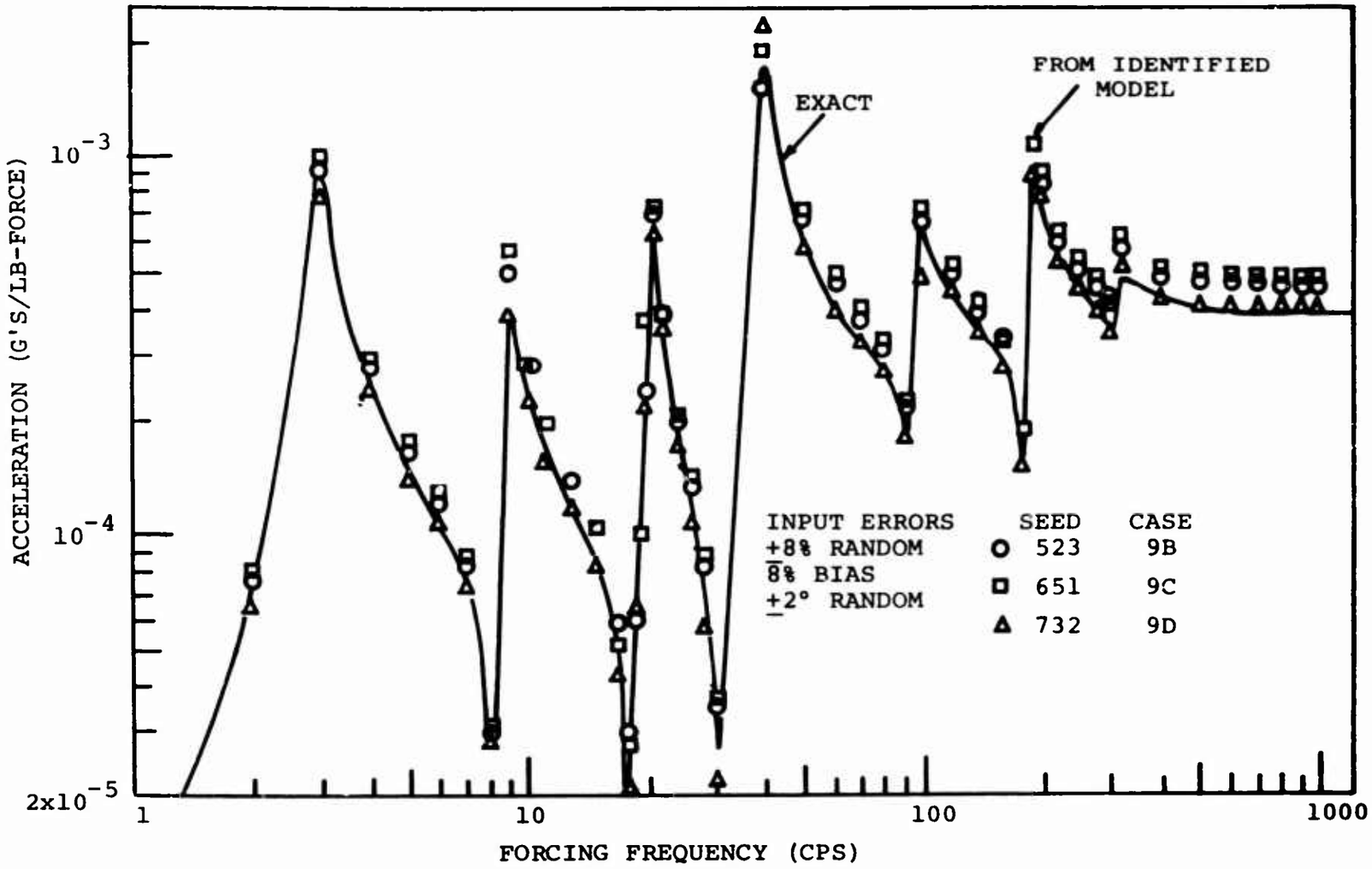

Figure 42. Response Obtained From Equations With Identified Parameters. Driving Point at Hub.

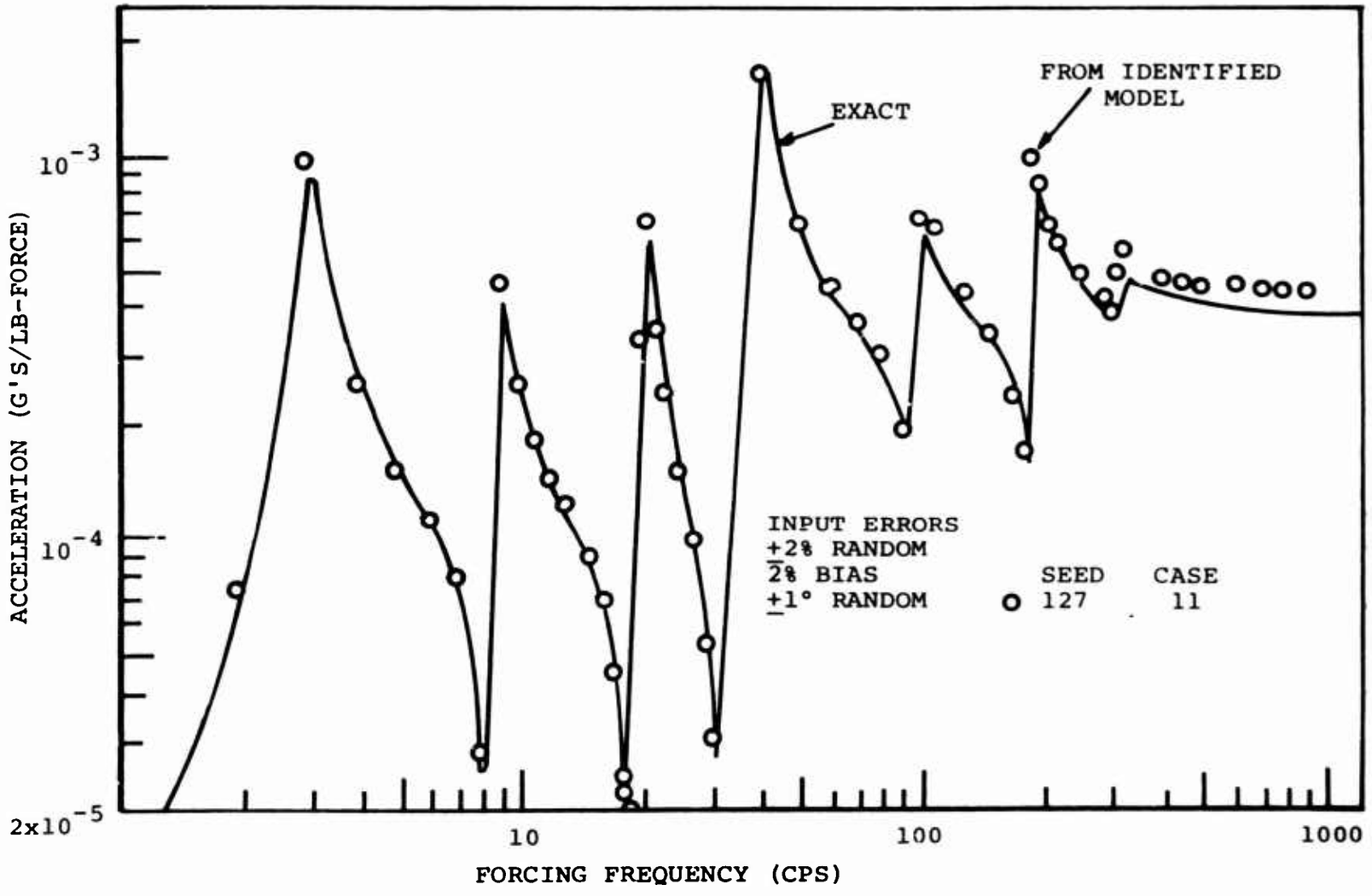

Figure 43. Response Obtained From Equations With Identified Parameters. Driving Point at Hub.

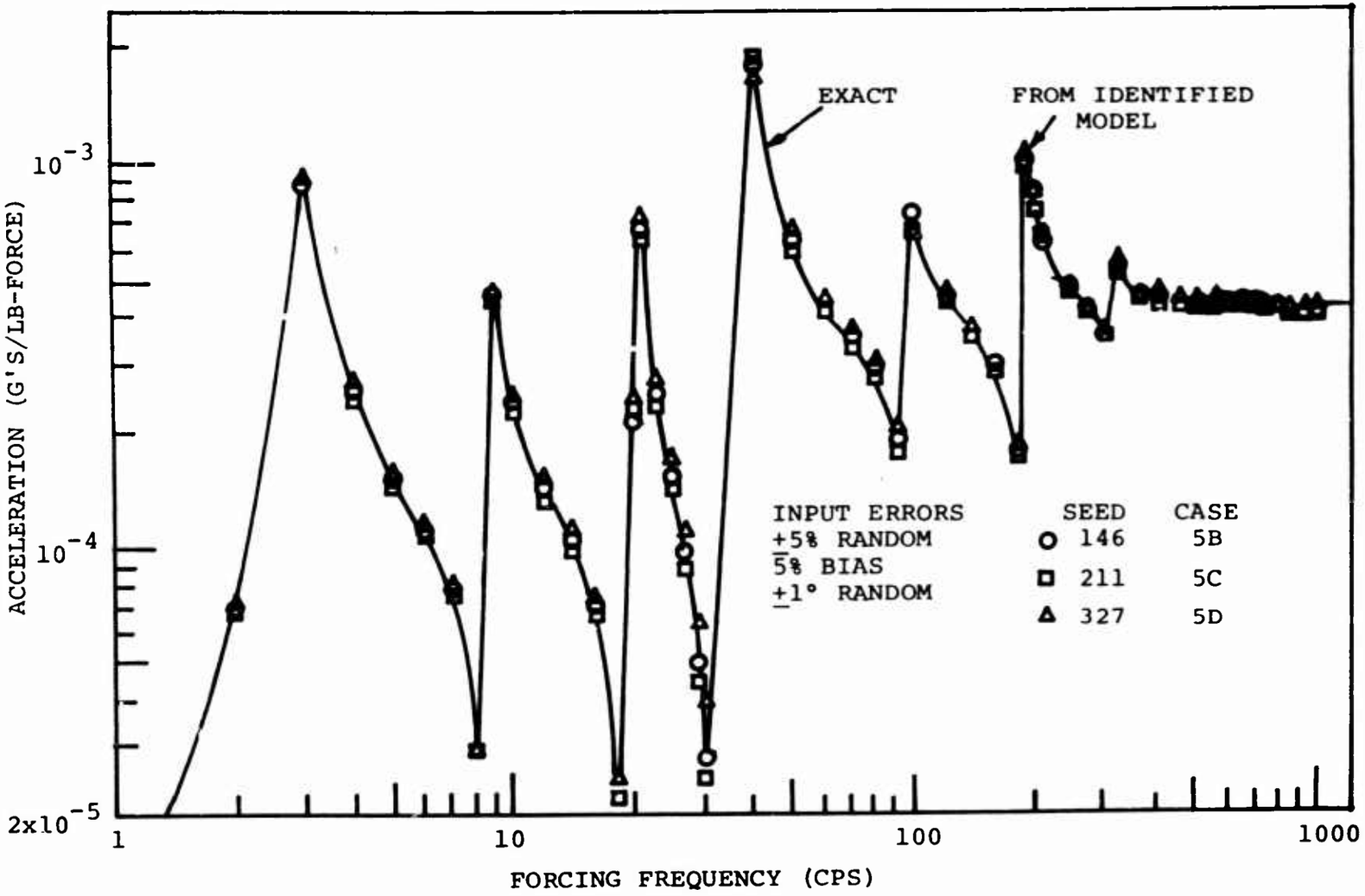

Figure 44. Response Obtained From Equations With Identified Parameters. Driving Point at Hub.

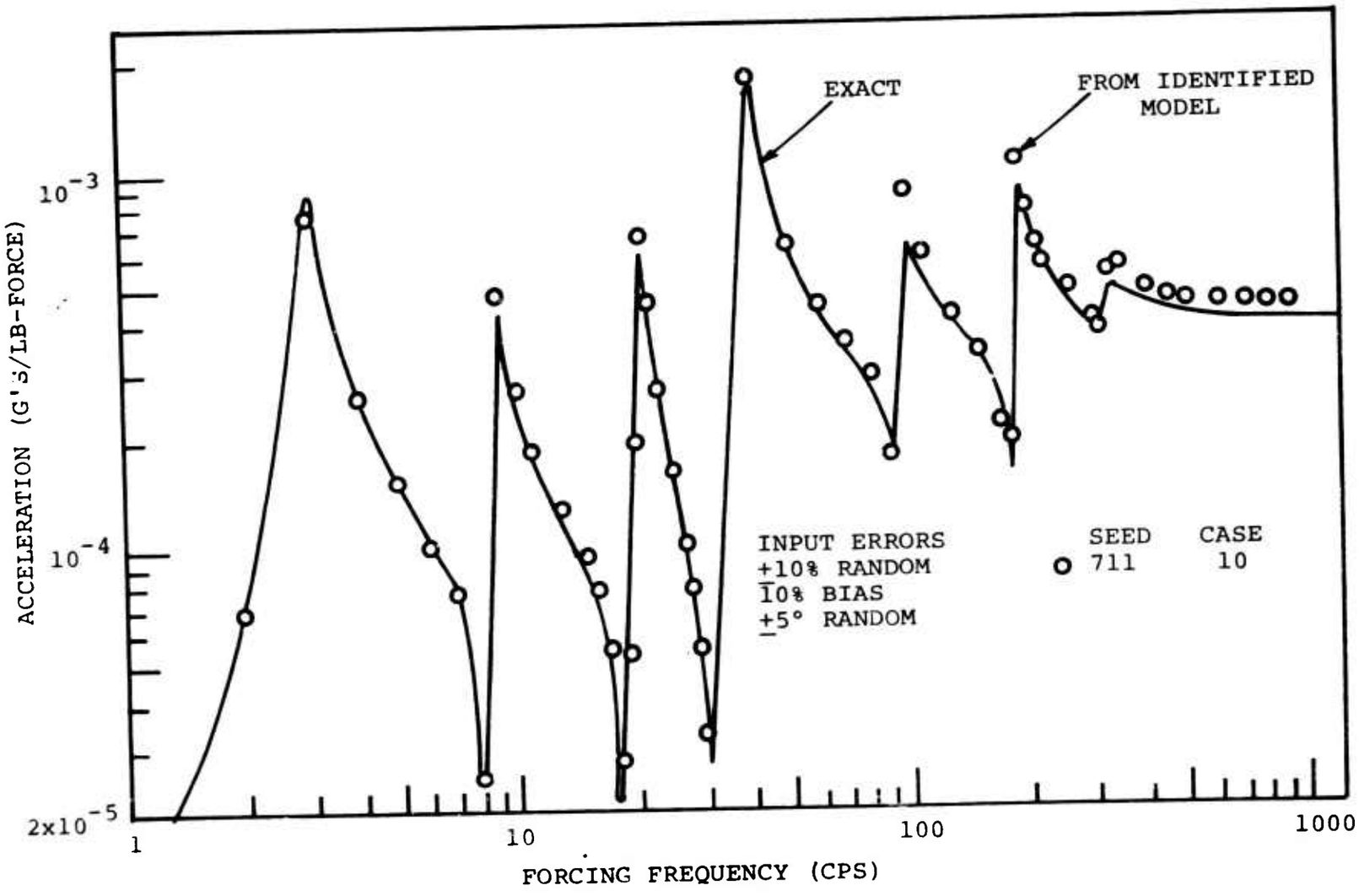

Figure 45. Response Obtained From Equations With Identified Parameters. Driving Point at Hub.

amplitude at the hub station due to forcing at the hub station in this one simulated test and rerun of the identified equations. Figure 47 shows the distribution of phase error for the same case.

Figures 50 through 53 display the data for response at the pilot seat station due to forcing at the hub station.

In general, there is a greater central tendency in the reproduced response than in the measured input data. This is a result of the averaging effect of the identifier. In Figures 46 and 50, the bias effect is noticeably diminished in the rerun distribution. The greater spread in the rerun error results, of course, from the fact that the measured data has "white" random spread between absolute limits while the rerun data is spread in a more Gaussian-like manner. The mode of the rerun mobilities is closer to the actual value than the bias of the input in Figures 46 and 50 and no worse than the bias in Figures 48 and 52.

It is practical to use the mean of the mobilities determined by rerunning each of many identifications and, as noted previously, practical to make one identification from the mean of measured mobilities. However, as previously discussed, it is not practical to operate with the mean of identified parameters. Averaging mobilities is beneficial; averaging parameters is not.

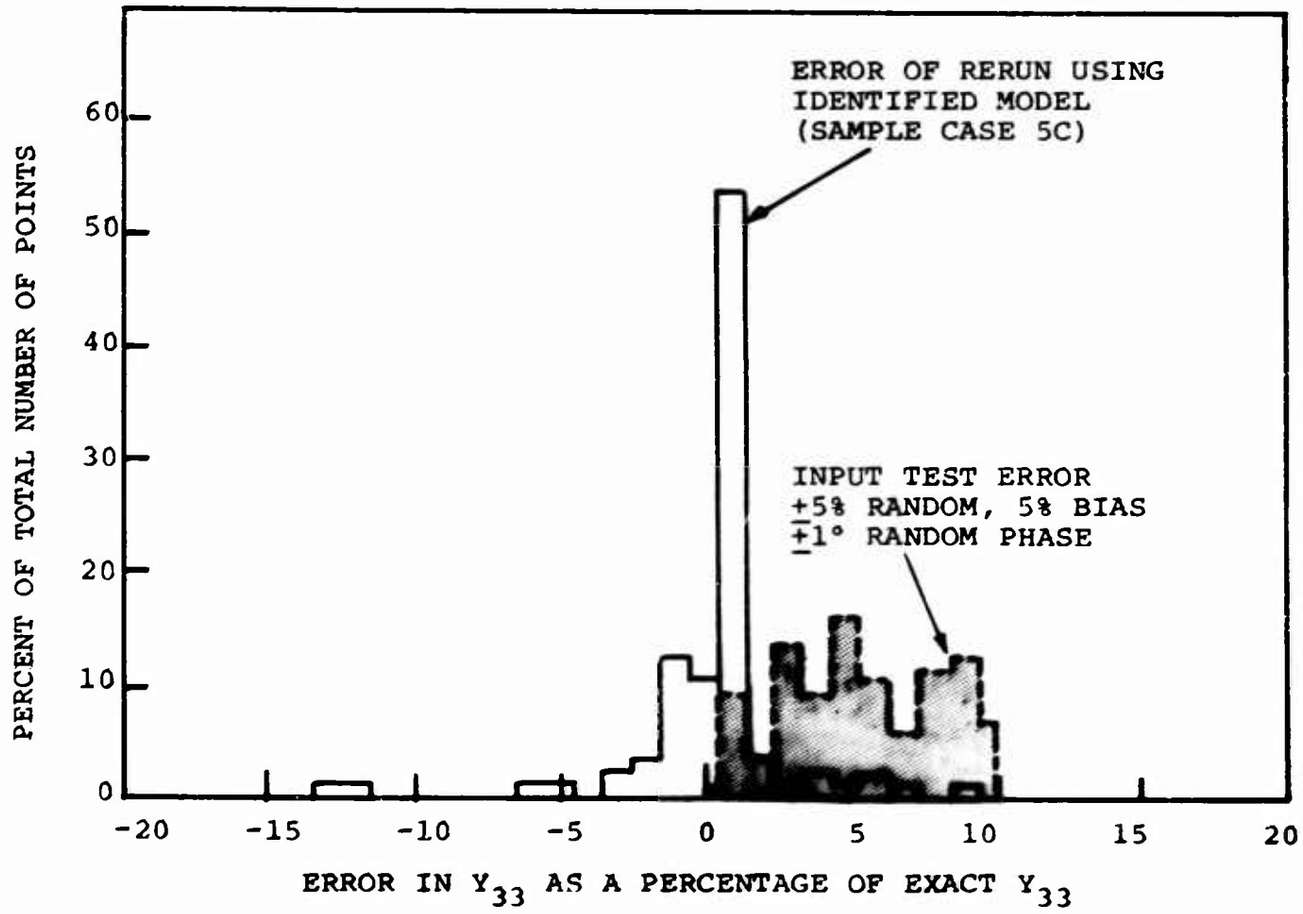

Figure 46. Error in Rerun Response at Hub Versus Error in Input Data.

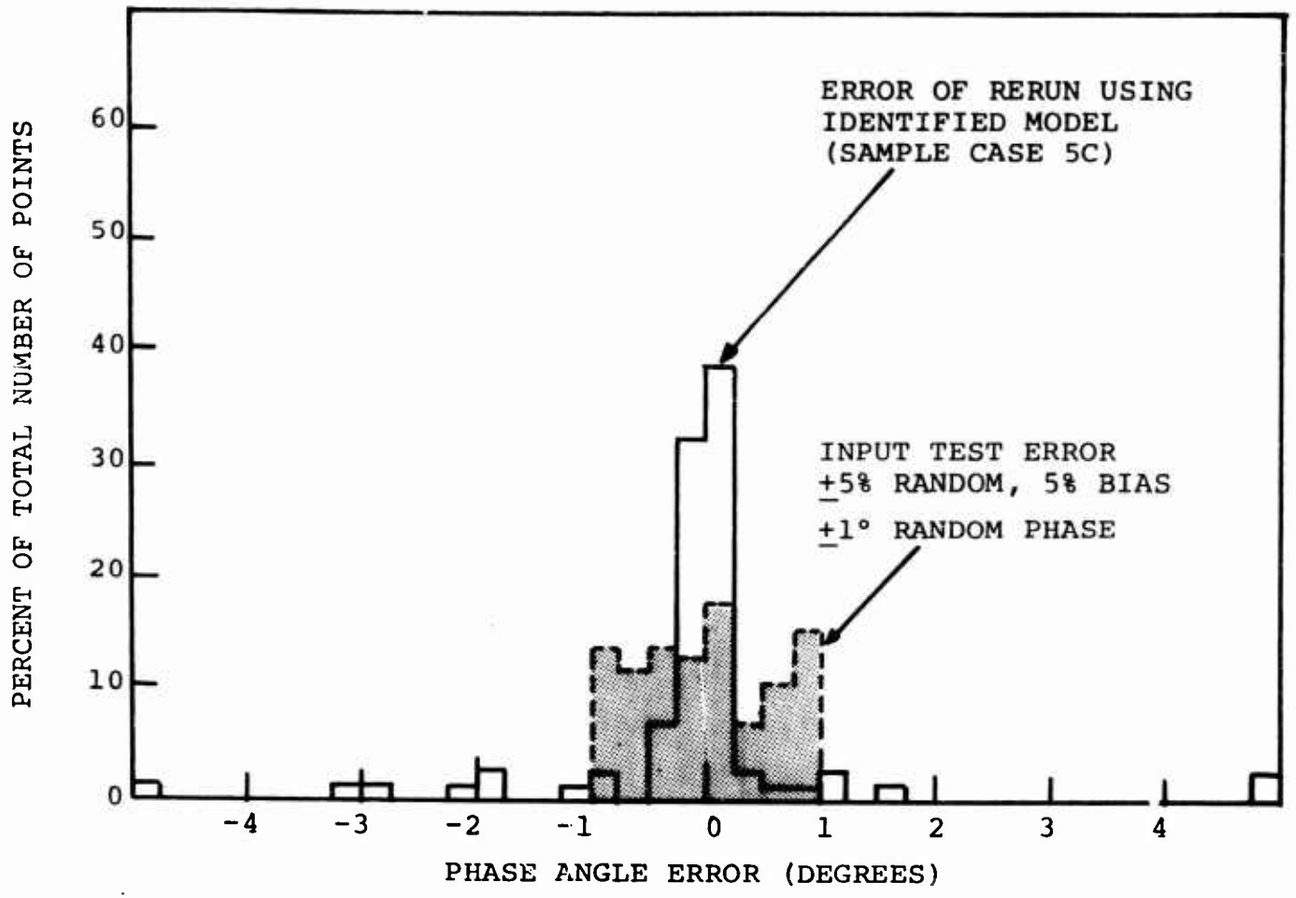

Figure 47. Error in Rerun Response at Hub Versus Error in Input Data.

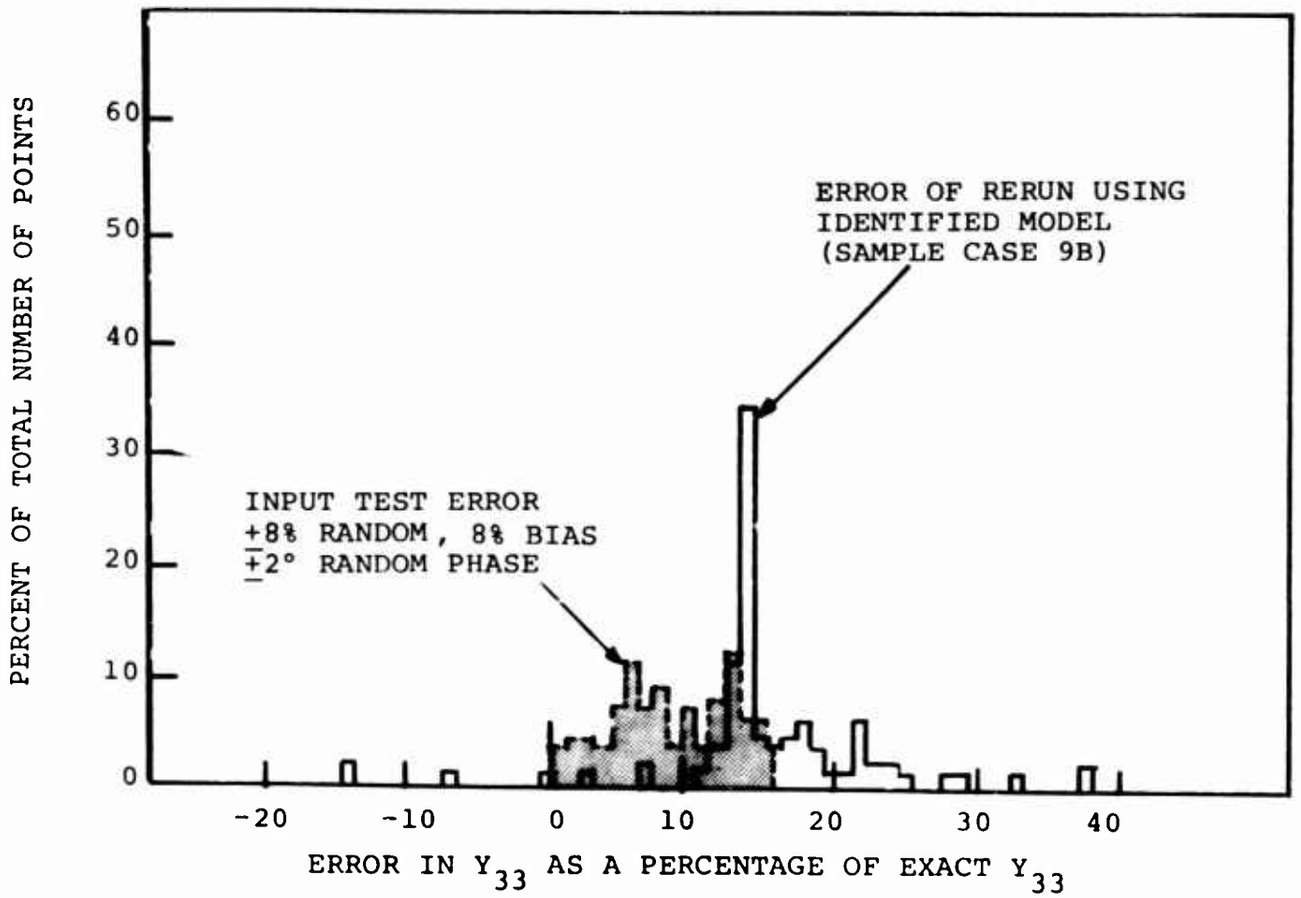

Figure 48. Error in Rerun Response at Hub Versus Error in Input Data.

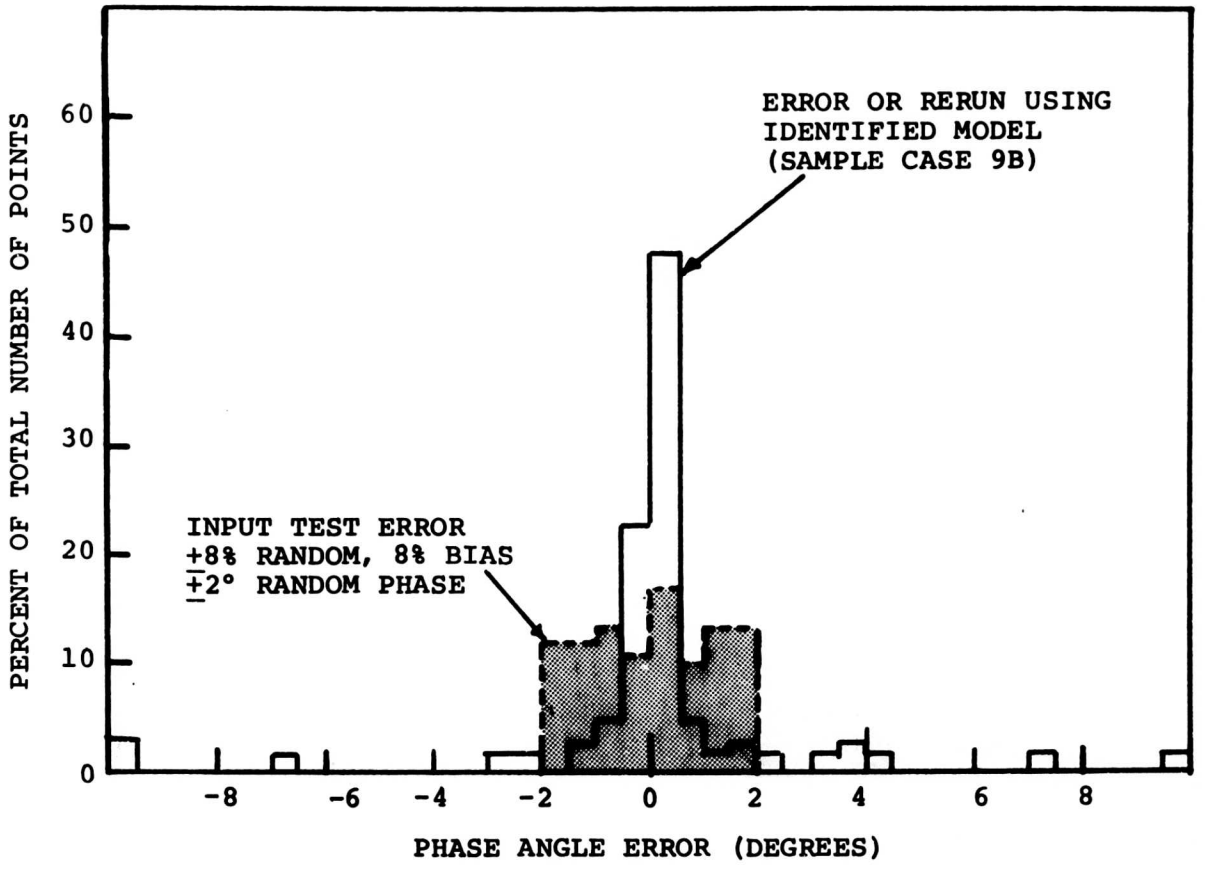

Figure 49. Error in Rerun Response at Hub Versus Error in Input Data.

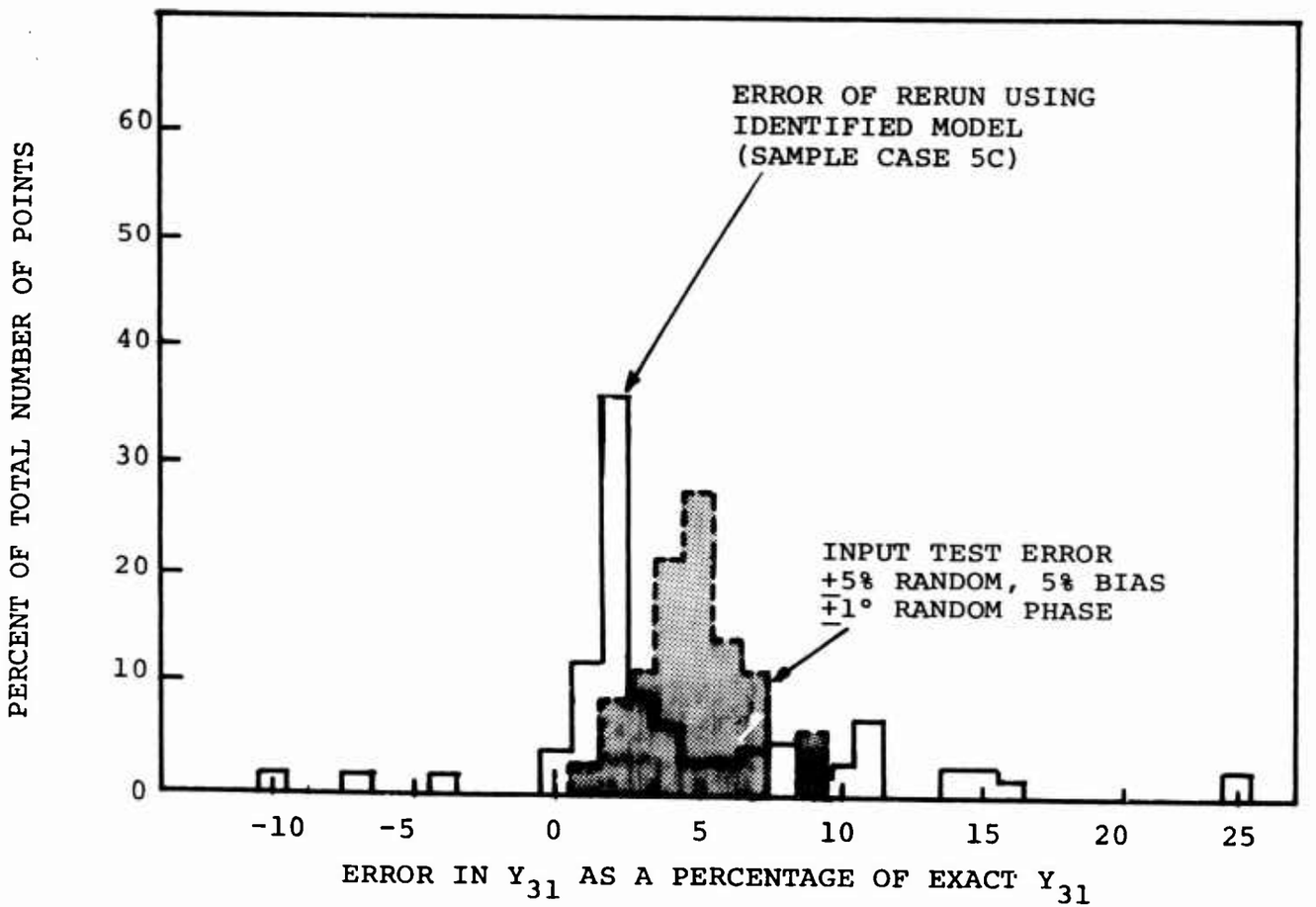

Figure 50. Error in Rerun for Response at Pilot's Seat Due to Force at Hub Versus Error in Input Data.

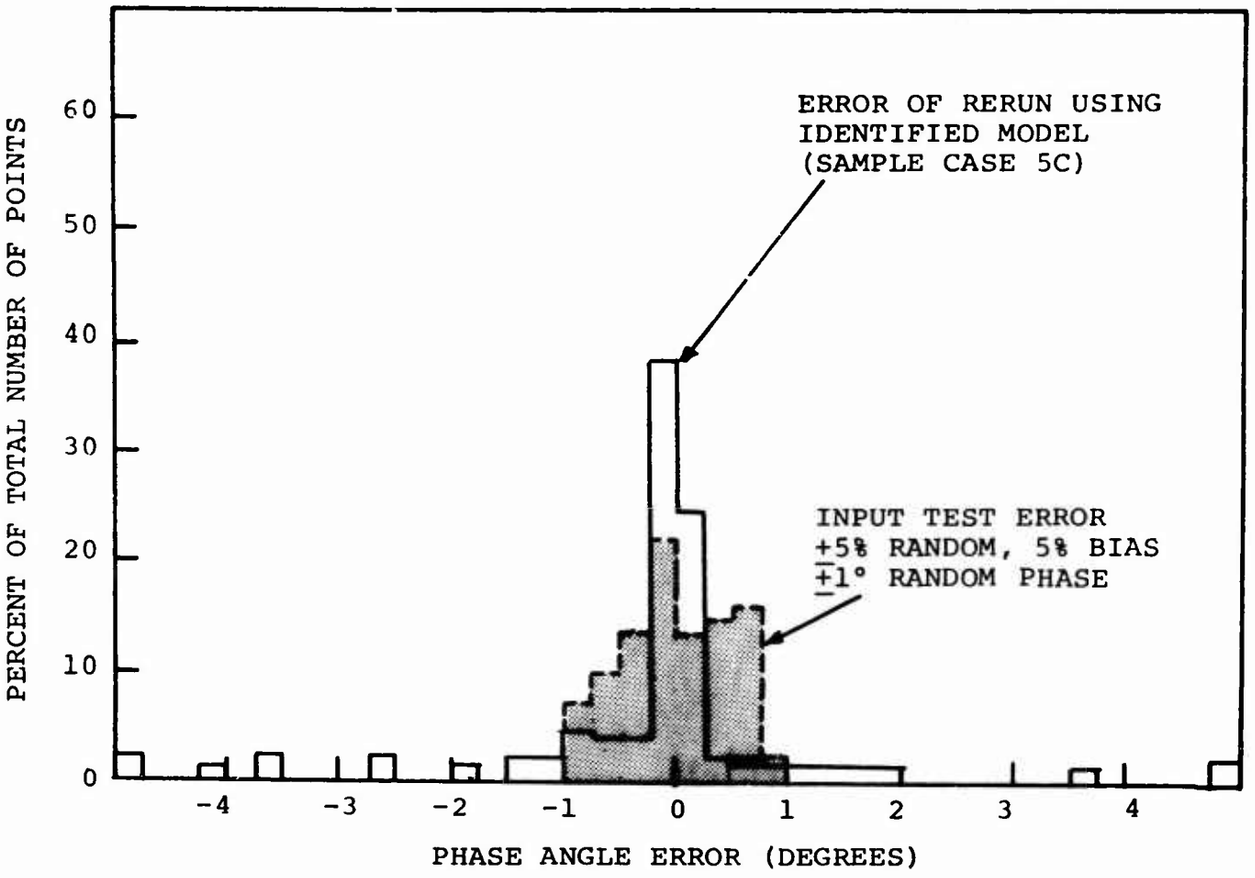

Figure 51. Error in Rerun for Response at Pilot's Seat Due to Force at Hub Versus Error in Input Data.

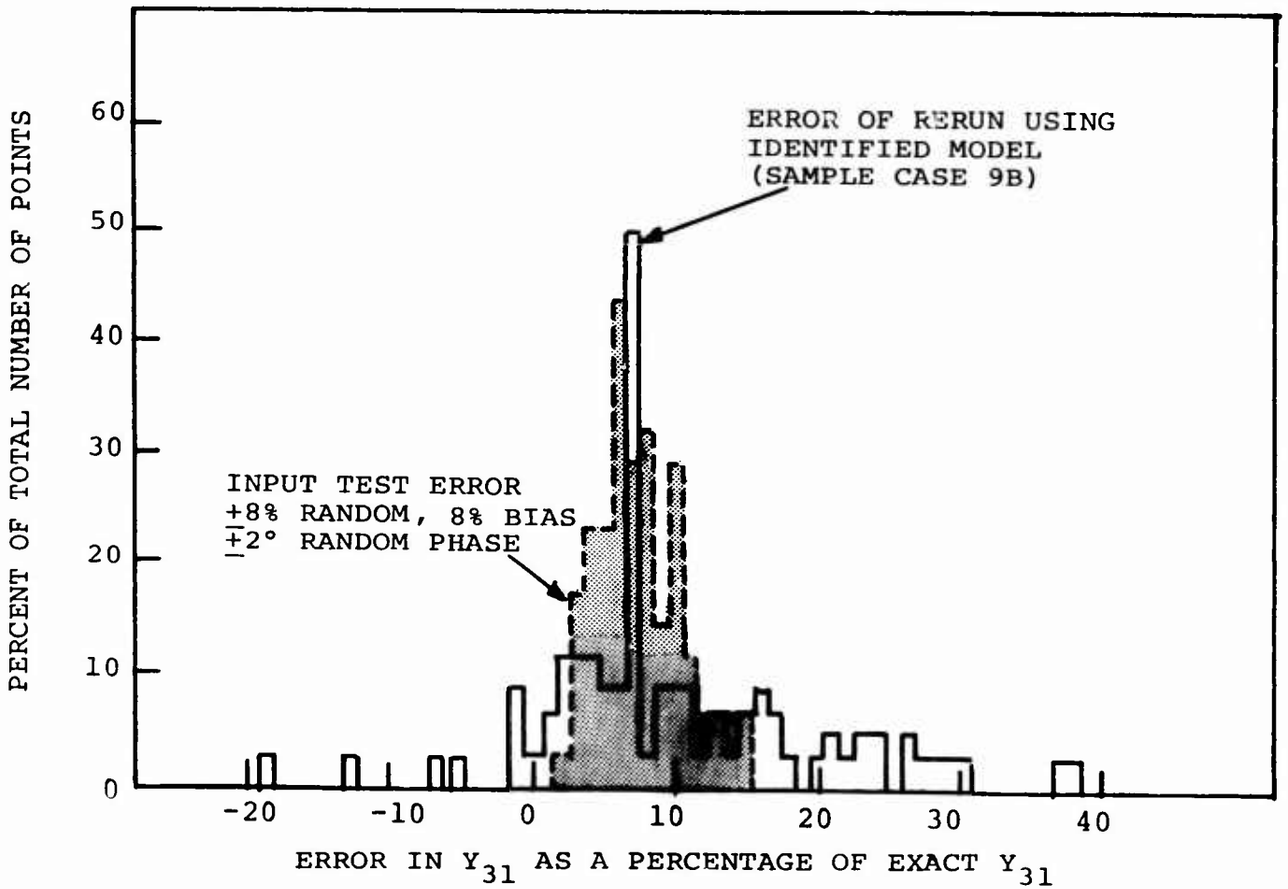

Figure 52. Error in Rerun for Response at Pilot's Seat Due to Force at Hub Versus Error in Input Data.

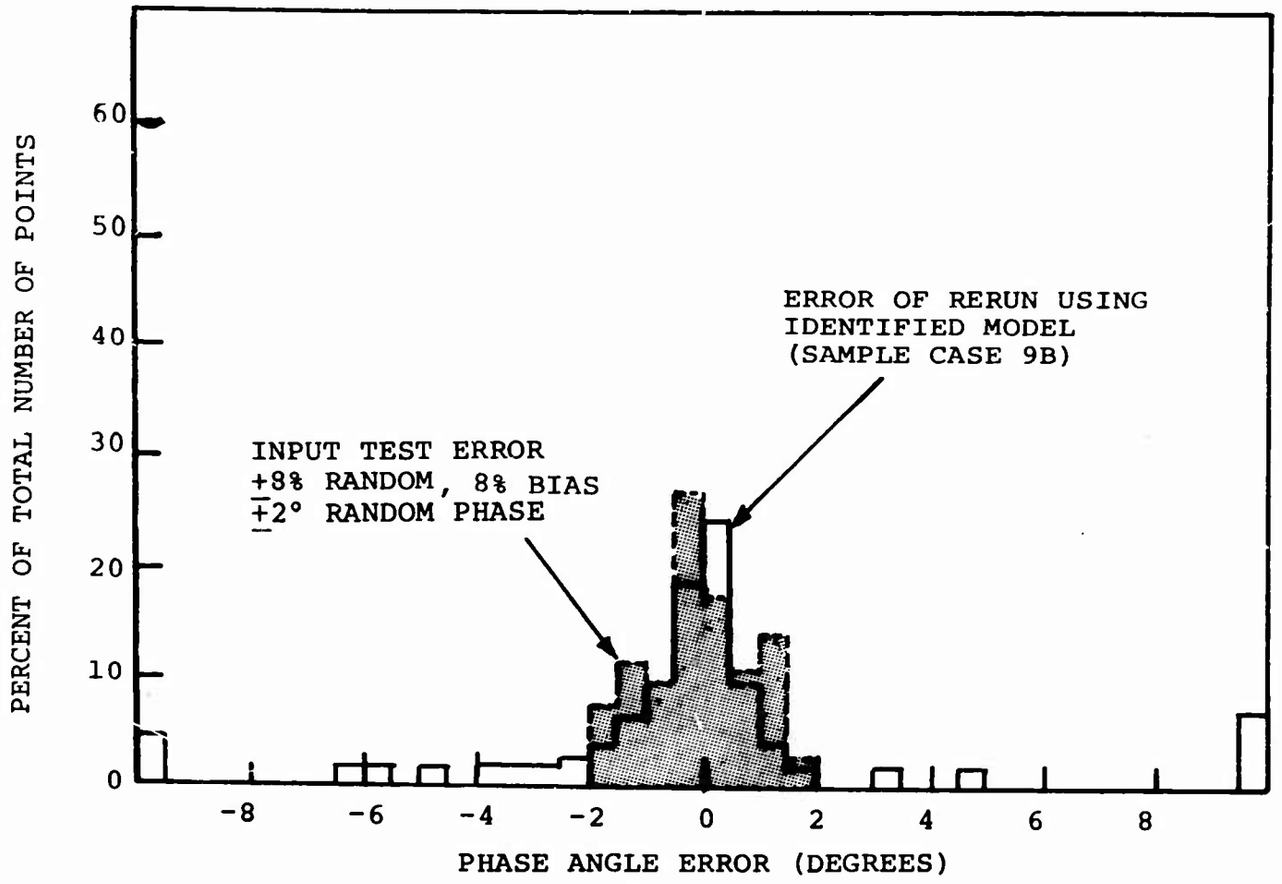

Figure 53. Error in Rerun for Response at Pilot's Seat Due to Force at Hub Versus Error in Input Data.

ADDITIONAL OBSERVATIONS

SWEEPING OUT THE DOMINANT MODE

Equation (20) describes a method of removing the dominant mode from the mobility eigenvalue equation, Equation (17), so that iteration will converge on the next most dominant mode. It is not necessary to use Equation (20) in a practical helicopter situation because mobilities will be measured throughout the frequency spectrum and, as demonstrated, each mode will be dominant at some frequency even if the driving point mobility shows no peak in that frequency band.

Equation (20) was, however, experimented with in the computer experiments and, as expected, the accuracy of the second most dominant mode calculation was substantially worse than the calculation of the dominant mode. It was judged that reasonable measurement errors in the mobility matrix would make calculations of successively less dominant modes than the dominant and second dominant numerically impractical.

Additional complications attended using Equation (20) for the second dominant mode. In whatever sequence the calculations proceed regarding frequency, there is quite a good chance that the second dominant mode at any frequency is a mode which was already calculated as the dominant mode in a previous calculation rather than being the nearest uncalculated mode. At frequencies "between modes" where dominance is seriously confounded by measurement errors, wild variations may be found in the calculated values of the second dominant mode.

Because the use of Equation (20) is unnecessary, and because of the confusion that might result from such calculations, Equation (20) was not used in the identification process in the computer experiments. The numerical results of computer experiments on Equation (20), being of no value to the engineering implementation of the theory, are not presented in this report.

DETERMINATION OF MODE SHAPES

Using Only Mobilities

It was mentioned in the Derivation of the Modal Eigenvalue Problem that iteration on the transpose of Equation (16) converges on the normal mode eigenvector. The normal modes are not used in this theory of identification; therefore,

none were calculated in the computer experiments. However, the accuracy with which the normal modes could be calculated, using the transpose of Equation (16), should be the same as that attending the calculation of the gamma vectors. As can be seen from Figures 5 through 14, a high degree of accuracy can be achieved allowing the assumptions upon which this study is based.

With Known Masses or Stiffnesses

There are situations in helicopter engineering in which the analyst has a legitimately high degree of confidence in the a priori determination of either stiffness or mass. For example, in a very light structure containing many highly concentrated loads which can be weighed on a scale (such as many widely separated packages of heavy, concentrated electronic gear in a structurally light boom), the engineer can rely reasonably well on the lumped mass matrix obtained from Weights Department data. In other situations, a very reliable stiffness distribution might be available from use of an advanced finite element technique (such as the generalized quadrilateral technique used on homogeneous bodies of revolution like long tapered shafts) while the mass is clearly distributed, leaving the accuracy of the lumped mass matrix questionable.

When either the mass or the stiffness matrices are so reliable that the parameter can be considered "known", then the engineer can obtain either the dominant gamma vector or normal mode vector from the mobility matrix without obtaining a mobility matrix measurement at any other frequency.

From Equation (15),

$$[Y^{R}_{(\omega)}] = \sum_{i=1}^{N} Y^{*R}_{i(\omega)} \{\phi\}_i \{\phi\}^{T}_i \qquad (15)$$

and from Equation (31),

$$[m] = \sum_{i=1}^{N} \mathcal{M}_i \{\gamma\}_i \{\gamma\}^{T}_i \qquad (31)$$

Postmultiplying Equation (15) by Equation (31) gives

$$[Y^{R}_{(\omega)}][m] = \sum_{i=1}^{N} \mathcal{M}_i Y^{*R}_{i(\omega)} \{\phi\}_i \{\gamma\}^{T}_i \qquad (40)$$

Therefore,

$$[Y^{R}_{(\omega)}][m]\{\phi\}_k = \mathcal{M}_k Y^{*R}_{k(\omega)}\{\phi\}_k \tag{41}$$

The left-hand eigenvector of Equation (40) is obtained by iteration on the transpose.

$$[m][Y^{R}_{(\omega)}]\{\gamma\}_k = \mathcal{M}_k Y^{*R}_{k(\omega)}\{\gamma\}_k \tag{42}$$

It is therefore also easily seen that

$$[Y^{I}_{(\omega)}][m]\{\phi\}_k = \mathcal{M}_k Y^{*I}_{k(\omega)}\{\phi\}_k$$

$$[m][Y^{I}_{(\omega)}]\{\gamma\}_k = \mathcal{M}_k Y^{*I}_{k(\omega)}\{\gamma\}_k$$

$$[Y^{I}_{(\omega)}][k]\{\phi\}_k = \Omega_k^2 \mathcal{M}_k Y^{*I}_{k(\omega)}\{\phi\}_k$$

$$[k][Y^{I}_{(\omega)}]\{\gamma\}_k = \Omega_k^2 \mathcal{M}_k Y^{*I}_{k(\omega)}\{\gamma\}_k$$

$$[Y^{R}_{(\omega)}][k]\{\phi\}_k = \Omega_k^2 \mathcal{M}_k Y^{*R}_{k(\omega)}\{\phi\}_k$$

$$[k][Y^{R}_{(\omega)}]\{\gamma\}_k = \Omega_k^2 \mathcal{M}_k Y^{*R}_{k(\omega)}\{\gamma\}_k \tag{43}$$

Equations (41) through (43) give four additional eigenvalue equations each for determination of the normal mode vectors and the gamma vectors by iteration. The authors feel that the eigenvalue equation formed by multiplication of the mobility matrix and the damping matrix would not be reliable in actual engineering practice for determination of the modal and gamma vectors because of the lack of reliable a priori damping parameters and the generally small numerical significance of damping.

INCOMPLETE SUMMATIONS

Equations (31) through (33) show that the physical parameters are equal to the sum of n n x n modal parameter matrices over the n modes of an n degree-of-freedom system. Each modal parameter matrix, $[m]_i^*$ for example, is of rank 1 and the sum of q of these, where $q < n$, is of rank q. The sum of q modal parameter matrices will not, in general, approximate the physical parameter matrix even when $n - q = 1$. The reason for this is that the generalized parameters, $\mathcal{M}_i$ and $\mathcal{K}_i$, do not necessarily become small for higher modes. In fact, the generalized stiffness usually grows larger with increasing natural frequency. The sum of the first nine modal stiffness matrices in this study has no resemblance to the physical stiffness matrix, but the addition of the tenth modal stiffness matrix causes the sum to approximate the physical stiffnesses very precisely.

Table IV shows the values of the generalized parameters mode-by-mode. The generalized mass and stiffness in Table IV were obtained by normalization on the modal eigenvector, not by normalization on the gamma vector as done in the identification program, and these values should be used only with a gamma matrix which is the unnormalized inverse of a normalized modal eigenvector matrix. However, Table IV illustrates the point that the scalar modal multiplier for stiffness grows larger, in this typical case, with increasing natural frequency and that the generalized mass does not become negligible for the higher modes.

It should be noted that the matrix $\{\gamma\}_i\{\gamma\}_i^T$ in Equations (31) through (33) are not idempotents and the vectors are not the eigenvectors of mass or stiffness. Neither are the generalized masses or generalized stiffnesses eigenvalues, of course, of their respective matrices. It follows that the gamma vectors are not orthogonal except with respect to the mobility matrix at any frequency, as shown in Equation (21). Any matrix of the form $\{\gamma\}_i\{\gamma\}_i^T$, when raised to any integer power p is, of course, equal to the matrix to the first power multiplied by the p-th power of the scalar $\{\gamma\}_i^T\{\gamma\}_i$.

Equations (31) through (33) superficially resemble the expression of a matrix in terms of the summation of principal idempotents in this respect, and in the fact that cross products of the gamma vectors do not occur. No relationship exists between the gamma vectors and the

eigenvectors of the mass matrix irrespective of the stiffness matrix, and vice versa.

INFLUENCE COEFFICIENTS

The influence coefficient matrix may be analytically expressed as the inverse of Equation (32).

$$[C] = \sum_{i=1}^{N} \frac{1}{\eta_i \Omega_i^2} \{\phi\}_i \{\phi\}_i^T \qquad (44)$$

Note in Table IV that the value of $\eta_i \Omega_i^2$ grows larger with increasing natural frequency; therefore, the scalars of Equation (44) will become small for the higher modes. For example, in Table IV, it is seen that the contribution of the tenth mode to the influence coefficient matrix is less than one one-thousandths the contribution of the first mode.

It is possible, therefore, to approximate the influence coefficient matrix quite accurately term-by-term by summing Equation (44) over less than the full n modes, and this approximation will hold for the fully populated influence coefficient matrix. If the calculations for the summation of Equation (44) over $p < n$ modes were exact, then the resulting influence coefficient matrix would be singular. However, measurements are not exact, and therefore it is very unlikely that the approximate flexibility matrix will be singular; it might even be well conditioned. It will have the fault of not containing information about the higher modes. However accurate, within reason, any measured influence coefficient matrix might be, the stiffness matrix obtained by inverting it should be regarded as having absolutely no physical meaning unless the order of the matrix is trivially small.

IDENTIFICATION OF DIAGONAL MASSES WITH ONLY A FEW MODES

If it is known, or can be reasonably assumed, that a diagonal mass matrix is a satisfactory representation of the inertial terms in the equations of motion of the helicopter, then the physical masses may be identified via this theory using only the first few modes.

TABLE IV. SCALAR MODEL PARAMETERS OF BEAM REPRESENTATION OF HELICOPTER

Mode	Natural Frequency (cps) Ω_i	Generalized Mass-Normalized Modal Vector (lb-sec^2/in.) η_i	Generalized Stiffness-Normalized Modal Vector (lb/in.) $\eta_i \Omega_i^2$
I	3.144	8.1375	3.176×10^3
II	9.103	4.5545	1.49×10^4
III	20.791	.4952	8.48×10^3
IV	41.121	1.662	1.111×10^5
V	101.35	.7054	2.86×10^5
VI	154.897	.0338	3.20×10^4
VII	190.12	.3504	5.00×10^5
VIII	309.35	.6856	2.59×10^6
IX	562.277	.3258	4.07×10^6
X	1145.31	.2970	1.54×10^7

For physical masses which are only diagonal, the following holds:

$$m_{kk} = \sum_{i=1}^{N} \mathcal{M}_i \gamma_{ki}^2 = \sum_{i=1}^{N} \sum_{j=1}^{N} \mathcal{M}_i \gamma_{ki} \gamma_{ji} \tag{45}$$

This leads immediately to the fact that

$$\sum_{i=1}^{N} \mathcal{M}_i \gamma_{ki} \sum_{\substack{j=1 \\ j \neq k}}^{N} \gamma_{ji} = 0 \tag{46}$$

for diagonal mass matrices. Equation (45) may also be expressed as

$$m_{kk} = \sum_{i=1}^{q} \mathcal{M}_i \gamma_{ki}^2 + \sum_{i=1}^{q} \mathcal{M}_i \gamma_{ki} \sum_{q \neq k}^{N} \gamma_{ji} \tag{47}$$

The first term obviously converges monotonically to the physical diagonal mass and the second converges to zero when q = N. The second term is likely, in many cases, to converge more or less nearly monotonically also because of the relatively large first generalized mass and increasing changes in sign of the gamma vector with increasing modes.

Table V shows a close approximation to the ten actual diagonal masses summing Equation (47) over only three modes for the specimen used in this study. The convergence is dramatic compared to that obtained using the first summation of Equation (45). As this matter is beyond the scope of this study, the subject is not being pursued further in this report.

TABLE V. APPROXIMATIONS OF DIAGONAL MASSES BY

$$m_{kk} \approx \sum_{i=1}^{q} \sum_{j=1}^{N} \mathcal{M}_i \gamma_{ki} \gamma_{ji}$$

Station k	Exact Masses ($lb\text{-}sec^2/in.$)	Approximate Masses: Mode I	Modes I + II	Modes I + II + III
1	.029	.046	.025	.029
2	7.337	9.322	7.020	7.352
3	6.540	5.760	6.783	6.482
4	5.179	3.741	5.361	5.193
5	3.129	1.784	3.172	3.161
6	.527	.222	.511	.532
7	.170	.047	.153	.170
8	.119	.016	.095	.116
9	.238	-.016	.145	.227
10	.298	-.081	.123	.300

IMPEDANCE AND MOBILITY

NETWORK THEORY AND IMPEDANCE

All systems which can be described by a set of second-order linear differential equations with constant coefficients can be depicted as a "network" or "circuit" of intersecting lines. The dependent variables are "potentials" and are a property of the points of intersections. The independent variables are "flows" and are a property of the connecting lines. Given the system in a steady state, the ratio of the difference between the sinusoidal maxima of the potentials at adjacent intersections of a line (or element) and the sinusoidal maximum of the flow through that element may be termed the absolute value of the "component impedance". As there will be a phasing between the potential difference and the flow, the component impedance will be a complex quantity and, in general, will be a function of frequency.

In many systems, such as electrical circuits and simple spring-mass-damper chains, the component impedances are physically measurable quantities directly and obviously identified with physical entities such as resistors, masses, capacitors, dampers, etc. In more complicated systems such as beams, for example, the component impedances are associated with combinations of the material properties of sections of the system such as the product of the modulus of elasticity and second moment of area (EI) divided by the cube of length. All linear structural systems, no matter how complicated, can be mathematically duplicated in terms of dynamic response by a network of springs, masses and dampers.

The component impedance between points i and j or a network where $i \neq j$ is minus one times the partial derivative of the flow phasor from i to ground with respect to the potential phasor at j. This partial derivative is here called the "element impedance" and is the ij-th term in the matrix of impedances in the equations of motion. The component impedance between point i and ground is the sum of the element impedances of the i-th row in the equations of motion.

In linear dynamic structures, the flow phasor to ground is an impressed force and the potential phasor is, by convention, the sinusoidal velocity at a point.

MOBILITY OF A NETWORK

In complex assembled systems, such as helicopters, it is generally only possible to measure the "response" of the total system. The "response" of a complete system may be defined as the partial derivative of the potential phasor at point i in the system with respect to the flow phasor to ground at point j in the system. In structural dynamics this is the complex value of the steady-state sinusoidal velocity phasor at point i on the structure to the force-to-ground phasor at point j when the force at point j is the only external force on the structure and is termed "mobility".

The response of any linear system of n components is an n x n matrix of the partial derivatives of the potential phasor at j with respect to the grounded flow phasor at i. The frequency-dependent terms in the equations of motion form an n x n matrix of the partial derivatives of the grounded flow phasor at j with respect to the potential phasor at i. Clearly, then, the equations of motion are related to the response by the inverse of a matrix because a partial derivative is related to its reciprocal only by the inversion of the matrix of the partials.

NETWORKS IN MATRIX FORM

It is fundamental to Network Analysis that the performance of the entire network is given by the inverse of the matrix of the element impedance terms formed from the components of the network. When networks are expressed in matrix form it is usually unnecessary to draw the network diagram. Kirchoff's Laws, Norton's Theorem, Thevenin's Theorem and other such rules are merely special cases of the matrix expression of a circuit or network.

IMPEDANCE MATRICES

Impedance matrices are lambda matrices[4]. In structural dynamics, impedance matrices are lambda matrices of the second degree. The response or mobility matrix is the inverse of the impedance matrix and is not a lambda matrix. In general, the inverse of a lambda matrix is not a lambda matrix, and therefore the mobility matrix cannot be expressed as a polynomial in forcing frequency. For this reason, we cannot draw a mobility or response network in which the components are coefficients of the p-th power of the forcing frequency; therefore, we find the network of response of no obvious practical value.

MATRIX INVERSION AND PHYSICAL RELEVANCE

If $[z']$ is approximately equal to the exact impedance matrix $[z]$, it does not follow that $[z']^{-1}$ is approximately equal to $[z]^{-1}$. To prove this, expand $[z]$ in terms of its principal idempotents[5] and let the n-th eigenvalue be small compared to the other eigenvalues. Let

$$[z'] = \sum_{i=1}^{n-1} \lambda_i \{\beta\}_i \{\beta\}_i^T + (\lambda_n + \varepsilon)\{\beta\}_n \{\beta\}_n^T \quad [z],$$

where ε is considered of the order of magnitude of λ_n. Then

$$[z]^{-1} = \sum_{i=1}^{h} \frac{1}{\lambda_i} \{\beta\}_i \{\beta\}_i^T$$

is not approximately equal to $[z']^{-1}$ because the smallest eigenvalue of $[z]$ is the largest eigenvalue of $[z]^{-1}$. The conditioning of a matrix which approximates an exact matrix does not necessarily indicate whether the inverse of the approximate matrix will approximate the inverse of the exact matrix. For the inverse of an approximate matrix to approximate the inverse of the exact matrix, it is necessary but not sufficient that the approximate matrix be well conditioned. Herein lies one of the chief difficulties in obtaining mathematical model parameters from test data.

THE MEASUREMENT OF MOBILITY AND IMPEDANCE

At a given frequency,

$$[z]\{\tilde{\dot{y}}\} = \{\tilde{f}\}$$

If $[z]$ is of order n, and n different force vectors are applied, then the mobility matrix is given by

$$[Y] \equiv [z]^{-1} = [\tilde{\dot{y}}][\tilde{f}]^{-1}$$

However, if any column of $[\tilde{f}]$ is a linear combination of the other columns, the matrix will be singular. One way

to insure that $\tilde{[f]}$ is both nonsingular and well conditioned is to make $\tilde{[f]}$ a diagonal matrix: that is, to apply only one force at a time and at a different station each time. This is a practical way to measure mobility because excitation force is generally an independent variable in structural testing.

It is impractical to measure impedance directly from

$$[z] = \tilde{[f]}\,\tilde{[y]}^{-1}$$

because the velocity phasor matrix is generally ill conditioned except at high frequency.

CONCLUSIONS AND OBSERVATIONS

1. In an n-degree-of-freedom structurally damped linear system, the mass, stiffness and damping matrices of Lagrange's equations of motion, the natural frequencies, mode shapes, generalized masses and generalized stiffnesses can be obtained directly from impedance-type test data.

2. The identification of these parameters can be obtained with sufficient accuracy to accurately reproduce the measured response using input data having errors that are within the state-of-the-measurement art.

3. The mean of replicated measurements can be used to identify a practical mathematical model. However, the mean of replicated parameter identifications should not be used because they can give a model which is not consistent within itself.

4. Bias phase error has negligible error on the identifications.

5. The eigenvectors of the product of a mobility matrix and the inverse of another mobility matrix are the modal eigenvectors.

6. The first eigenvector of the product of a mobility matrix measured at frequency ω and an imaginary mobility matrix measured near the n-th mode, for matrices of order n, is the eigenvector of the mode which is dominant at frequency ω.

7. Real mobility matrices are generally ill-conditioned. The higher the frequency at which an imaginary mobility matrix is measured, the better the conditioning.

8. The accuracy of identification of far off-diagonal parameters is less important to model response than the accuracy of identification of diagonal and near-diagonal parameters.

9. If the elements of a matrix A approximate those of a matrix B, the elements of the inverse of A will not necessarily approximate the elements of the inverse of B regardless of how well conditioned A might be.

10. Diagonal masses in a ten-degree-of-freedom model have been accurately identified using only data from three modes.

REFERENCES

1. Soroka, W.W., NOTE ON THE RELATIONS BETWEEN VISCOUS AND STRUCTURAL DAMPING COEFFICIENTS, Journal of the Aeronautical Sciences, Vol. 16, No. 7, July 1949, p. 409.

2. Raney, J.P., IDENTIFICATION OF COMPLEX STRUCTURES USING NEAR RESONANCE TESTING, The Shock and Vibration Bulletin, No. 38, Part 2, August 1968, pp. 23-32.

3. Kennedy, C.C. and Pancu, C.D.P., USE OF VECTORS IN VIBRATION MEASUREMENT AND ANALYSIS, Journal of the Aeronautical Sciences, Vol. 14, No. 11, November 1947, pp. 603-625.

4. Frazer, R.A., Duncan, W.J., and Collar, A.R., ELEMENTARY MATRICES, Cambridge, The Syndics of the Cambridge University Press, 1965, p. 57ff.

5. Rosanoff, R.A., A SURVEY OF MODERN NONSENSE AS APPLIED TO MATRIX COMPUTATIONS, AIAA Structural Dynamics and Aeroelasticity Specialist Conference, New Orleans, Louisiana, April 1969, p. 275.

Unclassified

Security Classification

DOCUMENT CONTROL DATA - R & D

(Security classification of title, body of abstract and indexing annotation must be entered when the overall report is classified)

1. ORIGINATING ACTIVITY (Corporate author) Kaman Aerospace Corporation Old Windsor Road Bloomfield, Connecticut	2a. REPORT SECURITY CLASSIFICATION Unclassified 2b. GROUP

3. REPORT TITLE

THEORY OF STRUCTURAL DYNAMIC TESTING USING IMPEDANCE TECHNIQUES, VOLUME I - THEORETICAL DEVELOPMENT

4. DESCRIPTIVE NOTES (Type of report and inclusive dates)

Final Report

5. AUTHOR(S) (First name, middle initial, last name)

William G. Flannelly Roger M. Barnsby
Alex Berman

6. REPORT DATE June 1970	7a. TOTAL NO. OF PAGES 113	7b. NO. OF REFS 5
8a. CONTRACT OR GRANT NO. DAAJ02-68-C-0106 b. PROJECT NO. Task 1F162204A13904 c. d.	9a. ORIGINATOR'S REPORT NUMBER(S) USAAVLABS Technical Report 70-6A 9b. OTHER REPORT NO(S) (Any other numbers that may be assigned this report) R-823	

10. DISTRIBUTION STATEMENT

This document is subject to special export controls, and each transmittal to foreign governments or foreign nationals may be made only with prior approval of U. S. Army Aviation Materiel Laboratories, Fort Eustis, Virginia 23604.

11. SUPPLEMENTARY NOTES Volume I of a 2-volume report	12. SPONSORING MILITARY ACTIVITY U. S. Army Aviation Materiel Laboratories Fort Eustis, Virginia

13. ABSTRACT

It is shown that the mass, stiffness and damping parameters in Lagrange's equations of motion of an n-degree-of-freedom damped linear elastic structure can be determined directly from impedance-type test data without prior assumption of an intuitive mathematical model. The damping is assumed to be such that the modal vectors are orthogonal with respect to damping.

A method is derived for determination of the exact modal eigenvector of the dominant mode at any forcing frequency by iteration on the damped impedance measurements in matrix form. A similar eigenvalue equation yields the vector in the inverse transpose of the modal matrix; this vector called the gamma vector, is identified with the dominant mode. The generalized masses, stiffnesses and damping terms are related to the mass, stiffness and damping matrices of the equations of motion through products of the gamma vectors.

Using the gamma vectors, obtained by iteration on test data, the natural frequencies and other modal parameters are determined. Natural frequencies which are not visible in response plots may be determined by this method.

Computer experiments were conducted to test the sensitivity of the theory to errors in input data.

The work performed under this contract is reported in two volumes. This volume contains the theoretical development, application of the theory and computer experiments demonstrating the theory's practicality.

DD FORM 1473 REPLACES DD FORM 1473, 1 JAN 68, WHICH IS OBSOLETE FOR ARMY USE.

Unclassified

Security Classification

14. KEY WORDS	LINK A		LINK B		LINK C	
	ROLE	WT	ROLE	WT	ROLE	WT
Structural Dynamic Testing						
Eigenvector						
Eigenvalue						
Gamma Vector						
Impedance Techniques						